ASYNTHESIS, CHARACTERISATION AND BIOLOGICAL ACTIVITY OF BISMUTH AND ANTIMONY 1,1-DITHIOLATES

DYG HAZWANI ABANG ISHAK

FACULTY OF SCIENCE
UNIVERSITY OF MALAYA
KUALA LUMPUR

2017

SYNTHESIS, CHARACTERISATION AND BIOLOGICAL ACTIVITY OF BISMUTH AND ANTIMONY 1,1-DITHIOLATES

DYG HAZWANI ABANG ISHAK

DISSERTATION SUBMITTED IN FULFILLMENT OF THE REQUIREMENTS FOR THE DEGREE OF MASTER OF SCIENCE

FACULTY OF SCIENCE
UNIVERSITY OF MALAYA
KUALA LUMPUR

2017

UNIVERSITI MALAYA
ORIGINAL LITERARY WORK DECLARATION

Name of Candidate: **DYG HAZWANI ABANG ISHAK**

Registration/Matric No: **SGR120118**

Name of Degree: **MASTER OF SCIENCE**

Title of Project Paper/Research Report/Dissertation/Thesis ("this Work"):

SYNTHESIS, CHARACTERISATION AND BIOLOGICAL ACTIVITY OF ANTIMONY BISMUTH 1,1-DITHIOLATES

Field of Study: **INORGANIC CHEMISTRY**

I do solemnly and sincerely declare that:

(1) I am the sole author/writer of this Work;
(2) This Work is original;
(3) Any use of any work in which copyright exists was done by way of fair dealing and for permitted purposes and any excerpt or extract from, or reference to or reproduction of any copyright work has been disclosed expressly and sufficiently and the title of the Work and its authorship have been acknowledged in this Work;
(4) I do not have any actual knowledge nor do I ought reasonably to know that the making of this work constitutes an infringement of any copyright work;
(5) I hereby assign all and every rights in the copyright to this Work to the University of Malaya ("UM"), who henceforth shall be owner of the copyright in this Work and that any reproduction or use in any form or by any means whatsoever is prohibited without the written consent of UM having been first had and obtained;
(6) I am fully aware that if in the course of making this Work I have infringed any copyright whether intentionally or otherwise, I may be subject to legal action or any other action as may be determined by UM.

Candidate's Signature   Date

Subscribed and solemnly declared before,

Witness's Signature   Date

Name:

Designation:

ABSTRACT

Motivated by the success of metal-based drugs in treatment of various diseases, 12 complexes of antimony (**7-12**) and bismuth (**13-18**) metal were synthesized and characterized by using ^{1}HNMR, ^{13}CNMR, FTIR, CHNanalyser, TGA, DSC, PXRD, SCXRD, UV-Visible and Fluorescence characterisation. After having verified the structure of the complexes, the prepared complexes were tested for their biological activity, anticancer in particular against a range of carcinoma cell lines, together with an evaluation of anti-microbial activities. Bismuth compound [Bi(S$_2$CNR$_2$)](**13**) with R=CH$_2$CH$_3$ was found to be cytotoxic towards an array of human carcinoma, more pronounced in HepG2 cells (liver cancer cells). This compoundalso induced apoptosis in the cell the death mechanism pathway and expressed death receptor-dependent pathway by generating CD40, CD40L and TNF-R1 (p55) protein. Moreover, complex **13** promotes tumour-suppressor, DAPK1 enzyme which naturally comes hand in hand with the down-regulation of XIAP gene and NF-κB, protein complex that controls the DNA transcription. The inhibition growth of HepG2 cells is in parallel with the findings that cell cycle arrest occurred at S and G$_2$/M phases. However, another bismuth compound in the testing, [Bi(S$_2$CNR$_2$)] (**16**) with R=CH$_2$CH$_2$OH, is found to be less formidable in almost all of the study performed. This result is further supported by the cell invasion rate study whereby the invasion rate of **16** is 10-fold higher than that of **13**, again, correlated with the down-regulation of XIAP and Survivin protein, extracted by **13**. Complexes **13** and **16** were also discovered to have different binding motifs in DNA where **13** interacts at AT- and TA- specific sites followed by inhibition digestion of restriction enzyme; **16** display an adverse effect.

ABSTRAK

Kejayaan ubat berasaskan logam yang digunakan untuk merawat pelbagai penyakit , 12 kompleks daripada antimoni dan bismut telah disintesis dan dicirikan menggunakan ^{1}H NMR, ^{13}C NMR, FTIR, CHN, TGA, DSC, PXRD, SCXRD, UV-Visible dan pendarfluor spektroskopi. Setelah struktur kompleks disahkan, ia kemudiannya diuji terhadap aktiviti biologi menfokuskan kepada ujian antikanser dengan menggunakan sel karsinoma, bersama-sama dengan pemeriksaan ke atas aktiviti-aktiviti mikrob. Sebatian bismut [Bi(S$_2$CNR$_2$)] (**13**) dengan R=CH$_2$CH$_3$ didapati sitotoksik kepada pelbagai sel karsinoma manusia, lebih ketara dalam sel-sel HepG2 (sel-sel kanser hati). Sebatian**13** juga menyebabkan sel mati melalui laluan mekanisme apoptosis dan mengekspresi laluan reseptor-kematian dengan menjana protein CD40, CD40L dan TNF-R1 (P55). Lebih-lebih lagi, **13** menggalakkan tumor-supressor, enzim DAPK1 yang secara semula jadi seiring dengan penurunan gen XIAP dan NF- κB, yang merupakan kompleks protein yang mengawal transkripsi DNA. Perencatan pertumbuhan sel-sel HepG2 adalah selari dengan penemuan bahawasanya perencatan kitaran sel berlaku di fasa S dan G$_2$/M. Walau bagaimanapun, satu lagi kompaun bismut yang diuji, [Bi(S$_2$CNR$_2$)] (**16**) dengan R=CH$_2$CH$_2$OH, adalah didapati tidak aktif secara biologi dalam hampir semua ujian yang dilakukan. Keputusan ini disokong oleh kajian kadar pencerobohan sel, dimana kadar pencerobohan **16** adalah 10 kali ganda lebih tinggi daripada **13**, sekali lagi, berkait rapat dengan penurunan gen XIAP dan protein Survivin, yang diekstrak oleh **13**. **13** dan **16** juga ditemui mempunyai motif yang berbeza dalam tindak balas dengan DNA dimana **13** berinteraksi di laman AT dan TA yang khusus diikuti oleh perencetan penghadaman sekatan enzim ;**16** memaparkan kesan disebaliknya.

ACKNOWLEDGEMENTS

TABLE OF CONTENTS

LIST OF FIGURES

LIST OF TABLES

LIST OF ABBREVIATIONS AND SYMBOLS

^{1}H-NMR	Proton NMR
^{13}C-NMR	Carbon-13 NMR
AEVD	Amino acid sequence
AFC	Antibody-forming cell
AIF	Apoptosis Inducing Factor
ATCC	American Type Culture Collection
BAD	Bcl-2-associated death promoter
Bi	Bismuth
BNIP3L	BCL2/adenovirus E1B 19 kDa protein-interacting protein 3-like
Bu	Butyl
c-Abl	Mammalian Abelson murine leukaemia viral oncogene homolog 1
CD40	Tumour necrosis factor receptor superfamily, member 5
CD40L	Tumour necrosis factor superfamily, member 5
CDCl$_3$	Deuterated chloroform
CT	Cycle threshold
CHN	Carbon, Hydrogen, Nitrogen Analysis
COX-2	Enzyme that causes pain and inflammation
DAPK1	Death-associated protein kinase 1
DFFA	DNA fragmentation factor subunit alpha
DMSO	Dimethyl sulfoxide
DNA	Deoxyribonucleic acid
Dnase	Deoxyribonuclease
DPBS	Dulbecco's phosphate-bufferred saline
DSC	Differential Scanning Calorimetry

EDT	Ethylenediaminetetraacetic acid
Et	Ethyl
EtOH	Ethanol
FTIR	Fourier Transform Infrared Spectroscopy
G_2	Gap 2 phase; gap between DNA synthesis and mitosis
GPC	Gel Permeation Chromatography
HepG2	Human hepatocellular carcinoma (human liver cancer cell)
HSQC	Heteronuclear Single Quantum Correlation
ICAM-1	Intercellular Adhesion Molecule 1
iPr	Isopropyl
K	Kelvin
M	Mitosis phase; cell division to 2 daughter cells
Me	Methyl
NF-κB	Nuclear factor kappa-light-chain-enhancer of activated B cells
NMR	Nuclear magnetic resonance spectroscopy
PXRD	Powder X-ray Diffractometry
RPMI	Roswell Park Memorial Institute
S	Synthesis phase where DNA replication occurs
Sb	Antimony
SCXRD	Single-crystal X-ray Diffraction
SEM	Standard error of the mean
TAE	Tris-Acetate-EDTA
TE	Tris-EDTA
TGA	Thermogravimetric analysis
TNF	Tumour necrosis factor receptor
TNF-R1	Tumour necrosis factor receptor superfamily, member 1A

UV-Vis   Ultraviolet-visible Spectroscopy

XIAP   X-lined mammalian inhibitor of apoptosis protein

CHAPTER 1 : INTRODUCTION AND LITERATURE REVIEW

1.1 INTRODUCTION TO COORDINATION COMPOUNDS

Coordination compounds or metal complexes consist of two components: a metal center and ligand(s) (Garnovskii *et. al.*, 2009). It is a product of a reaction between a Lewis base: in which neutral molecules or anions that contain at least one pair of electrons to be donated to a Lewis acid: a metal atom/ion accepted the electrons lone pair to form a coordination covalent bond (Fiorillo *et. al.* 2004).

Research on coordination compounds have potrayed different kind of ligands which varies from the O, N and S donor. Examples of O-donor ligands are aqua ligand, H_2O and ligands containing carbonato ion, CO_3^{2-}. Studies on O-donor ligands include (Martirosyan *et. al.*, 2013) that reported on the interaction of tetrahydrofuran (THF), an O-donor ligand with ferrous nitrosyl complex Fe(TTP)(NO) (TTP^{2-} is *meso*-tetra-*p*-tolyl-porphyrinatodianion). The inspection was done through electronic and absorption spectroscopy. It was shown that the complexation of THF and ferrous nitrosyl complex occurs at low temperature as opposed to high temperature. Bhalla *et. al.*, 2016 had synthesized and characterised through X-ray crystallography on the geometry of $MF_3 \cdot 3H_2O$ (M = Al, Ga or In) complexes with dimethylsulfoxide (dmso), $[MF_3(OH_2)_2(dmso)]$. Lippert *et. al.*, 2016 had reviewed on the structural compatibility of platinum complexes with aqua, hydroxido, oxido, and peroxido ligands, all of which are O-donor ligands. It was shown that the complexes' interesting bonding gave rise to medicinally important antitumor drugs as well as catalytically relevant species.

N-donor ligands are lewis bases that utilize nitrogen as its donor atom, for example, ammine, NH_3 and pyridine ligand. Studies on N-donor ligands include (Jabali *et. al.*, 2016) which has synthesized and characterised a series of Zn(II) complexes: $[Zn_2(Indo)_4]$, $[Zn_2(indo)_4(pico)_2]$, $[Zn(indo)_2(apy)_2]$, $[Zn(indo)_2(ampy)]$, $[Zn(indo)_2(phen)]$, $[Zn(indo)_2(dmph)]$ and $[Zn(indo)_2(admp)_2]$ (indo = indomethacin, apy = 2-amino pyridine, dmph = 2,9-dimethyl-1,10-phenanthroline, pico = 3-picoline, ampy = 2-aminomethyl pyridine, phen = 1,10-phenanthroline, admp = 2-amino-4,6-dimethylpyrimidine) complexes. It was found that all the complexes have anti-bacterial effects against *P. aeruginosa*, and *S. aureus* while they were inactive toward *E. coli* and *L. monocytogenes*. In a more recent study, (Lalegani *et. al.*, 2017) had reported on the structure of four new coordination polymers of $[Cu(\mu\text{-bip})_2(N_3)_2 \cdot 2H_2O]_n$, $[Cu(\mu\text{-bbd})_2(\mu_4\text{-}N_3)_4]_n$, $[Mn(\mu\text{-bip})_2(NCS)_2]_n$ and $[Mn(\mu\text{-bip})_2(N_3)_2]_n$ that were prepared by using the neutral N-donor ligands 1,3-bis(imidazolyl)propane (**bip**) and 1,4-bis(3,5-dimethylpyrazolyl)butane (**bbd**), mono-anionic NCS^- or N_3^- ligands and appropriate metal salts of Cu(II) and Mn(II) ions. Yi-Yun *et. al.*, 2017 had reported on five new coordination polymers based on unsymmetrical tetracarboxylic acid and varied auxiliary N-donor ligands, $[Ln(\alpha\text{-Hbptc})(H_2O)_4] \cdot H_2O$ where Ln = Eu or Tb, $[Cu_2(\alpha\text{-bptc})(bipy)(H_2O)_4] \cdot H_2O$, $[Cd_2(\alpha\text{-bptc})(phen)_2(H_2O)_2] \cdot H_2O$, $[Cd_2(\alpha\text{-bptc})(bpee)_{0.5}(H_2O)_4] \cdot 3H_2O$ where $\alpha\text{-H}_4bptc = 2,3,3',4'$-biphenyl tetracarboxylic acid, bipy = 4,4'-bipyridine, bpee = 1,2-bis(4-pyridyl)ethylene, phen = 1,10-phenanthroline.

Various research have been done focusing on the specialty of S-donor ligands particularly on its geometry, electrochemistry and bioinorganic chemistry, for instance. The chemistry of S-donor ligands is of interest as they can bind to a wide range of metal ion (Collinson *et. al.*, 2011), making it the focus of this study. Examples of S-donor ligands are sulfido, S^{2-} containing compounds and organosulfur compounds that contain

thiocynato, SCN⁻ and thiolato RS⁻ group for example thiocarbamate and thiourea as illustrated in **Figure 1.1A**.

| i | ii |
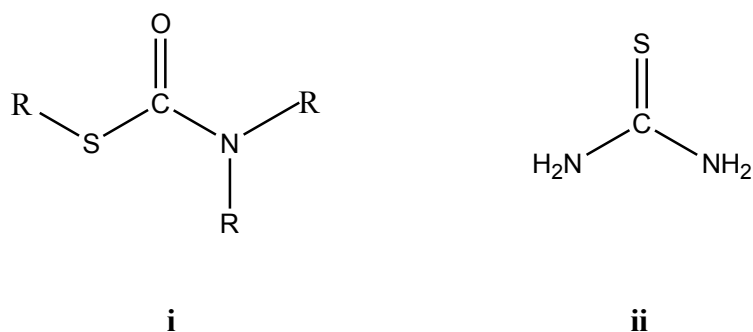
Figure 1.1A: General structure of (i) *S*-thiocarbamate (ii) and thiourea

1.2 INTRODUCTION TO 1,1-DITHIOLATE

Thiolate ligands are obtained from the general reaction of carbon disulphide and different types of nucleophiles. Thiolate ligands can be classified into two categories: mono- and di-thiolate ligands, depending on the number of sulfur atom(s) that is accessible for coordinating. Mono thiolate ligand provides one sulfur atom for coordinating. Examples of mono thiolate ligands are mercapto, HS-R and thioamide, ROC(=S)NHR') where R, R' is an alkyl and/or an aryl group as illustrated in **Figure 1.1B**.

| i | ii |
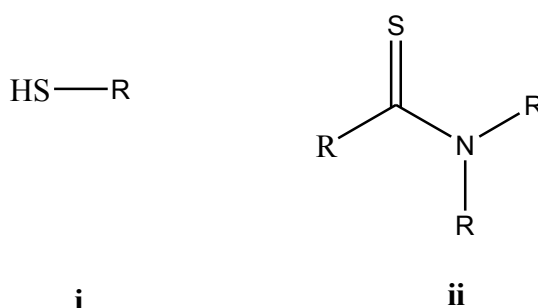
Figure 1.1B : General structure of (i) mercapto and (ii) thioamide

Dithiolate ligands on the other hand, contain two sulfur atoms available for coordinating. There are four main types of 1,1-dithiolate ligands: xanthate ($^-$S$_2$COR), dithiophosphate [$^-$S$_2$P(OR)$_2$], dithiphosphinate ($^-$S$_2$PR$_2$) and dithiocarbamate ($^-$S$_2$CNR$_2$), as shown in **Figure 1.1C**.
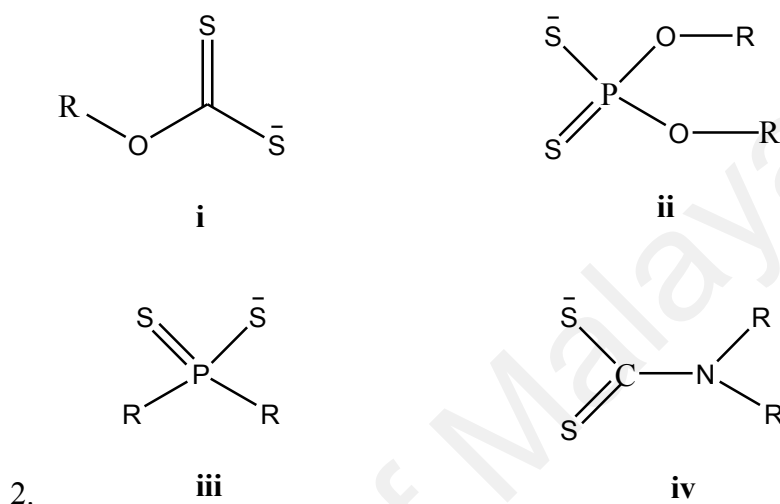
Figure 1.1C: General structure of (i) xanthate ($^-$S$_2$COR), (ii) dithiophosphate [$^-$S$_2$P(OR)$_2$], (iii) dithiphosphinate ($^-$S$_2$PR$_2$) and (iv) dithiocarbamate ($^-$S$_2$CNR$_2$)

Dithiocarbamate, with a general formula $^-$S$_2$CNRR', in which R and R' can be identical or different, offer remarkable coordination chemistry. Dithiocarbamates can be synthesized by reacting carbon disulfide with a primary or secondary amine. The dithiocarbamate ligand exists as milky white or pale yellow with an unpleasant smell (Aly *et. al.*, 2012). They are lipophilic and work best when complexed with metals in a symmetrical chelate fashion. They form stable complexes with the majority of main group elements through a wide range of oxidation states and have good solubility in water or organic solvent, depending on the nature of its cation. 1,1-dithiocarbamate ligands are planar making it non-demanding ligands that can be electronically tuned to selectively bind to substituents (Hogarth, 2012).

Mensforth *et. al.*, 2013 wrote a review on the importance of sulfur-based metal complexes containing dithiocarbamate, dithiocarboxylate and xanthate ligands due to their ability to produce materials for applications such as gas storage, catalysis, magnetism, conductivity, nonlinear optical responses, catalysis, and ion exchange. The study had shown that various dithiocarbamate, dithiocarboxylate and xanthate polymeric complexes can be prepared with a variety of metals and displayed a variety of coordination modes.

Han-Dong *et. al.*, 2008 had successfully synthesized and inspected the structure of three antimony(III) dithiocarbamate complexes: $(OC_4H_8NCS_2)SbBr$ which had shown to have a trigonal bipyramidal geometry, $[(C_5H_{10}NCS_2)_3Sb]$ which had shown to have a distorted octahedral geometry, and that $[(HOCH_2CH_2)_2NCS_2]_3Sb$ complex is stabilized by strong intermolecular hydrogen bonds between the ethanolic hydrogen.

Joshi *et. al.*, 2017 had synthesized six mixed metal derivatives of antimony(III) and bismuth(III) by the reaction of ethane-1,2-dithiol and metal *bis* derivatives of dithiocarbamates and/or dithiophosphates ligands. These derivatives have been characterized by physicochemical studies and have nano-ranged crystallite size (8.18–18.04 nm) with monoclinic crystal system. In addition to the structural studies, all the synthesized derivatives were found to have elevated the zone for the inhibition against four bacterial and two fungal species as compared to single metal species (metal precursors) as well as standard drugs.

Apart from the spectroscopic and structure evaluation, dithiocarbamates were also synthesized to be applied in wide range of applications. This was shown when a few Cu dithiocarbamate complexes showed semiconducting properties (Mensforth *et. al.*, 2013). The study also showed that a tridentate dithiocarbamate based ligand gave rise to macrocyclic arrays which extended its supramolecular interactions. This gives

rise to a promising structural chemistry and potential future various applications.

In biological activity studies, (Banti *et. al.* 2017) had synthesized and characterized complexes with the general formula $[Ag(CH_3OCS_2)(Ar_3P)_2]$ (Ar_3P = triphenylphosphine, tri(p-tolyl)phosphine and tri(m-tolyl)phosphine). All three complexes were tested for their *in vitro* cytotoxic activity against human adenocarcinoma cancer cell lines: MCF-7 (breast, estrogen receptor (ER) positive), MDA-MB-231 (breast, estrogen receptor (ER) negative) and MRC-5 (normal human fetal lung fibroblast cells) with sulforhodamine B (SRB) colorimetric assay. Complex $Ag(CH_3OCS_2)(Ar_3P)_2](Ar_3P$ =tri(m-tolyl)phosphine) exhibits higher activity against MCF-7 cells. The results are correlated with those obtained from heteroleptic silver complexes of its tri-aryl-phosphines and carboxylates analogs where the xanthate is replaced by carboxylate. The structure-activity relationships (SAR) study underlines the significance of the ligand type on its bioactivity of these compounds.

Amir *et. al.*, 2017 reported on the presence of various dithiocarbamates moiety in palladium(II) complexes which had significantly improves the anticancer action and reduces the possibility of any damaging side effects, as opposed to the widely used *cisplatin*. Kemahli *et. al.*, 2016 had investigated the histopathological and biochemical effects of pyrrolidine dithiocarbamate, PyDT, an antioxidant and inhibitor of NF-kβ, on ischemiareperfusion injury in rats. The study shows the beneficial effects of PyDT for the alleviation of ischemiareperfusion injury in testicular tissue in rats, which in turn, could be potent in combating ischemiareperfusion injury in human testicular tissue.

Milacic *et.al.*, 2013 has found that PyDT-copper(II) complex is more potent to inhibit cellular proteasomal activity, suppress proliferation and induce apoptosis in various human breast and prostate cancer cell lines as compared to (PyDT)-zinc(II) complex. It was also discovered that the potencies of these PyDT-metal complexes

depend on the nature of metals and also on the ratio of PyDT to the metal ion within the complex, which probably affects their stability and availability for interacting with and inhibiting the proteasome in tumor cells.

Jamaludin *et. al.*, 2013 had reported on the synthesis and characterisation of $R_3PAu[S_2CN(^iPr)CH_2CH_2OH]$, for R = Ph, Cy and Et. All the compounds synthesized are cytotoxic against the doxorubicin-resistant MCF-7R with $Ph_3PAu[S_2CN(^iPr)CH_2CH_2OH]$ exhibiting greater potency and cytotoxicity than either of doxorubicin and cisplatin. Based on human apoptosis PCR-array analysis, caspase activities, DNA fragmentation, cell apoptotic assays, intracellular reactive oxygen species (ROS) measurements and human topoisomerase I inhibition, induction of apoptosis by $Ph_3PAu[S_2CN(^iPr)CH_2CH_2OH]$, and necrosis by both $R_3PAu[S_2CN(^iPr)CH_2CH_2OH]$, for R = Cy and Et, are demonstrated, by both extrinsic and intrinsic pathways. Compound $Ph_3PAu[S_2CN(^iPr)CH_2CH_2OH]$ activates the p53 gene, $Cy_3PAu[S_2CN(^iPr)CH_2CH_2OH]$ activates only the p73 gene, whereas $Et_3PAu[S_2CN(^iPr)CH_2CH_2OH]$ activates both the p53 and p73 genes. Compounds $Ph_3PAu[S_2CN(^iPr)CH_2CH_2OH]$ and $Et_3PAu[S_2CN(^iPr)CH_2CH_2OH]$ activate NF-κB, and each inhibits topoisomerase I.

Tan *et. al.*, 2015 reported that $\{Zn[S_2CN(R)CH_2CH_2OH]_2\}_2$ for R = iPr, CH_2CH_2OH and Me, and an all alkyl species, $[Zn(S_2CNEt_2)_2]_2$, are broadly cytotoxic, specifically against human cancer cell lines compared with normal cells, with greater potency than cisplatin. Notably, some selectivity were indicated with $\{Zn[S_2CN(CH_2CH_2OH)CH_2CH_2OH]_2\}_2$ being the most potent against human ovarian carcinoma cells (cisA2780), and $[Zn(S_2CNEt_2)_2]_2$ being more cytotoxic toward multidrug resistant MCF-7R, human colon adenocarcinoma cells (HT-29), and human lung adenocarcinoma epithelial cells (A549). Based on human apoptosis PCR-array analysis, caspase activities, DNA fragmentation, cell apoptotic assays, intracellular

reactive oxygen species (ROS) measurements and human topoisomerase I inhibition, induction of apoptosis in HT-29 cells is demonstrated via both extrinsic and intrinsic pathways. Compounds {Zn[S$_2$CN(R)CH$_2$CH$_2$OH]$_2$}$_2$ for R = CH$_2$CH$_2$OH and Me, and an all alkyl species, [Zn(S$_2$CNEt$_2$)$_2$]$_2$ activate the p53 gene while {Zn[S$_2$CN(iPr)CH$_2$CH$_2$OH]$_2$}$_2$ activates both p53 and p73. Cell cycle arrest at the S and G$_2$/M phases correlates with inhibition of HT-29 cell growth. Cell invasion is also inhibited by all the compounds synthesized this correlated with down-regulation of NF-κB.

Based on the above studies done by (Milacic *et.al.*, 2013), (Jamaludin *et. al.*, 2013) and (Tan *et. al.*, 2015) on *N, N'*-diethyl dithiocarbamate, pyrrolidine dithiocarbamate, *N*-Isopropyl-*N*-hydroxyethyl dithiocarbamate, *N, N'*-diethanol dithiocarbamate and *N*-ethanol-*N*-methyl dithiocarbamate ligands as successful antitumour drugs, it is then worthwhile to look further look into these dithiocarbamate complexes and its biological activity, making it the focal point of this dissertation.

1.3   BIOLOGICAL ACTIVITY OF ANTIMONY COMPLEXES

As a result of the success of antimony's wide usage in the treatment of leishmaniasis (Haldar *et. al.*, 2011), interest was gained recently to inspect other antimicrobial and anticancer activities of antimony complexes. Ru-Zhong Sun, 2012 asserts that antimony dibutyldithiocarbamate exerts a positive inhibitory effect in overcoming bacterial infections as compared to standard drugs used (e.g. Penicillin and Furacilin). Biological screening studies done by (Chauhan *et. al.*,2014) shows that *bis*(*N*,*N*-dimethyldithiocarbamato-*S*,*S'*)antimony(III) complexes sodium benzoate, sodium thioglycolate, phenol, sodium 1-propanethiolate, potassium thioacetate, sodium

salicylate, ethane-1,2-dithiolate and disodium oxalate having greater activities against some human pathogenic bacteria and fungi than the activities of standard drugs. Tunç, *et. al.*, 2015 had synthesized novel binuclear antimony(III) compound of {Sb[5,5′-disulfanediylbis(2-amino-4,6-dimetoxypyrimidine)]Cl$_3$}$_2$, mononuclear antimony(III) compounds, SbL$_2$Cl$_3$, [L: 2-amino-5-thiol-4,6-dimethoxy pyrimidine and 2-amino-5-(1H-tetrazol-5-ylthio)-4,6-dimethoxypyrimidine were synthesized and characterized. The complexes were tested *via* in vitro against both *Leishmania Tropica* promastigote and glutathione reductase inhibitory activity. The results showed that {Sb[5,5′-disulfanediylbis(2-amino-4,6-dimetoxypyrimidine)]Cl$_3$}$_2$ has the best biological activity.

Antimony(III) halide compounds (SbX$_3$, X = Cl and Br) of thioureas; tetramethylthiourea (TMTU), *N*,*N*′-diethylthiourea (DETU) and 1,3-diisopropyl-2-thiourea (DIPTU) of formulae {[SbCl$_3$(TMTU)]$_n$}, {[SbBr$_3$(TMTU)]$_n$}, {[*mer*-SbCl$_3$(DIPTU)$_3$] [*fac*-SbCl$_3$(DIPTU)$_3$] C$_6$H$_6$} and {[SbBr$_2$(DETU)$_2$]$^+$·Br$^-$}$_n$ were synthesized and characterized by (Han *et. al.*, 2014). The complexes and their ligands were shown to have higher activity against human cervical adenocarcinoma (HeLa) than human breast adenocarcinoma (MCF-7) cells. Ozturk *et. al.*, 2017 conducted an *in vitro* cytotoxic activity against MCF-7 and HeLa adenocarcinoma cells for three novel antimony(III) complexes (SbX$_3$, X = Cl and Br) with N-substituted thioureas; N,N-dimethylthiourea (DMTU) and N,N-diethylthiourea (DETU) of formulae [*fac*-SbCl$_3$(DMTU)$_3$], [*mer*-SbBr$_3$(DMTU)$_3$] and b,c,d-Cl-[SbCl$_3$(DETU)$_2$]. QSAR studies show that the selectivity exhibited by antimony(III) thiourea derivatives against HeLa cells and the corresponding selectivity of antimony(III) dithiocarbamates against MCF-7 cells should be attributed to the ligand type.

1.4   BIOLOGICAL ACTIVITY OF BISMUTH COMPLEXES

Bismuth sulfapyridine was shown to display great potential for both antimicrobial and anticancer treatment (Marzano IM1, 2013). A study done by (Chauhan *et. al.*, 2016) shows that a number of mixed bismuth(III)bis(*O*-alkyldithiocarbonato-*S,S′*) complexes with dialkyldithiocarbamates have been observed to have an anisobidentate mode of coordination between the dithiolato ligands and the central metal atom which leads to monoclinic crystal system. All the synthesized complexes have also exhibited greater antimicrobial activity than standard antibacterial drug chloramphenicol and antifungal drug terbinafine. In a recent study, (Tamilvanan *et. al.*, 2017) had prepared and characterized three bismuth(III) dithiocarbamate complexes namely tris(N-furfuryl-N-propyldithiocarbamato-S,S′)bismuth(III), tris(N-furfuryl-N-butyldithiocarbamato-S,S′)bismuth(III) and tris(N-furfuryl-N-benzyldithiocarbamato-S,S′)bismuth(III). All the compounds were screened against a panel of microbes *viz. Vibrio cholerae*, *Bacillus subtilis*, *Klebsiella pneumoniae*, *Escherichia coli*, *Staphylococcus aureus*, *Aspergillus niger* and *Candida albicans*.It was found that tris(N-furfuryl-N-propyldithiocarbamato-S,S′)bismuth(III) and tris(N-furfuryl-N-benzyldithiocarbamato-S,S′)bismuth(III) complex have better activity against *K. pneumoniae*, *V. cholerae*, *A. niger* and *C. albicans* and *in vitro* cytotoxic activity against KB cells as compared to tris(N-furfuryl-N-butyldithiocarbamato-S,S′)bismuth(III).

Ozturk *et. al.*, 2014 had synthesized and characterized bismuth(III) complexes of formulae $[Bi(Et_2DTC)_3]_2$ and $[BiCl(Me_2DTC)_2]_n$ (Et_2DTCH = diethyldithiocarbamate, $C_5H_{11}NS_2$, Me_2DTCH = dimethyldithiocarbamate, $C_3H_7NS_2$). The study revealed that $[Bi(Et_2DTC)_3]_2$ complex is active against HeLa cells while $[BiCl(Me_2DTC)_2]_n$ is active against MCF-7. *In vitro* biological studies were done by (Ferreira *et. al.*, 2016) on $[Bi(2AcpNO_2Ph)Cl_2]$ (-*para*-nitro-phenyl (H2Ac*p*NO_2Ph)) complex which shows that

led to 99% decrease in the clonogenic survival. The IC_{50} values of these compounds were three-fold smaller when cells were cultured in soft-agar (3D) than when cells were cultured in monolayer (2D), suggesting further studies aiming to develop new drug candidates for the treatment of colon cancer. Novel bismuth(III) complex derived from pentadentate 2,6-pyridinedicarboxaldehyde bis (^4N-methylthiosemicarbazone), $[BiL(NO_3)_2]NO_3\{L = $ 2,6-pyridinedicarboxaldehyde bis(^{4}N-methylthiosemicarbazone)$\}$ prepared by (Ouyang *et.al.*, 2017) indicates that the complex greatly suppressed colony formation, migration and significantly induced apoptosis of human lung cancer cells A549 and H460 and showed much higher anticancer activities than its parent ligands. The results were supported by *in vivo* study that the treatment with $[BiL(NO_3)_2]NO_3$ complex effectively inhibited A549 xenograft tumor growth in tumor-bearing mice and did not indicate the harmful effect on mouse weight and liver, leading to an interesting and potent strategy in the discovery of new anticancer drug candidates.

In view of the above prospective, it is of interest to further inspect on the characteristics and biological application of antimony and bismuth complexes with *N, N'*-diethyl dithiocarbamate, pyrrolidine dithiocarbamate, *N*-Isopropyl-*N*-hydroxyethyl dithiocarbamate, *N, N'*-diethanol dithiocarbamate, *N*-ethanol-*N*-methyl dithiocarbamate and *N, N'*-dibutyl dithiocarbamate ligands.

Moreover, the synthesis methods for the twelve complexes above had been reported using rigorous methods that involve multiple steps reaction, under high or low temperature, the use of reflux and harsh solvent system/condition. For example, (Qu *et.al.*, 1996) has synthesized antimony(III) diethyldithiocarbamate through the reflux of Sb_2O_3 with CS_2 and diethylamine. Heating was required in this process as to remove the unreacted. (Hongyu *et. al.* 2007) on the contrary had synthesized bismuth(III) diethyl and pyrrolidine dithiocarbamate that uses rotary evaporator instead of slow and natural recrytallisation process. (Han-Dong *et. al.*, 2008) had synthesized antimony(III) diethyl

and diethanol dithiocarbamate by stirring for 5 hours and uses tetrahydrofuran as the solvent system. (Jamaluddin *et. al.*, 2015) on the other hand had synthesized antimony(III) and bismuth(III) methylethanol dithocarbamate by stirring for 5 hours and had required washing process through cold solvent. Therefore, it is also of interest in to find a more subtle reaction to synthesized the complexes.

The biological appraisals were done against both healthy and cancer cells through cell death measurement. Cell death can be divided into necrosis and apoptosis. Necrosis involves rupturing of the cell membranes and releasing the cell content. Apoptosis refers to programmed cell death whereby the cell breaks into apoptotic bodies that in turn will be engulfed by the phagocyte. Dead cells released during necrosis may migrate to other sites and potentially promotes undesirable spread to healthy cells. As a consequence, apoptosis is the preferred pathway for cell death. The delineation of the cell death mode is crucial in this dissertation.

1.5   AIM OF STUDY

On the basis of the research, the purposes of this study are to:

- Successfully synthesize the dithiocarbamate ligands and their metal complexes of antimony and bismuth by using a different, more subtle reaction conditions.

- Perform complete characterisation of the metal complexes to affirm their structure and its chemical nature e.g. the existence of polymorphism; Different crystal system for a compound could be achieved by fine-tuning the parameters for crystal growing. For instance, changing the solvent system for slow evaporation and/or controlling the working temperature during crystallisation process. This gives rise

to a number of morphisms: polymorphism, solvomorphism (pseudo-polymorph) and supramolecular isomerism. Polymorphism refers to multiple crystal systems for a molecule. 13

- Execute a biological appraisal to inspect these biological activity properties. Potential complex that displays positive results, will then go through in-depth experiments, in quest to understand its possible mechanism and effects that gave rise to the bioactivity

CHAPTER 2 : METHODOLOGY

2.1   MATERIALS AND REAGENTS

The ligands and complexes in this dissertation were synthesized by using the following materials and reagents:

Diethyl dithiocarbamate (purchased from Sigma-Aldrich), ammonium pyrrolidine dithiocarbamate (purchased from Sigma-Adrich), 2-(Isopropylamino)ethanol (purchased from Sigma-Aldrich), acetone (purchased from Merck), carbon disulphide (purchased from Merck), sodium hydroxide (purchased from Merck), diethanolamine (purchased from Sigma-Aldrich), potassium hydroxide (purchased from Riendemann Schmidt), 2-(methylamino)ethanol (acquired from Sigma-Aldrich), diethyl ether (bought from Merck), dibutylamine (acquired from Sigma-Aldrich), chloroform (purchased from Merck), acetonitrile (purchased from Merck), antimony(III)chloride (purchased from R&M Chemicals), bismuth(III) chloride (purchased from R&M Chemicals), Chloroform-D (purchased from Merck), DMSO-D (purchased from Merck) and DMF-D (purchased from Merck).

2.2   INSTRUMENT AND MEASUREMENT PARAMETERS

After synthesizing the complexes, ten characterisation methods were done to verify the twelve complexes. This includes the ^{1}H-NMR, ^{13}C-NMR, FTIR, CHN, TGA, DSC, PXRD, SCXRD, UV-Visible and Fluorescence studies. It is of vital to confirm the complexes synthesized based on the characterisation results prior to any biological appraisals work.The following are the instruments used together with its measurement parameters:

FT-NMR LAMBDA 400 MHz and FT-NMR ECA 400 (JEOL); for both ^{1}H-NMR and ^{13}C-NMR experiments, an average of 8 scans, at 22 Hz spins and a frequency of 400 MHz were used throughout the experiments. This is to obtain an optimum average signal reading. **Perkin Elmer Spectrum 400 FT-IR/FT-FIR Spectrometer**; the data was collected by passing through the samples through at the mid-infrared section (wavelength between 2.5-25 μm), **Perkin Elmer 2400 Series II CHNS/O Elemental Analyzer**; the samples were heated up to 900 °C, **Perkin Elmer TGA 4000 Thermogravimetric Analyzer**; the samples were heated up to 900 °C at a scan rate of 10 °C or 20 °C depending on the samples, **DSC Q 20**; the samples were heated up to their melting point at a scan rate of 10 °C or 20 °C depending on the samples, **PANalytical EMPYREAN Multi-Function XRD**, the data were obtained by using the following parameters: Slit size = 0.4785° ; Time per step = 73.5s, step size = 0.026 [°2Th], **Cary-60 UV-Visible Spectrophotometer;** The results was obtained by using chloroform or DMSO as the solvent, at the concentration of 1.0×10^{-5} or 1.0×10^{-7} depending on the compound and **Cary Eclipse Fluorescence Spectrophotometer;** The compounds were dissolved in chloroform or DMSO and scan was run through based on the compound's absorption wavelength.

2.3 EXPERIMENTAL

2.3.1 SYNTHESIS OF LIGANDS
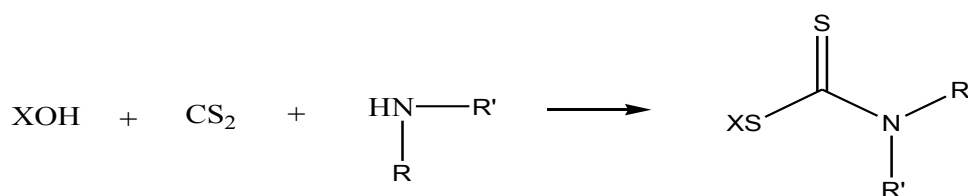
X: Na, K   R: Et, Me, Bu, iPr, EtOH, Pyrrole

R': Et, EtOH, Bu

Figure 2.3.1A: General reaction of amine with carbon disulfide and base

A total of six DTC ligands are used in the study: diethyl DTC (**1**), ammonium pyrrolidine DTC (**2**),isopropylethanol DTC (**3**), diethanol DTC (**4**), methylethanol DTC (**5**) and dibutyl DTC (**6**). Ligands **1** and **2**were purchased from Sigma-Aldrich while ligands **3-6** were being synthesized. Carbon disulphide was added to the solution followed by its respective amine and base under low temperature (1-5 °C). The reaction was stirred for 1-2 hours. The precipitate obtained were collected and was left to air-dry overnight.
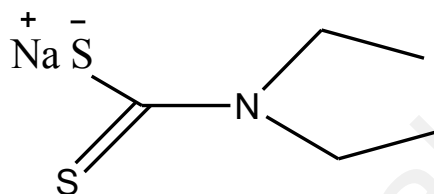
Figure 2.3.1B: Structure of diethyl DTC ligand, Na[$S_2CN(CH_2CH_3)_2$], **1**
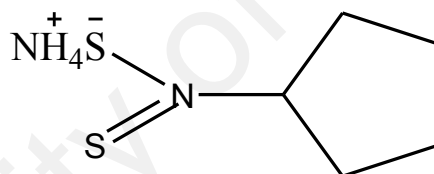
Figure 2.3.1C: Structure of ammonium pyrrolidine DTC ligand, NH$_4$[$S_2CN(CH_2)_4$], **2**

Throughout the experiments, it was noted that for ligands **5** and **6**, precipitation did not occur upon reaction. These DTC ligands will not be synthesized prior to complexation; instead, they were generated through in-situ reaction with the metal salt.

2.3.1.1 SYNTHESIS OF ISOPROPYL DITHIOCARBAMATE, NaS$_2$CN(IPR)(CH$_2$CH$_2$OH)], **3**
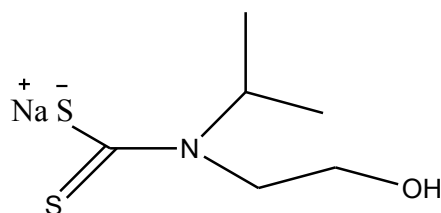
Figure 2.3.1.1: Structure of isopropylethanol DTC ligand, **3**

2-(Isopropylamino)ethanol (0.05 mol, 5.8 mL) in acetone (52.0 mL), was reacted with carbon disulphide (0.05mol, 3.0 mL) and sodium hydroxide, NaOH (50% concentration). The reaction was carried out in an ice bath for about 1-2 hours. The white precipitate formed were filtered out and washed with 5 mL of water. It was then left for overnight to air dry. Mass of the product obtained is 7.47 g.

2.3.1.2 SYNTHESIS OF DIETHANOL DITHIOCARBAMATE, $K[S_2CN(CH_2CH_2OH)_2]$, 4
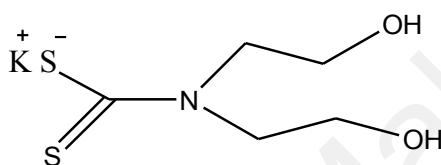
Figure 2.3.1.2: Structure of diethanoldithiocarbamate ligand, **4**

Ligand **4** was synthesized by using diethanolamine (0.06 mol, 4.8 mL) and carbon disulfide (0.06 mol, 3.0 mL) with potassium hydroxide as the base (0.06 mol) under low temperature (0-5 °C). After stirring for about an hour, the white-yellowish precipitate formed were collected before rinsing with water several times. The precipitate were then left dry overnight. Mass of the product obtained is 4.87 g.

2.3.1.3 SYNTHESIS OF METHYLETHANOL DITHIOCARBAMATE, $K[S_2CN(CH_3)(CH_2CH_2OH)]$, 5
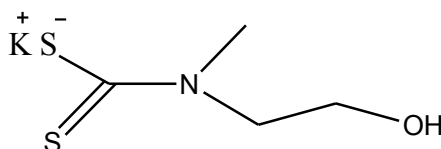
Figure 2.2.3: Structure of methylethanol DTC ligand, **5**

Ligand **5** was synthesised prior to reaction with metal chloride, by using 2-(methylamino)ethanol (0.01 mol, 0.8 mL), potassium hydroxide (concentration of 50%) and carbon disulphide (0.01 mol, 0.7 mL) in diethyl ether (1.0 mL). The reaction proceeded through stirring in an ice bath for about 1-2 hours.

2.3.1.4 SYNTHESIS OF DIBUTYL DITHIOCARBAMATE, $Na[S_2CN(CH_2CH_2CH_2CH_3)_2]$, **6**

Figure 2.3.1.4: Structure of dibutyl DTC ligand, **6**

Ligand **6** was also synthesised prior to the complexation reaction. Dibutylamine (0.05 mol, 8.4 mL) was reacted with sodium hydroxide (50% concentration) and carbon disulphide (0.05 mol, 3.0 mL) in acetone (31.0 mL). The reaction was carried out for about 1-2 hours while stirring in an ice bath.

2.3.2 SYNTHESIS OF ANTIMONY AND BISMUTH COMPLEXES

X: Na, K   M: Bi, Sb   R: Et, Me, Bu, iPr, EtOH, Pyrrole

R': Et, EtOH, Bu

Figure 2.3.2: General overview of the reaction of metal with ligands

The methods for metal complexation are also *via* a straightforward reaction. DTC in distilled water was added to the mixture/suspension of metal chloride in methanol. The reaction was stirred for about 2-3 hrs. The precipitate formed will then be filtered out through gravitational filtration. Simple recrytallisation method was administered if necessary.

2.3.2.1   ANTIMONY DIETHYL DITHIOCARBAMATE, **7**
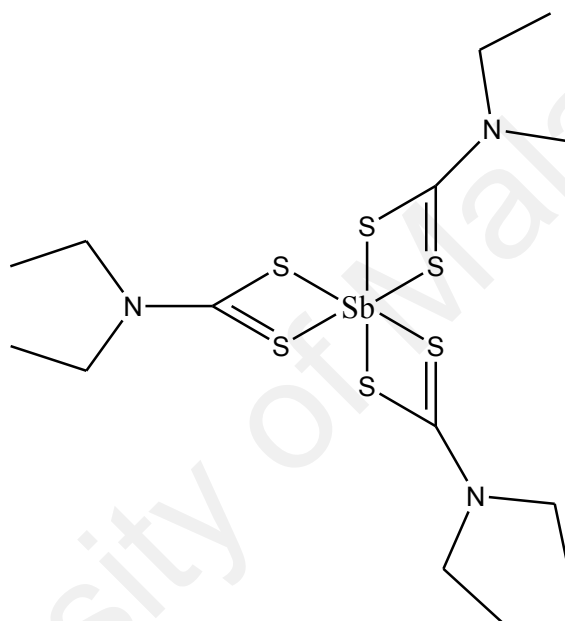
Figure 2.3.2.1: Tris(N,N'-diethyldithiocarbamato)antimony(III), **7**

Ligand **1** (10.00 mmol, 2.25g) dissolved in distilled water (37.5 mL), was added slowly to a suspension of antimony(III)chloride (3.39mmol, 0.77 g) in ethanol (25 mL). After two hours of stirring, bright-yellow precipitate was obtained. The crude yellow precipitate was then recrystallised by using acetonitrile:chloroform mixture (1:3), resulting in bright-yellow crystalline material, after it was left overnight. Mass of the product obtained was 1.79 g. Complex**7** has a melting point of 405.2-407.2 K.
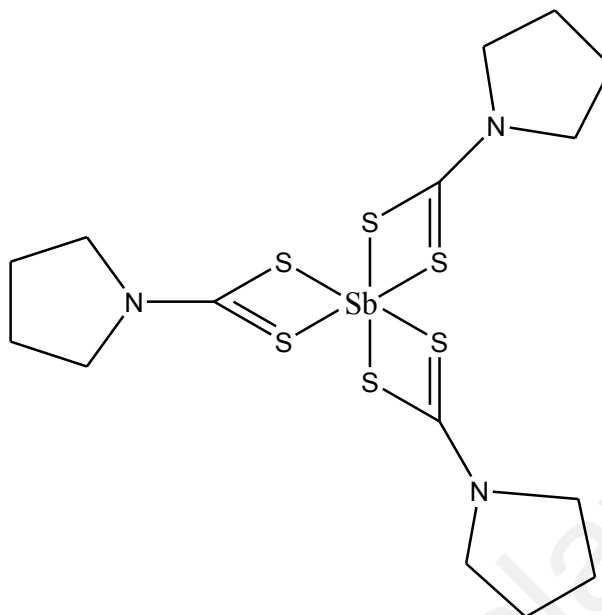
Figure 2.3.2.2: (Pyrrolidinedithiocarbamato)antimony(III), **8**

Ligand **2** (10.00mmol, 1.69g) in 38.0 mL of distilled water was added to the solution of antimony(III)chloride (3.39mmol, 0.83g) in 28.0 mL of ethanol. The reaction mixture was stirred for three hours. The precipitate was filtered and yellow crystals were obtained in the filtrate after two hours. The yellow crystals were then harvested and were left to air dry overnight. Mass of the product obtained was 1.74 g and has a melting point range of 519.7 - 521.1 K.
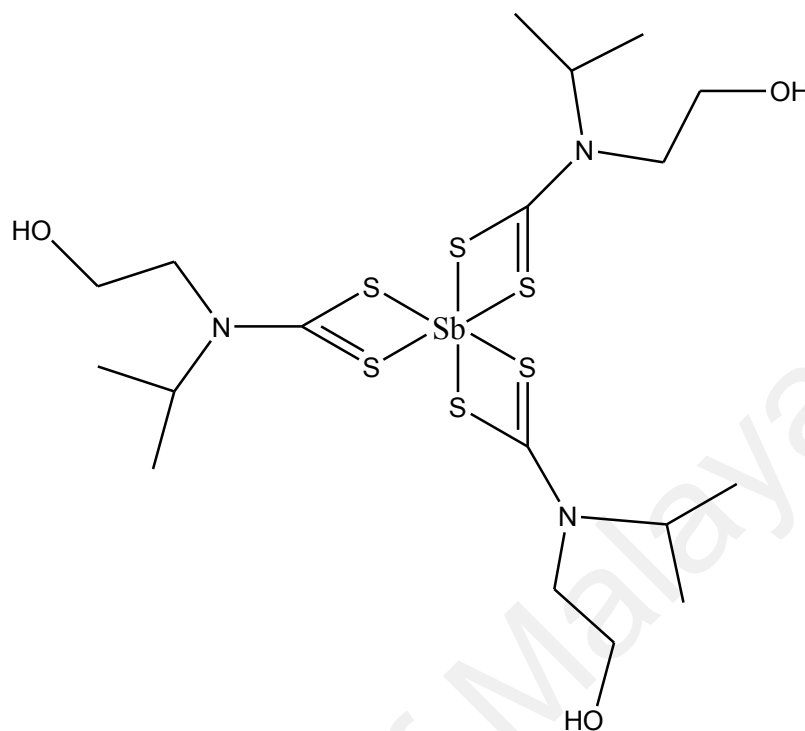
Figure 2.3.2.3: Tris(N, N'-Isopropylethanoldithiocarbamato)antimony(III), **9**

Antimony(III)chloride (3.39mmol, 0.83 g) dissolved in 28.0 mL ethanol was added to a suspension of ligand **3** (10.00mmol, 1.69g) in 25.0mL distilled water. The reaction mixture was stirred for three hours. The yellow precipitate obtained were then recrystallised in acetonitrile:chloroform (3:1) solvent system to yield yellow crystals after three days. Mass of the product obtained was 1.58 g and has a melting point of 412.8 – 414.8 K.
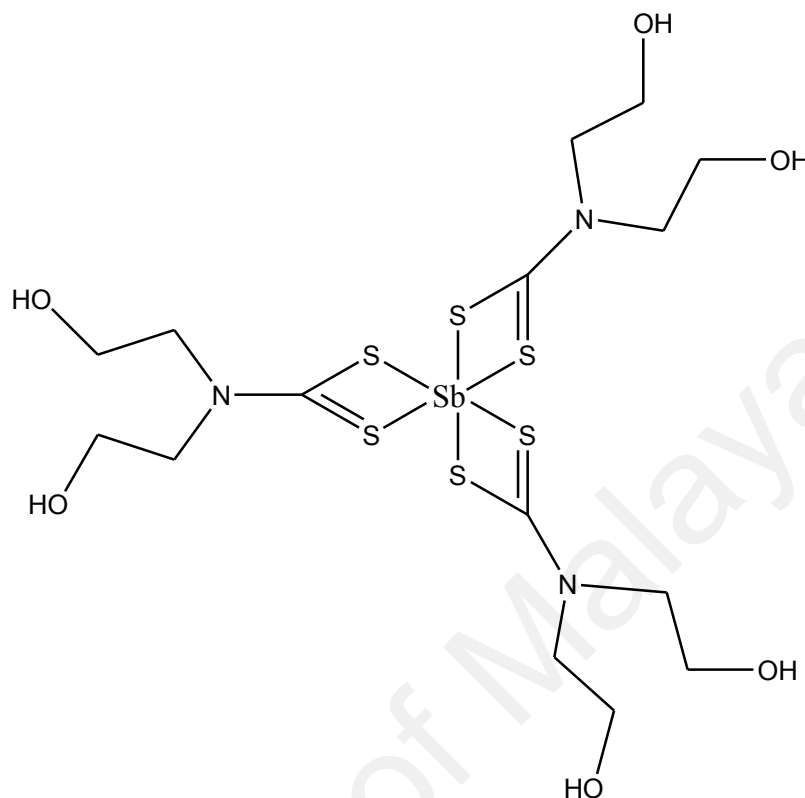
Figure 2.3.2.4: Tris(N, N'-diethanoldithiocarbamato)antimony(III), **10**

Antimony(III)chloride(3.39mmol, 0.87g) in 28.0 mL of ethanol was added to a solution of ligand **4** (10.00mmol, 2.24g) in 38.0 mL of distilled water. The reaction proceeded for three hours. The mixture was then left overnight before pale yellow crystals were obtained. The crystals were then further purified by acetonitrile:chloroform (3:1) solvent system to get pure yellow crystals of complex **10**. Mass of the product obtained was 1.16 g and has a melting point range of 411.3-413.5 K.

2.3.2.5   ANTIMONY METHYLETHANOL DITHIOCARBAMATE, **11**
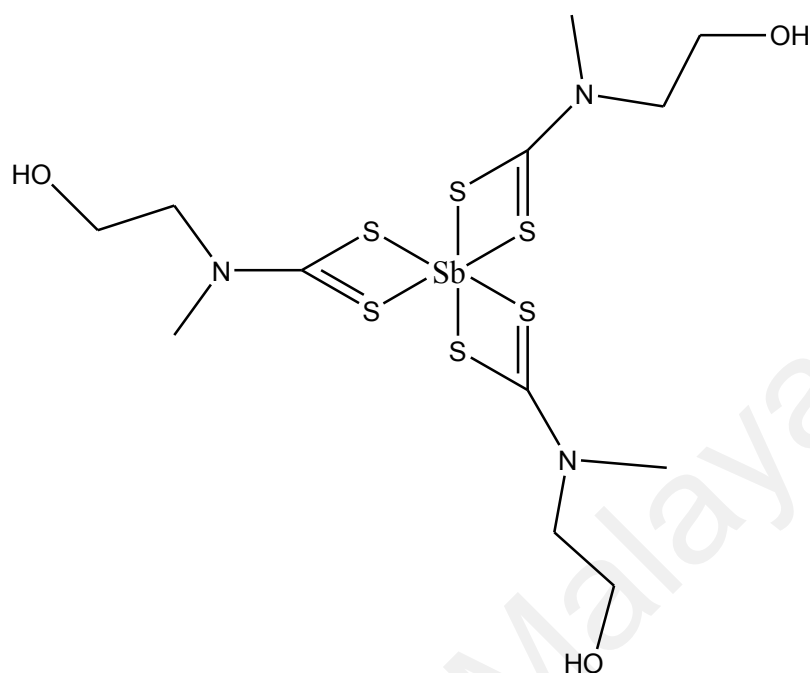
Figure 2.3.2.5: Tris(N, N'-methylethanoldithiocarbamato)antimony(III), **11**

In situ reaction of antimony(III)chloride and ligand **5** was preceded by using 2-(methylamino)ethanol (10mmol, 0.8 mL), KOH (concentration of 50%), CS_2 (0.01 mol, 0.7mL) in diethyl ether (1.0 mL) and antimony(III)chloride (3.39mmol, 0.77g) in 38.0 mL of distilled water. The yellow precipitate was filtered and further purified by using acetonitrile:chloroform (3:1). The solution was then left for a few days before pale yellow crystals were harvested. Mass of the product obtained was 1.21 g and a melting point range of 424.4-425.4 K.
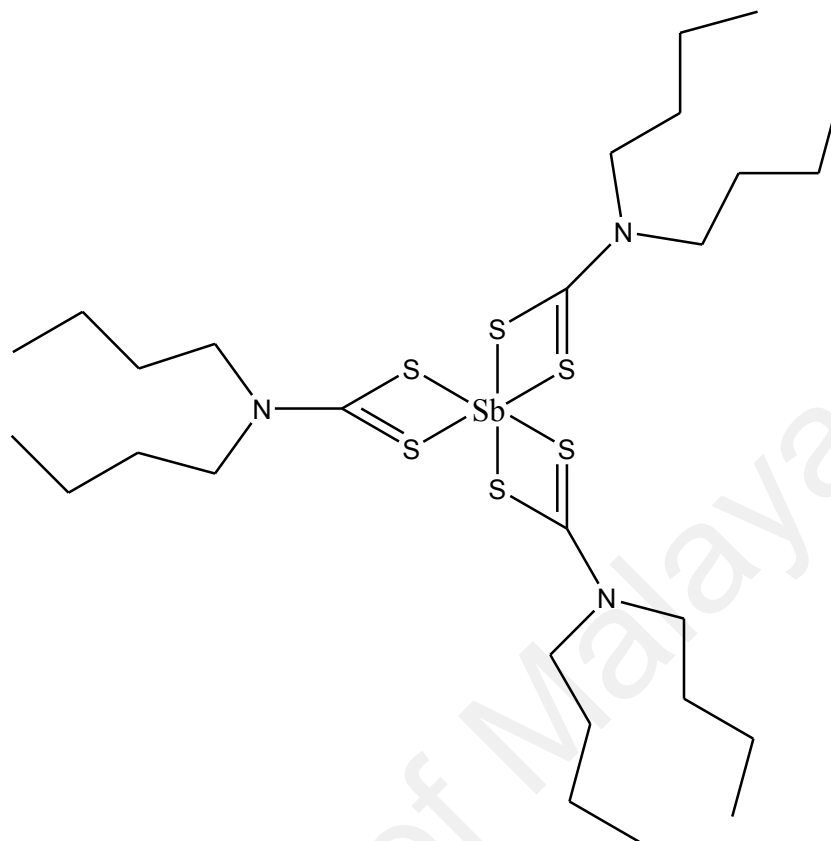
Figure 2.3.2.6: Tris(N, N'-dibutyldithiocarbamato)antimony(III**), 12**

Complex **12** was produced by the in-situ reaction of ligand **6** and metal salt. Ligand **6** was firstly prepared by using dibutylamine (0.05 mol, 8.4 mL), NaOH (50% concentration) and CS_2 (0.05 mol, 3.0 mL). The reaction was stirred in an ice bath for 1-2 hours in acetone (31.0 mL). 2.04g of the ligand was produced consequently antimony(III)chloride (3.39 mmol, 0.77 g) in 38.0 mL of distilled H_2O was added to the reaction. Further purification was done by acetonitrile:chloroform(3:1), after the yellow precipitate was filtered out. Pale yellow crystals were harvested after a few days. Mass of the product obtained was 1.34 g. Complex **12** has a melting point range of 520.3-521.3 K.
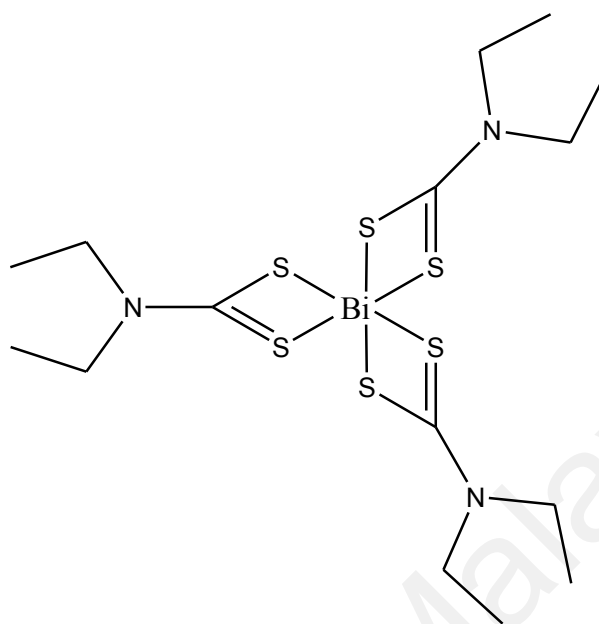
Figure 2.3.2.7: Tris(N, N'-diethyldithiocarbamato)bismuth(III), **13**

Ligand **1** (10.00mmol, 2.25g) dissolved in distilled water (39.0mL), was added slowly to a suspension of bismuth(III)chloride (3.39 mmol, 1.07 g) in ethanol (26.0ml). After two hours of stirring, bright-yellow precipitate were obtained. The crude yellow precipitate were then recrystallised by using acetonitrile:chloroform mixture (1:3), resulting in bright-yellow crystalline material, after it was left overnight. Mass of the product obtained was 2.10 g with a melting point range of 467.8-468.2 K.
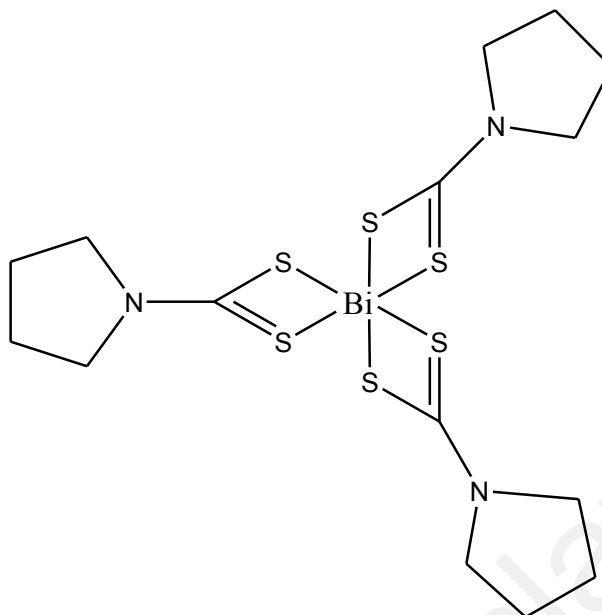
Figure 2.3.2.8: (Pyrrolidinedithiocarbamato)bismuth(III), **14**

Ligand **2** (10.00 mmol, 1.68 g) in 38.0 mL of distilled water, was added to bismuth(III)chloride (3.39 mmol, 1.12 g) in 25.0 mL of ethanol for three hours. The precipitate were filtered and yellow crystals were obtained in the filtrate after overnight. The yellow crystals were then harvested and were left to air dry. Recrystallisation of the complex was *via* acetonitrile:chloroform (3:1). Mass of the product obtained was 2.21 gand has a melting point range of 534.2-265.2 K.
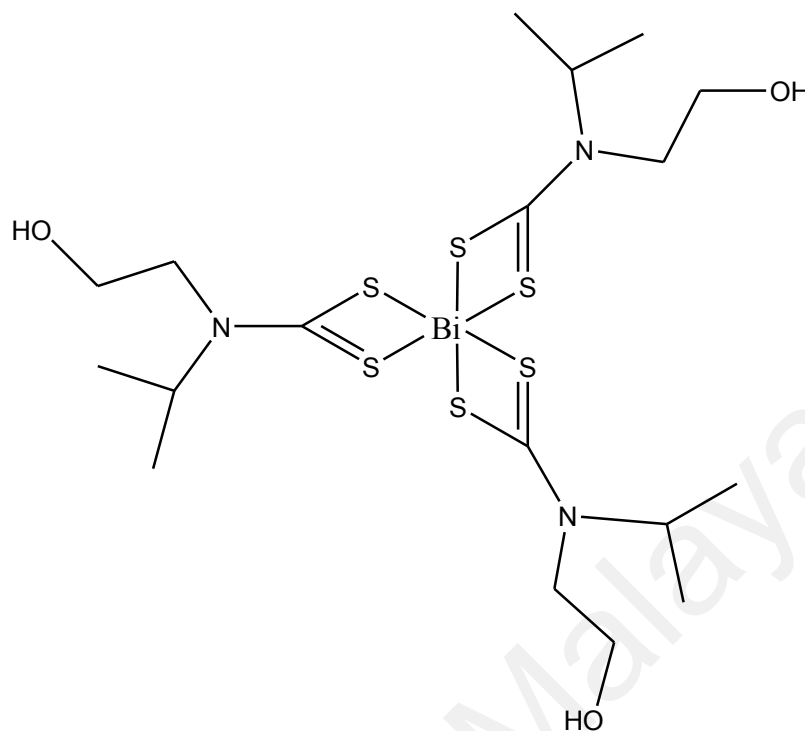
Figure 2.3.2.9: Tris(N, N'-Isopropylethanoldithiocarbamato)bismuth(III), **15**

T

o a suspension of bismuth(III)chloride (3.39mmol, 1.07g) in 28.0 mL of ethanol, ligand **3** (10.00mmol, 2.02g) in 38.0mL of distilled water, was added. The reaction was stirred for three hours. The precipitate formed were filtered out before it was recrystallise in chloroform:acetonitrile (3:1) to get pale yellow powder. Mass of the product obtained was 1.93 g with a melting point range of 436.8-437.0 K.

BISMUTH DIETHANOL DITHIOCARBAMATE, **16**
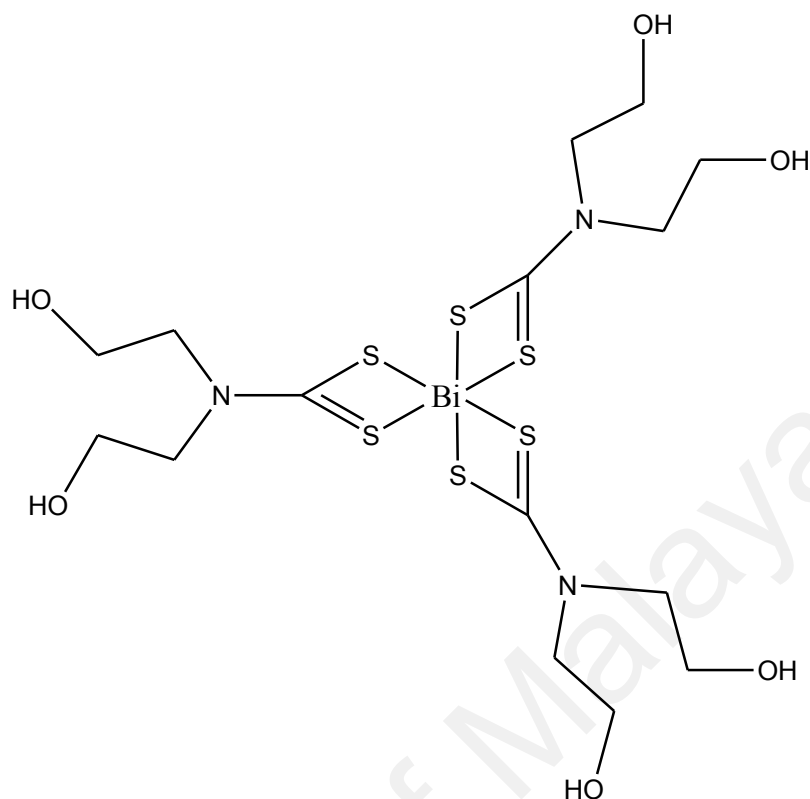
Figure 2.3.2.10: Tris(N, N'-diethanoldithiocarbamato)bismuth(III), **16**

Ligand**4** (10.00mmol, 2.19g) dissolved in distilled water (37.5mL), was added to a suspension of bismuth(III)chloride(3.39mmol, 1.07g) in ethanol (25.0mL). After two hours of stirring, the product was left overnight and pure yellow-brown crystals were formed. Crystals will only formed under room temperature as opposed to low temperature of the fridge.Mass of the product obtained was 1.62 g and Complex**16** has a melting point range of 430.2-431.2 K.
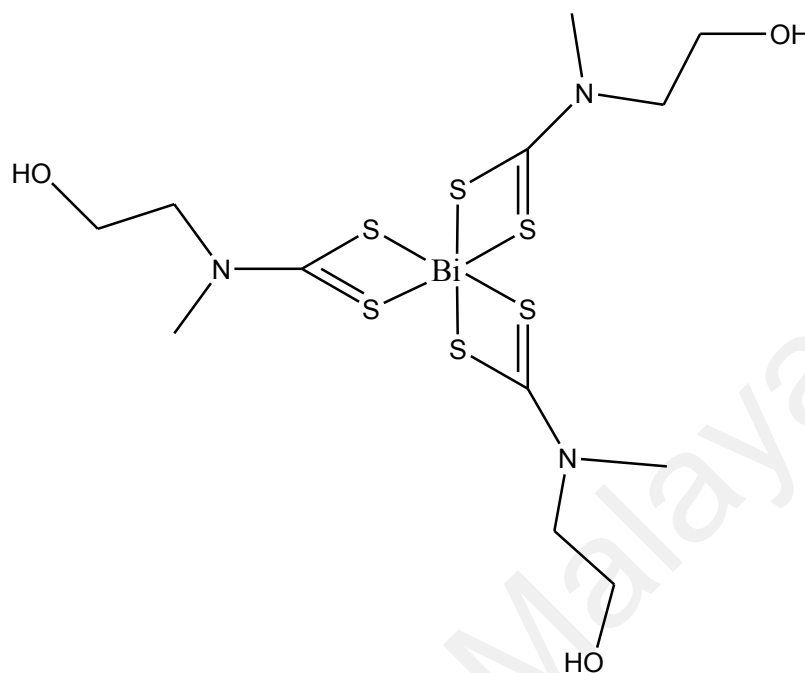
Figure 2.3.2.11: Tris(N, N'-methylethanoldithiocarbamato)bismuth(III), **17**

Ligand **5** was synthesised by using 2-(methylamino)ethanol (10 mmol, 0.8 mL), potassium hydroxide (concentration of 50%) and carbon disulphide (0.01 mol, 0.7 mL) in diethyl ether (1.0 mL). Subsequently, antimony(III)chloride (3.39 mmol, 0.77 g) in 38.0 mL of distilled water was added to the solution of ligand **5**. The yellow precipitate were filtered and further purified by recrystallising with chloroform:acetonitrile (3:1) solvent system. The solution was then left for a few days before yellow-orange crystals were harvested and left to dry. Mass obtained was 1.02 g and has a melting point range of 397.15 K.

2.3.2.12   BISMUTH DIBUTYL DITHIOCARBAMATE, **18**
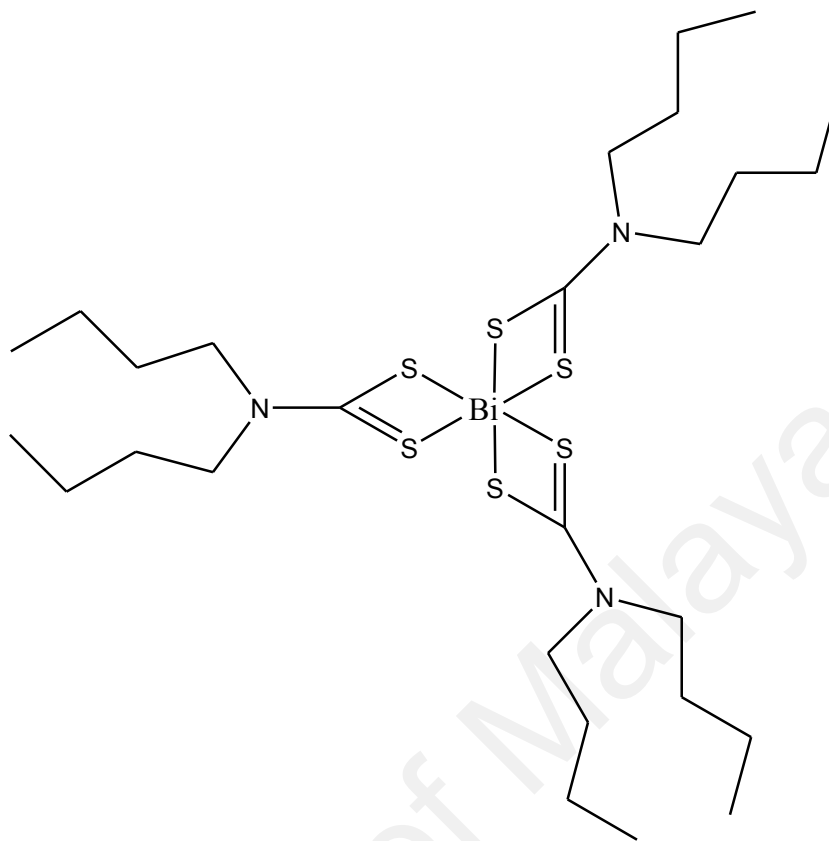
Figure 2.3.2.12: Tris(N, N'-dibutyldithiocarbamato)bismuth(III**)**, **18**

2.04g of ligand **6** was added to a suspension of bismuth(III)chloride (3.39mmol, 1.069g) in 38.0 mL of distilled water. The pale yellow precipitate were collected and further purified by using chloroform:acetonitrile (3:1) as the recrystallisation solvent system. Orange crystals were harvested after a few days. Mass obtained was 1.62 g and has a melting point of 527.15 K.

2.3.3 BIOASSAY EVALUATION

Cell viability assay is an initial measurement to inspect the cytotoxicity and drug potential of a compound. There are many types of cell viability assay methods that can be employed to obtain the desired results. In this dissertation, apart from a cell viability assay, nine additional studies are conducted to inspect the biological activity of compound **13** & compound **16**. The additional assays are membrane permeability study, DNA fragmentation, restriction enzyme inhibition assay, apoptosis and cell cycle analysis, caspase activity, reactive oxygen species (ROS) measurements, flow cytometry analysis, cytochrome c detection and cell invasion assay.

2.3.3.1 CELL VIABILITY ASSAY

Following the experimentation methods given by American Type Culture Collection (ATCC), the seven cancer cell lines for testing (HepG2, MCF-7R, A2780, HT-29, A549 and 8505C) were then incubated in culture. Using standard procedures, the cells were grown in an RPMI 1640 medium (10% foetal calf serum and antibiotics at 37°C) and 6% CO_2. The cells were seeded in 96-well plates (Techno Plastic Products, TPP, Plastik für die Zellkultur, Switzerland) and were let to develop for 24h in complete medium. The stock solutions with concentrations of 10^{-2} M, were prepared by dissolving test compounds (**7-18**) in 1 mL of DMSO. The solutions were then further diluted to obtain a final concentration ranging from 0-80 μM in an RPMI medium before adding it to the wells (100μL). DMSO (present) <1% does not show any effects on cell cytotoxicity. To achieve the required concentrations, the stock solutions were directly diluted to the culture medium, prior to the addition in the cell culture. 20 μL solution of MTT (3-[4,5-dimethylthiazole-2-yl]-2,5-diphenyltetrazolium bromide) in

PBS (phosphate buffer saline, 2 mg mL^{-1}) was added to each well after incubation at 37°C for 24h. The plates were then enclosed in the well at 37°C for 2h. The medium was then withdrawn and DMSO (100μL) was added to dissolve the precipitate. Using 96-well microplate reader, the absorbance of each well was measured at 580nm and the values obtained were compared to the figures obtained for the control cells that were incubated without a test compound. By fitting the plot of the percentage of surviving cells against the drug concentration using a sigmoidal function (Origin v7.5^{TM}), the IC$_{50}$ values for the inhibition of cell growth were determined.

2.3.3.2   MEMBRANE PERMEABILITY STUDY

Based on the results of cell viability experiments, the chosen cancer cell line were treated with the IC$_{50}$ concentration of each compound at a concentration of 5×10^3 cells/well in 96 well plates and enclosed in it for 24 h. Untreated cells were included as a negative control. From the culture flask, the treated cells were harvested and washed twice with 1X EDTA free-PBS before transferring to a microcentrifuge tube. At 1000 g, the cells were centrifuged for 10 min. Next, the cells were suspended in 100 μL 1X PBS. Subsequently, a 5 mg/mL mixture of acridine orange (AO) (Sigma) and propidium iodide (PI) (Sigma) was added to the cells in a 1:1 ratio for staining followed by chilling on ice for 10 min. On a slide, the mixture (20 μL) was introduced fractionally and the slide was then covered with a cover slip. The slide was then viewed under a fluorescence microscope (Olympus BX-51). An Olympus CMAD-2 camera was attached to the fluorescence microscope and the images were captured. The manner of cell death was then determined.

2.3.3.3   DNA FRAGMENTATION

For a DNA fragmentation, in an RPMI medium, 2×10^6 of the chosen cancer cells were treated with the IC_{50} concentration of the compounds at 37°C and 5% CO_2 for 24 h. The cells were then collected and centrifuged at 300 x g/15 min/10 ºC prior to washing with PBS. At a concentration of 1×10^6 cells mL^{-1} in an extraction buffer (10 mmol L^{-1} TriseHCl, 0.1 mol L^{-1} EDTA, 5 g mL^{-1} SDS), the cells were then re-suspended and treated with RNase A (20 mg L^{-1}, at 37°C for 60 min) followed by addition of proteinase K (100 mg L^{-1}, also at 37 ºC for 60 min). An equal volume of saline solution (NaCl 6 M) was added to the cells, prior to centrifuging for 10 min of 13,000 x g. Two equivalent volumes of ethanol (20 °C) were added to the collected supernatant. At 4 °C, the samples were centrifuged for 30 min at 13,000 x g. The pellets were collected by removing the supernatant. Next, the pellets were dissolved in TE buffer (1 x). Using a BioPhotometer Spectrophotometer UV/VIS (Eppendorf, Germany) and electrophoresis, the DNA concentration and quality were analysed. Consequently, electrophoresis of the samples applied to a 1.5% agarose gel with running buffer of TAE was carried out at 80 V for 2 h. Under UV light using a Syngene Bio Imaging system, the gel was stained, destained and photographed. The Gene Flash software™ was used to view the digital image.

2.3.3.4   RESTRICTION ENZYME INHIBITION ASSAY

The determination of the restriction enzyme inhibitory activity was determined by observing the resultant band of lambda (λ). The reaction mixture was prepared for each trial contained 0.25 μg of λ DNA, 2 μl of 10x restriction enzyme reaction buffer, 50 μM of tested compound and five units of restriction enzyme. Sterile deionized water

was added as well, making the total volume of the initial reaction to be 20 μL. Prior to the addition of the restriction enzyme, λ DNA was incubated at 37°C for 60 min with the test compound. At the same temperature, the reaction mixture was further incubated for 2h. 2 μl of 10 % SDS, 3 μl of dye solution comprising 0.02 % bromophenol blue and 50 % glycerol were added to terminate the reaction. The function of SDS in this experiment is to prevent further enzymatic activity by denaturating the restriction enzyme. The reaction mixture was added to a 2.0 % agarose gel, followed by electrophoresis for 2 h at 80 V with a running buffer of TAE. Again, the gel was stained, destained and photographed using Syngene Bio Imaging system. The digital image was viewed by using the Gene Flash software™.

2.3.3.5 EXTRACTION OF RNA AND RT^2 PROFILER PCR MICROARRAY (APOPTOSIS AND CELL CYCLE ANALYSIS)

At a density of 3 x 10^6 cells per T-75 cm^2 per flask, the chosen cancer cells were plated. Using a high-purity RNeasy Mini Kit (Qiagen, USA), according to the producer's protocols, total RNA samples were extracted from cultivated chosen cancer cells. The concentrations and quality of the total RNA samples dissolved in diethylpyrocarbonate-treated water were analysed by using electrophoresis and UV/visible (UV-vis) spectroscopy (BioPhotometer Spectrophotometer UV/VIS by Eppendorf, Germany).

Following the guidelines set by the manufacturer (Qiagen, Germany), a RT^2 Profiler PCR microarray (Apoptosis (PHAS-012) was used to measure the real-time PCR microarray analysis whilst (PHAS-020) was used for cell cycle analysis. The expressions of 84 key genes involved in programmed cell death were profiled by the human apoptosis RT^2 Profiler PCR microarray. Genes that have positive or negative

effects on cell cycle, the transitions between each of the phases, DNA replication, checkpoints and arrest were contained in this array. The CT values obtained from the results were used to compare the gene expression on each test.

2.3.3.6   CASPASE ACTIVITY (CASPASES 3, 7, 8, 9 AND 10)

The caspase activities were evaluated by measuring the light intensity using a kit (Caspase Assay, Milipore) and a luminometer (Perkin Elmer HTS 7000, France). In short, in 96-well plates with the final volume of 200 mL, the cells were cultured. Prior to the measurement at 37 °C, 50 mL of caspase reaction buffer was added to the plates and then incubated for 1 h at room temperature.

2.3.3.7   INTRACELLULAR REACTIVE OXYGEN SPECIES (ROS) MEASUREMENTS

Intracellular ROS, 5-(and-6)-Carboxy-2' was detected by using 7'-dichlorodihydrofluorescein diacetate (carboxy-H2DCFDA) (Sigma, USA). The cells were seeded in 96-well plates (Greiner Bio-One, France) and treated with the test compound for 24 h at the corresponding IC_{50} concentrations. The cells were then washed with PBS and kept for 1 h in a mixture of 10 μM carboxy H2DCFDA and DPBS. Fluorescence was measured at an excitation wavelength of 485 nm and emission wavelength of 535 nm using a plate reader (Perkin Elmer, France), after the cells were washed.

2.3.3.8 FLOW CYTOMETRY ANALYSIS (FLUORESCENCE-ACTIVATED CELL-SORTING)

At 1 x 10^6 cells per T-75 cm^2 flask the chosen cancer cell lines were plated. The IC$_{50}$ concentration of the test compounds in DMSO were embedded in the cells for treatment. A control experiment was carried out by applying only DMSO in the medium of the chosen cancer cell lines. At interval of 6 h, 12 h and 24 h, the treated cells were collected, harvested in 70% ethanol and kept at 20 °C. Ice-cold PBS was used to wash the cells prior to incubation with RNase and PI (a DNA intercatalyting dye). Using a Becton Dickinson Facstar flow cytometer, the cell-cycle analysis phase was performed. The Becton Dickinson™ cell-fit software was operated to corroborate the data.

2.3.3.9 CYTOCHROME C DETECTION

At 1 x 10^6 cells per T-75 cm^2 flask the chosen cancer cell lines were plated. The IC$_{50}$ concentration in 1% DMSO of the test compounds were embedded in the cells for treatment while a control experiment was carried out by incorporating 1% DMSO only in the medium. According to the manufacturer's protocol, Cytochrome c activity was analysed through FlowCellect™ Cytochrome C Kit (Millipore, Germany).

2.3.3.10 CELL INVASION ASSAY

BioCoat™ Matrigel™ Invasion Chamber (BD Biosciences, San Jose, CA) was used to carry out the cell invasion study. Briefly, to the bottom of the well, 0.75 mL of the complete medium was added. Simultaneously, with or without the IC$_{50}$ value of the compound for testing, 5 x 10^4 cells were placed back into the suspension in 0.5 mL of the complete medium and then were added to the insert of the well. All inserts achieved

a final concentration of 0.01% DMSO. For 22 h under 5% CO_2 and at 37 ºC, the cells were then enclosed in the well. The non-invaded cells were removed from the inside of the insert by using cotton tips. Methanol was used to fix the invaded cells for 2 min, stained with 1% of Toluidine Blue O (Sigma-Aldrich) and washed with water. An inverted microscope at 200x magnification was used to observe the membrane. The number of invaded cells was counted by randomly choosing ten fields. Three independent experiments were carried out and the data collected are shown as mean ± SEM.

CHAPTER 3 : RESULTS AND DISCUSSIONS

The twelve antimony and bismuth complexes were successfully synthesized and nine types of characterisation were used to identify the complexes. Although these complexes were known to have been synthesized and characterized in separate studies, this dissertation covers the compilation of all the chemical characterization for the twelve antimony and bismuth complexes, of which, the work has not been done previously. Following are the results and discussions for the characterization of antimony and bismuth complexes.

3.1 CHARACTERIZATION OF ANTIMONY AND BISMUTH COMPOUNDS

3.1.1 GENERAL SPECTROSCOPIC CHARACTERISATION

Through ^{1}H-NMR, ^{13}C-NMR, CHN, FTIR, UV-Visible and Fluorescence analysis, the spectroscopic characteristics of the complexes were verified.

Following are the results of ^{1}H-NMR and ^{13}C-NMR results for the twelve compounds. The ^{13}C-NMR data were collected by using PENDANT (polarization enhancement nurtured during attached nucleus testing) ^{13}C-NMR NMR method (Gentçen *et. al.*, 2006). PENDANT method was used as the time taken to gather the ^{13}C-NMR data was shorter as compared to its conventional method. Both ^{1}H-NMR and ^{13}C-NMR data were collected by using CDCl$_3$ and DMSO as the solvent (**Table 3.1.1A – 3.1.1F**).

Table 3.1.1A : ^{1}H-NMR and ^{13}C-NMR Peaks for complex **7** and complex **13**
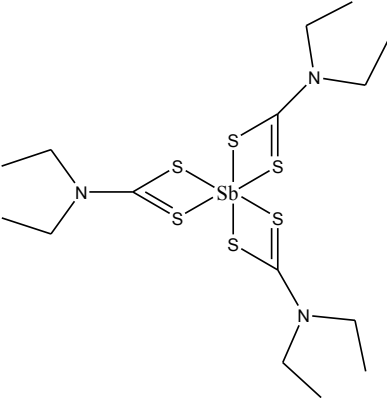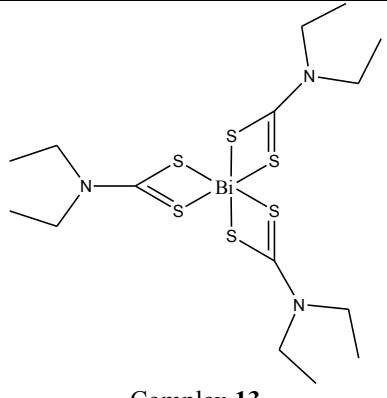
Structure	Chemical formula	^{1}H-NMR Peaks		^{13}C-NMR Peaks (ppm)		
Ligand **1**	$C_5H_{10}NS_2$	CH$_2$C<u>H</u>$_3$	C<u>H</u>$_2$CH$_3$	N<u>C</u>H$_2$CH$_3$	NC<u>H</u>$_2$CH$_3$	N<u>C</u>S$_2$
Complex **7**	[(H$_3$CH$_2$C)$_2$NCS$_2$]$_3$Sb	1.30 ppm, *t*, 6.99Hz	3.87 ppm, *q*, 7.19Hz	12.0	49.0	197.0
Complex **13**	[(H$_3$CH$_2$C)$_2$NCS$_2$]$_3$Bi	1.33 ppm, *t*, 7.07Hz (0 hours) 1.23 ppm, *t*, 7.07Hz (24 hours) 1.23 ppm, *t*, 7.07Hz (36 hours)	3.82 ppm, *q*, 7.15Hz (0 hours) 3.57 ppm, *t*, 7.07Hz (24 hours) 3.75 ppm, *t*, 7.07Hz (36 hours)	12.0	48.5	202.0

Table 3.1.1B : ^{1}H-NMR and ^{13}C-NMR Peaks for complex **8** and complex **14**
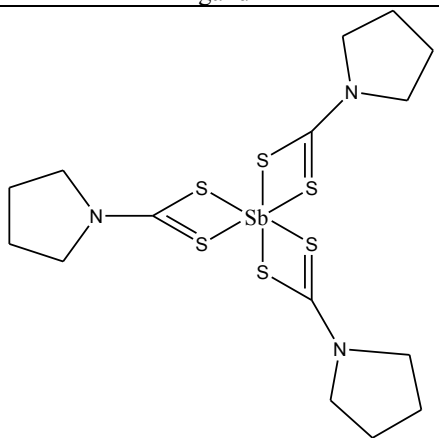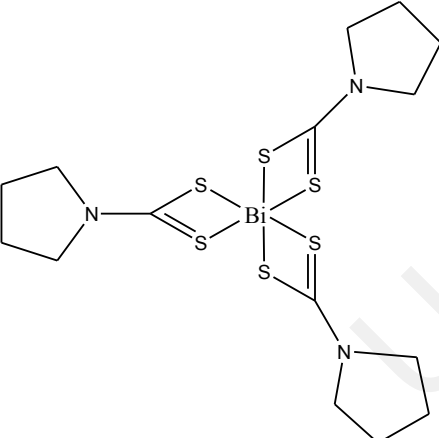
Structure	Chemical formula	^{1}H-NMRPeaks		^{13}C-NMRPeaks		
Ligand **2**	$C_5H_8NS_2$	$CH_2\underline{C}H_2CH_2$,	$N\underline{C}H_2CH_2$	$\underline{C}H_2\underline{C}H_2CH_2$	$N\underline{C}H_2CH_2$	NCS_2
Complex **8**	$[(CH_2)_4NCS_2]_3Sb$	2.03ppm, *tt*, 3.81Hz	3.92ppm, *t*, 2.03Hz	26.0	53.0	195.0
Complex **14**	$[(CH_2)_4NCS_2]_3Bi$	2.03ppm, *tt*, 3.48Hz	3.91ppm, *t*, 2.03Hz	26.0	54.0	199.0

Table 3.1.1C : ^{1}H-NMR and ^{13}C-NMR Peaks for complex **9** and complex **15**
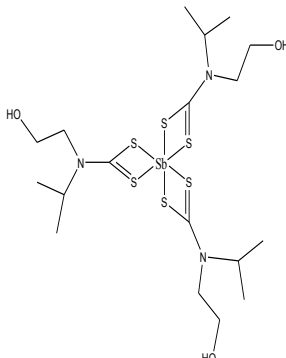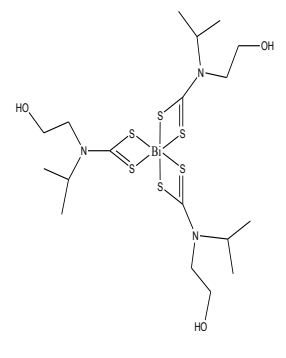
Structure	Chemical formula	^{1}H-NMRPeaks					^{13}C-NMRPeaks				
Ligand **3**	$C_6H_{12}NOS_2$	NCH(C$\underline{H}_3$)$_2$	CH$_2$C$\underline{H}_2$OH	C$\underline{H}_2$CH$_2$OH	CH$_2$O$\underline{H}$	NC$\underline{H}$	NCH($\underline{C}H_3$)$_2$	$\underline{C}$H$_2$CH$_2$OH	CH$_2$$\underline{C}H_2$OH	N$\underline{C}$H	N$\underline{C}$S$_2$
Complex **9**	[(HOCH$_2$CH$_2$)(CH$_3$(CH$_2$)$_2$)NCS$_2$)]$_3$Sb	1.21 ppm, *d*, 6.67 Hz	3.36 ppm, *m*, 6.70 Hz	3.73 ppm, *t*, 6.87 Hz	4.98 ppm, *t*, 5.50 Hz	5.10p pm, *s*, 5.18 Hz	20.2	55.4	58.5	49.7	199.5
Complex **15**	[(HOCH$_2$CH$_2$)(CH$_3$(CH$_2$)$_2$)NCS$_2$)]$_3$Bi	1.24 ppm, *d*, 6.71 Hz	3.36 ppm, *m*, 5.25Hz	3.65 ppm, *t*, 5.18 Hz	4.92 ppm, *t*, 5.20 Hz	5.21 ppm, *s*, 6.67 Hz	20.1	54.9	58.7	49.8	202.5

Table 3.1.1D : ^{1}H-NMR and ^{13}C-NMR Peaks for complex **10** and complex **16**

Structure	Chemical formula	^{1}H-NMRPeaks			^{13}C-NMRPeaks		
Ligand **4**	$C_5H_{10}NO_2S_2$	$CH_2\underline{CH_2}OH$	$\underline{CH_2}CH_2OH$	$O\underline{H}$	$CH_2\underline{CH_2}OH$	$\underline{CH_2}CH_2OH$	NCS_2
 Complex **10**	$[(HOCH_2CH_2)_2NCS_2]_3Sb$	3.68 ppm, *dt*, 5.60 Hz	3.87 ppm, *q*, 7.19Hz	4.98 ppm, *q*, 5.34Hz	40.0	59.0	199.0
 Complex **16**	$[(HOCH_2CH_2)_2NCS_2]_3Bi$	3.72 ppm, *q*, 5.61Hz (0 hours) 3.73 ppm, *q*, 5.69Hz (24 hours) 3.73 ppm, *q*, 5.77Hz (36 hours)	3.88 ppm, *t*, 4.27Hz (0 hours) 3.90 ppm, *t*, 5.85Hz (24 hours) 3.90 ppm, *t*, 5.97Hz (36 hours)	4.95 ppm, *t*, 5.26Hz (0 hours) 4.99 ppm, *t*, 6.21Hz (24 hours) 4.99 ppm, *t*, 5.97Hz (36 hours)	42.0	59.0	203.0

42

Table 3.1.1E : ^{1}H-NMR and ^{13}C-NMR Peaks for complex **11** and complex **17**

Structure	Chemical formula	^{1}H-NMRPeaks				^{13}C-NMRPeaks			
Ligand **5**	C₄H₈NOS₂	CH₂CH₂OH	CH₂CH₂OH	CNCH₃	OH	CH₂CH₂OH	CH₂CH₂OH	CNCH₃	NCS₂
Complex **11**	[(HOCH₂CH₂)(CH₃)NCS₂]₃ Sb	3.38 ppm, *dt*, 5.60Hz	3.91 ppm, *t*, 5.64Hz	5.02 ppm, *t*, 5.34Hz	3.38 ppm, *s*	43.1	58.4	58.9	199.3
Complex **17**	[(HOCH₂CH₂)(CH₃)NCS₂]₃ Bi	3.70 ppm, *dt*, 5.64Hz	3.84 ppm, *t*, 5.79Hz	4.93 ppm, *t*, 5.34Hz	3.70 ppm, *s*	43.2	58.4	59.0	202.4

43

Structure	Chemical formula	^{1}H-NMRPeaks				^{13}C-NMRPeaks				
Ligand **6**	C$_9$H$_{18}$NS$_2$	CH$_2$C$\underline{H}_3$	CH$_2$C$\underline{H}_2$CH$_3$	CH$_2$C$\underline{H}_2$CH$_2$	NC$\underline{H}_2$CH$_2$	CH$_2$$\underline{C}H_3$	CH$_2$$\underline{C}H_2CH_3$	CH$_2$$\underline{C}H_2CH_2$	N$\underline{C}$H$_2$CH$_2$	N$\underline{C}$S$_2$
Complex **12**	[(H$_3$CH$_2$CH$_2$CH$_2$C)(CH$_3$)NCS$_2$]$_3$ Sb	0.94 ppm, *t*, 7.31Hz	1.35 ppm, *sex*, 6.21Hz	1.72 ppm, *quin*, 6.15Hz	3.78 ppm, *t*, 5.28Hz	13.9	20.2	29.1	54.0	199.0
Complex **18**	[(H$_3$CH$_2$CH$_2$CH$_2$C)(CH$_3$)NCS$_2$]$_3$Bi	0.94 ppm, *t*, 7.31Hz	1.35 ppm, *sex*, 6.22Hz	1.75 ppm, *quin*, 6.39Hz	3.73 ppm, *t*, 7.91Hz	13.9	20.3	29.1	54.1	199.0
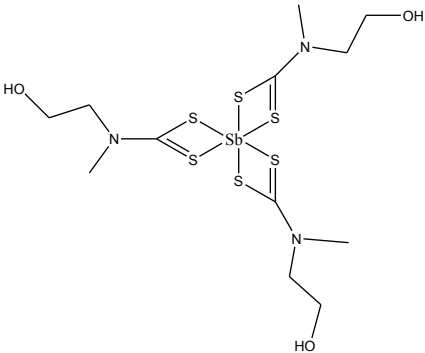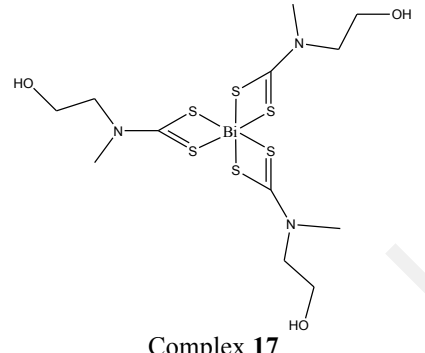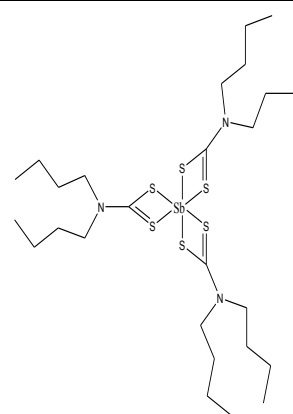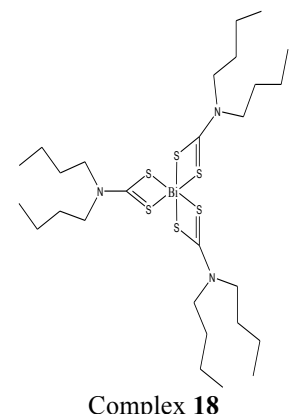
Based on the shift range of ^{1}H-NMR, all the twelve complexes display similar results within its series, confirming its composition. As reported by (Li, 2007), complex **13** showed a promising anti-tumour activity. Complex **13** is therefore selected as one of the first complex in the series to undergo further biological evaluation in this study. ^{1}H-NMR data for complex **13** was collected in the span of 0, 24 and 36 hours. This is to inspect the stability of the complex over time when it is being incorporated in the biological system. ^{1}H-NMR data at 0 hours was collected by using CDCl$_3$asthe solvent and DMSO-d6 solvent is being used to collect the data at 24 and 36 hours as it mimicked the solubility of the complex in an aqueous environment of the biological system.On the other hand, the presence of the hydroxyl group increases the solubility of complex **16**, hence its anti-tumour activity is worth to be looked into. Like complex **13**, ^{1}H-NMR data for complex **16** were collected in the span of 0, 24 and 36 hours under the same conditions. Both complex **13** and **16** showed similar shift range up until 36 hours, hence confirming the stability its structure. The ^{13}C-NMR results on the other hand showed that the shift range of all the twelve complexes display similar results within its series, confirming thus, confirming the structure of the complex.

The functional groups in the complexes were analysed through FTIR. **Table 3.1.1G** summarizes the FTIR results for all the twelve complexes:

Table 3.1.1G: FTIR results for complexes **7** - **18**

Complexes	Frequency, v				
	C-S		C-N	C-O	OH
7	981.3	1074.0	1462.9	-	-
8	942.7	1035.0	1432.7	-	-
9	960.3	1045.7	1448.4	1241.1	3175.7
10	976.2	1060.1	1465.7	1216.8	3271.7
11	978.6	1063.2	1435.5	1246.7	3386.3
12	953.4	1093.6	1479.7	-	-
13	979.0	1065.0	1489.4	-	-
14	939.9	1040.6	1432.2	-	-
15	974.2	1036.7	1445.3	1239.0	3328.8
16	969.7	1039.4	1471.9	1204.9	3251.5

| 17 | 943.2 | 1056.2 | 1432.6 | 1255.2 | 3167.0 |
| 18 | 952.5 | 1093.6 | 1478.8 | - | - |

Generally, the FTIR results can be summarized as follow: C-S functional group was displayed as strong peaks at 939.9-981.3v and 1035.0-1093.6v, C-N functional as a weak/medium peak at 1432.2-1489.41v, (if present) C-O functional as a strong peak at 1204.9-1255.2v and (if present) OH functional as a medium broad peak at 3167.0-3386.3v. By correlating the ^{1}H-NMR and ^{13}C-NMR, the FTIR results strengthened the composition of the complexes.

The CHN data (**Table 3.1.1H**) gives out the percentage of carbon, hydrogen and nitrogen atoms for the complexes.

Table 3.1.1H: CHN results for complexes **7 - 18**

Complex	Found Values (%)			Calculated Values (%)			Difference (±%)		
	C	H	N	C	H	N	C	H	N
7	43.82	7.82	5.59	44.13	7.41	5.72	0.31	0.41	0.13
8	31.64	4.04	7.37	32.14	4.37	7.50	0.50	0.33	0.13
9	33.00	5.60	6.60	32.90	5.50	6.30	0.10	0.10	0.30
10	31.64	4.04	7.37	32.14	4.32	7.50	0.50	0.28	0.13
11	25.27	4.13	7.27	25.19	4.23	7.34	0.08	0.10	0.07
12	43.82	7.82	5.59	44.13	7.41	5.72	0.31	0.41	0.13
13	27.57	4.72	6.41	27.56	4.63	6.43	0.01	0.09	0.02
14	27.94	3.12	6.27	27.82	3.74	6.49	0.12	0.62	0.22
15	26.52	5.63	5.62	26.50	5.89	5.15	0.02	0.23	0.47
16	23.79	3.45	5.51	24.03	4.03	5.61	0.24	0.58	0.10
17	22.00	3.50	6.36	21.85	3.67	6.37	0.15	0.17	0.01
18	40.03	7.00	5.03	39.45	6.62	5.11	0.58	0.38	0.08

As the difference between the theoretical percentages of the atoms and the experimental percentages is less than ± 0.6% (to take into account errors in the analysis), it is concluded that the synthesized complex contains the same number of carbon, hydrogen and nitrogen atoms as expected.

The results of UV-Visible and Fluorescence spectroscopy studies were done to obtain the molar absorptivity value of the complexes. The molar absorptivity values were calculated by using the Beer-Lambert law. This value is used to determine the

concentration of the complexes in biological appraisals. **Table 3.1.1j** shows the results obtained for both UV-Visible and Fluorescence spectroscopy:

Table 3.1.1J: UV-visible and fluorescence spectroscopy results for complexes **7** - **18**

Complex	Concentration, M	Absorption wavelength, nm	Molar absorptivity, $M^{-1}\ cm^{-1}$	Emission wavelength, nm
7	1×10^{-5}	261	6.4×10^{4}	398
8	1×10^{-5}	256	1.3×10^{5}	372
9	1×10^{-7}	274	4.4×10^{5}	356
10	1×10^{-5}	263	1.9×10^{5}	376
11	1×10^{-5}	262	9.1×10^{4}	373
12	1×10^{-5}	259	1.3×10^{5}	373
13	1×10^{-7}	259	7.1×10^{5}	370
14	1×10^{-5}	259	1.2×10^{5}	365
15	1×10^{-5}	264	9.5×10^{4}	359
16	1×10^{-5}	265	1.1×10^{5}	376
17	1×10^{-5}	263	1.3×10^{5}	407
18	1×10^{-5}	267	9.5×10^{4}	407

UV-Visible spectra for both antimony and bismuth complexes were recorded between 256-274 nm range. The similarity of the spectra is consistent with lack of significant influence of the alkyl group on electronic transitions (Bevilacqua et al., 1994; Buntine et al., 2003; Kang et al., 2010). This too, corresponds that all twelve complexes have the same distorted octahedra geometry. Based on the molar absorptivity value of more than $10^{5}\ M^{-1}\ cm^{-1}$, it is also shown that all the complexes displayed strong spin-orbit coupling by having spin-allowed transitions (intra-ligand $\pi \rightarrow \pi^{*}$ charge transfer) in their electronic arrangements which further confirms the predicted distorted octahedra geometry of the complexes. The fluorescence wavelength for the complexes were measured to be between 356-407 nm range which again can be correlated to the similar electronic transition from the excited state to the ground state of the complexes.

3.1.2 THERMAL CHARACTERISATION

The thermal characterisation of the complexes can be evaluated by the analysis of TGA and DSC results, which indicated the crystallisation temperature (T_c) and whether the complexes show any phase changes or polymorphs throughout the thermal experiments. TGA analysis for the complexes are shown in the **Table 3.1.2A** below:

Table 3.1.2A: TGA analysis results for complexes **7 - 18**

Complex	Suggested compound	Total mass loss (%)	Percentage of residue (%)	Theoretical percentage (%)	Difference (±%)
7	H$_3$CH$_2$CN		38.137	37.834	0.303
	CS$_2$		41.369	40.242	1.127
	Sb	79.506	20.494	21.177	0.683
8	[(CH$_2$)$_4$NC]$_3$S$_4$		65.781	66.917	1.136
	SbS$_2$	66.871	34.219	33.129	1.100
9	HOCH$_2$CH$_2$NC(CH$_3$)$_2$		45.465	45.748	0.283
	CS$_2$		35.334	34.786	0.548
	Sb	80.799	19.201	18.568	0.633
10	HOCH$_2$CH$_2$NC		51.503	52.586	1.083
	SbS$_6$	63.629	48.497	47.414	1.083
11	[OHCH$_2$CH$_2$(CH$_3$)NC]$_3$S$_4$		66.603	67.529	0.926
	SbS$_2$	66.603	33.397	32.471	0.926
12	(H$_3$CH$_2$CH$_2$CH$_2$)NC]$_3$S$_4$		73.601	73.071	0.530
	SbS$_2$	73.601	25.9	24.8	1.1
13	(H$_3$CH$_2$CNC)$_3$S$_4$		57.769	58.227	0.458
	BiS$_2$	57.769	42.231	41.773	0.458
14	[(CH$_2$)$_4$NC]$_3$S$_4$		59.208	57.837	1.371
	BiS$_2$		15.930	17.377	1.447
15	OHCH$_2$CH$_2$N		23.146	23.822	0.676
	(CH$_3$)$_2$C		15.930	17.377	1.447
	CS$_2$		11.959	10.236	1.723
	BiS$_4$	51.035	48.965	45.336	3.629
16	HOCH$_2$CH$_2$NCS		58.109	59.298	1.189
	BiS$_3$	58.109	41.891	40.702	1.189
17	[OHCH$_2$CH$_2$(CH$_3$)NC]$_3$S$_5$		61.757	63.462	1.701
	BiS	61.757	38.243	36.538	1.701
18	(H$_3$CH$_2$CH$_2$CH$_2$)NC]$_3$S$_4$		67.862	65.318	2.544
	BiS$_2$	67.862	32.138	33.221	1.083

The TGA analysis results show that the residue is indeed as expected and that the ±3% difference in the experimental and theoretical mass loss was due to negligible errors during the experiments.

Listed in **Table 3.1.2B** are the DSC analysis results for the twelve antimony and bismuth complexes:

Table 3.1.2B: DSC analysis results for complexes **7** - **18**

Complex	Crystallization temperature, T_c (°C)	Change of heat (J/g)
7	66.7	11.56
	119.5	45.40
8	178.7	10.09
9	141.1	102.07
10	141.0	109.08
11	140.6	55.08
12	78.0	49.79
13	193.3	33.44
14	178.7	10.09
15	180.7	22.91
16	111.4	0.73
17	130.1	73.80
18	96.7	57.57

From the twelve complexes, only complex **7** displays polymorphism based on its DSC results whereby, there were two T_c observed. The possible polymorphism phenomena will be further discussed under complex **7** PXRD results.

3.1.3 PXRD

The correlation between the PXRD and SCXRD data of all twelve complexes verifies the structure of the complexes. SCXRD data were extracted *via* Mercury Software (Que, 2009), (Kavounis, 1980), (Low, 2001), (Tiekink, 2006), (Sun, 2012), (Lai, 2008), (Chian, 2007), (Handong, 2004) and (Venkatachalam, 1997). These data were converted into PXRD diffractogram by using X'pert HighScore Plus software. The generated PXRD diffractogram will then be used to compare with the PXRD diffractogram of the synthesized complexes. The diffractogram in red designates the synthesized complexes PXRD diffractogram while the diffractogram in blue represents

the simulated diffractogram from the single crystal X-ray. The results obtained are compared below:
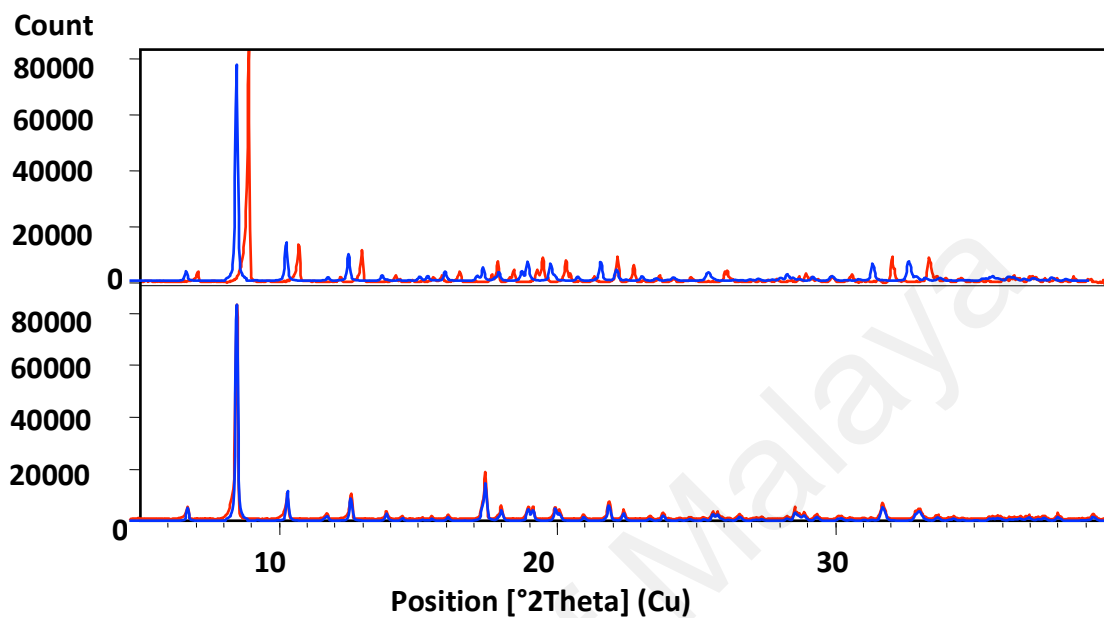
Figure 3.1.3A: (Top) PXRD diffractorgram for complex **7** and (below) PXRD diffractogram for complex **13**.
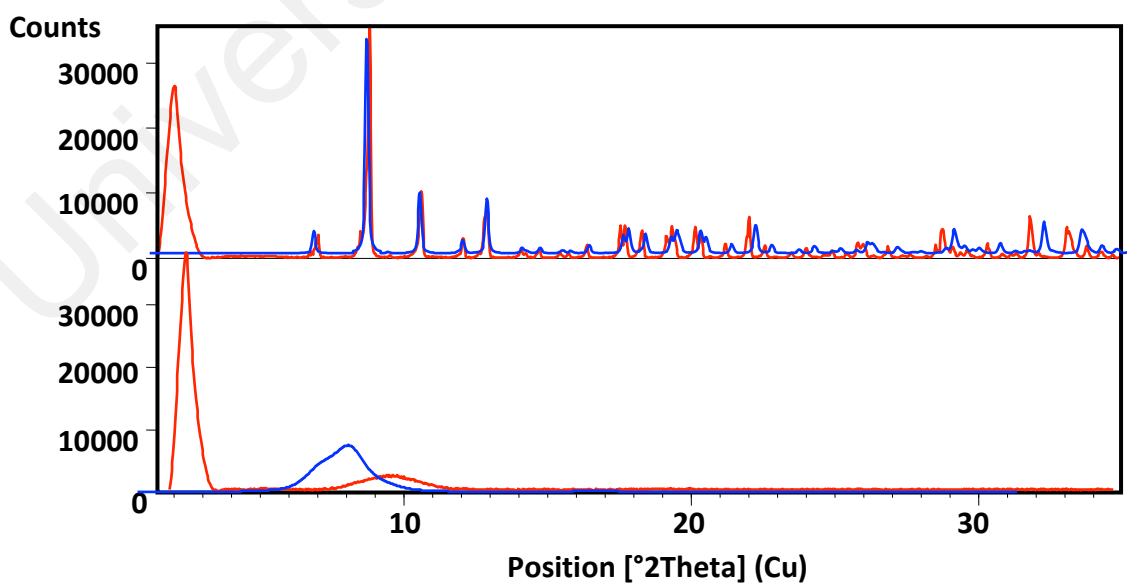
Figure 3.1.3B: (Top) PXRD diffractorgram for complex **13** at temperature 116 °C and (below) PXRD diffractogram for complex **13** at temperature 190 °C.
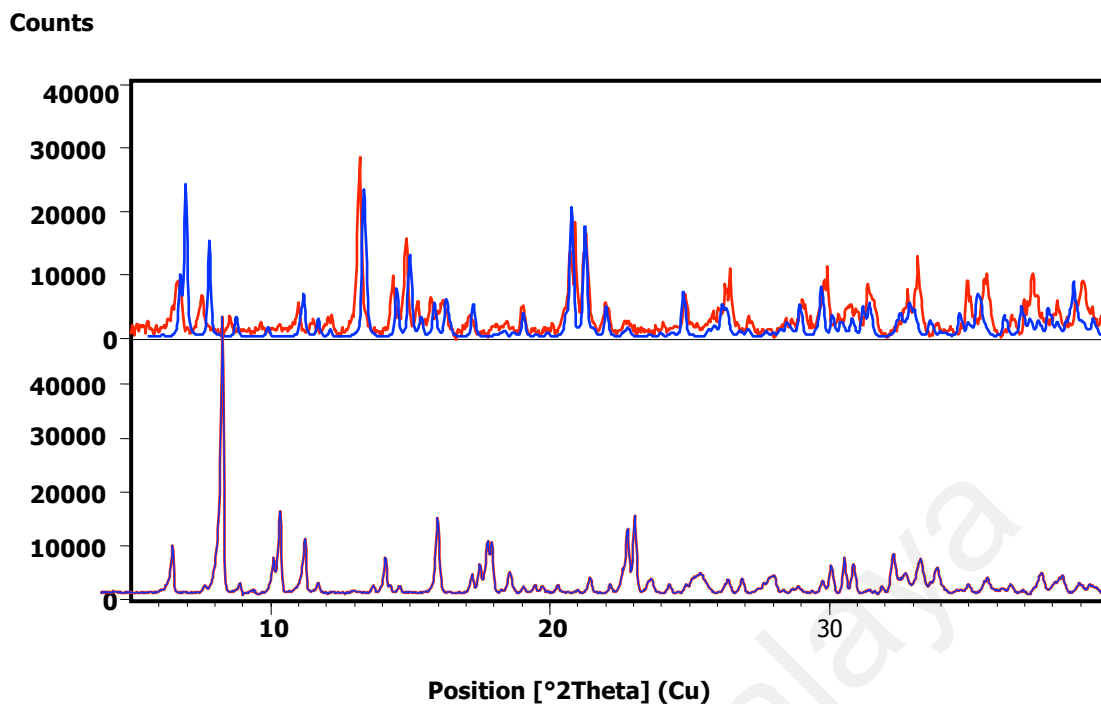
Figure 3.1.3C: (Top) PXRD diffractorgram for complex **8** and (below) PXRD diffractogram for complex **14**.
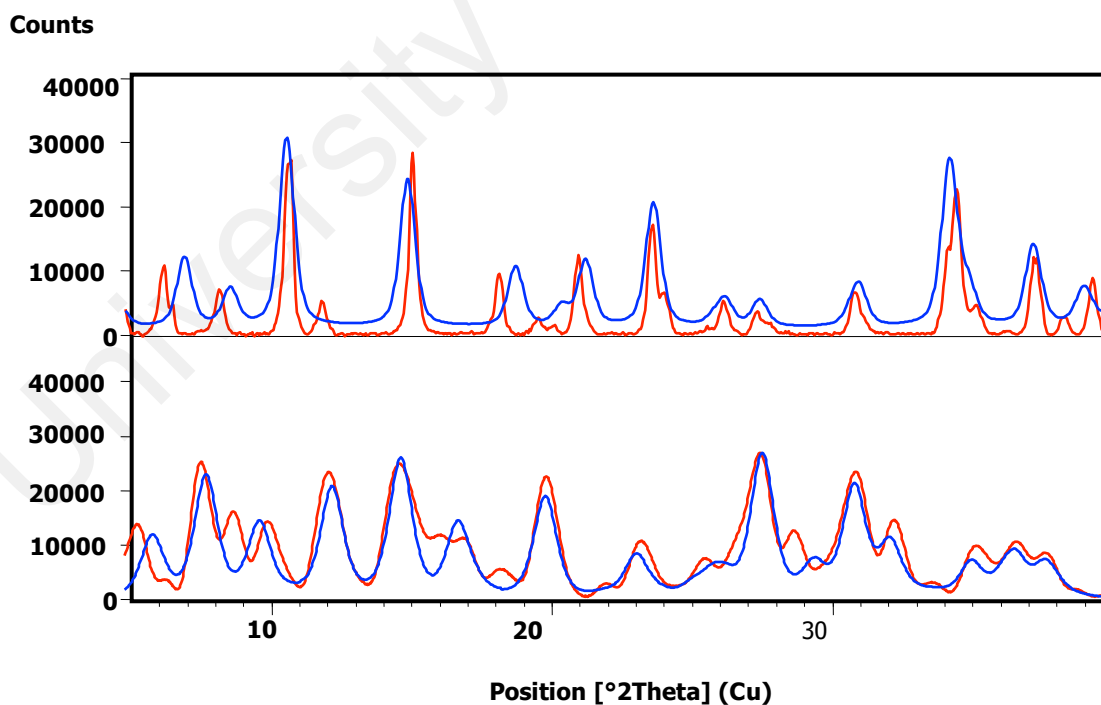
Figure 3.1.3D: (Top) PXRD diffractorgram for complex **9** and (below) PXRD diffractogram for complex **15**.
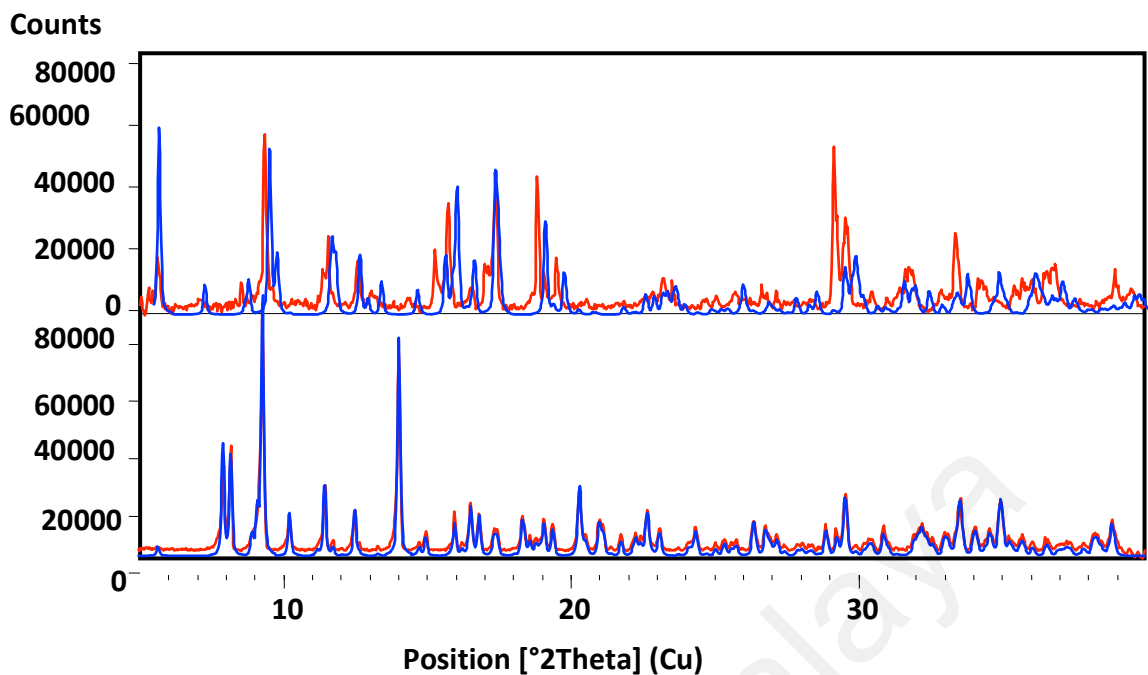
Figure 3.1.3E: (Top) PXRD diffractorgram for complex **10** and (below) PXRD diffractogram for complex **16**.
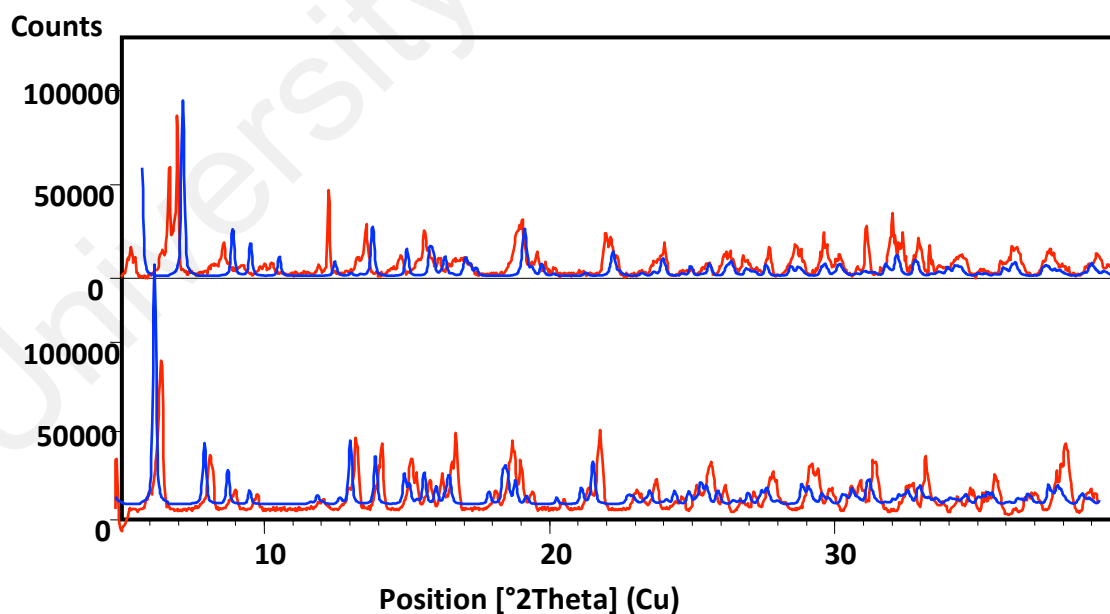
Figure 3.1.3F: (Top) PXRD diffractorgram for complex **11** and (below) PXRD diffractogram for complex **17**.
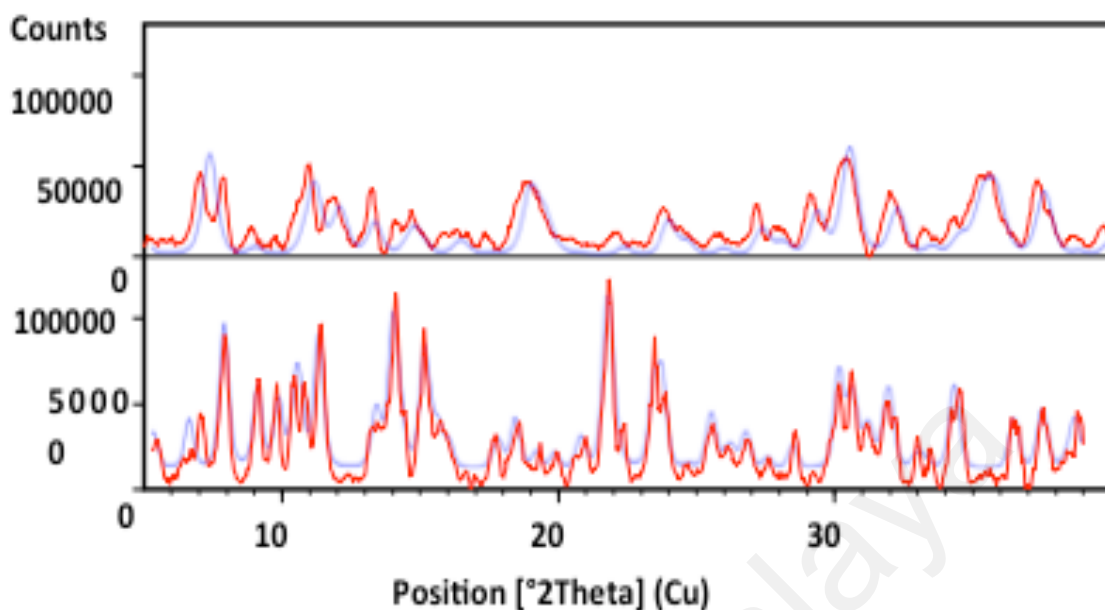
Figure 3.1.3G: (Top) PXRD diffractorgram for complex **12** and (below) PXRD diffractogram for complex **18**.

As shown above, the same pattern of PXRD diffractograms were obtained by correlating with the PXRD diffractograms from the generated from the SCXRD data. This verifies that the complexes are indeed having the exact structure as per reported by its respective literature. From the PXRD data, it was shown that complex **7** showed a similar pattern to its generated PXRD. This in turn concluded that the possible polymorphism observed for complex **7** based on its DSC result is not dominant in determining the structure of complex **7**, hence, giving the same pattern as predicted by the literature. Due to the antitumour activity potential for complex **13**, additional PXRD data was collected at 116 and 190 °C. Based on the results obtained, complex **13** structure is still retained at 116 °C but deforms at temperature of 190 °C. The data were collected at the designated temperatures based on its T_c (refer to DSC results).

3.2 Bioassay of complex **13** and **16**

3.2.1 Cancer cell proliferation inhibitory study (cell viability assay)

A cancer cell proliferation inhibitory is a study designed to measure the number of cancer cells successfully inhibited from growing and dividing. The compounds under investigation were appraised for their potential to inhibit cell proliferation against six human carcinoma cell lines, namely HepG2, MCF-7R, A2780, HT-29, A549 and 8505C, together with Cisplatin, Doxyrobucin and Paclitaxel as the positive controls. After 24 h, the data were collected to inspect the effects of the test compounds on cell growth and proliferation of the selected cancer cell. From the data evaluation, the IC_{50} values were obtained.

Due to time constraints, the complete biological evaluation data for only two compounds were obtained and they are evaluated compounds **13** and **16** while the other compounds in this dissertation are still being appraised at the time of writing. **13** and **16** were chosen to be the first to be inspected fully due to their promising and interesting cytotoxicity results against HepG2 cells.

3.2.1.1 Bismuth diethyl dithiocarbamate, **13**

The effects of **13** on the growth and proliferation of the selected carcinoma cells were appraised after 24 hand IC_{50} values obtained. The data are presented in **Table 3.2.1.1** by taking the mean and standard deviation from two independent experiments conducted in triplicate except for values >80:

Table 3.2.1.1: Cytotoxic activity of **13** and standard drugs against six human carcinoma cells after 24 h

Cell line	IC_{50} (µM)			
	Cisplatin	Doxorubicin	Paclitaxel	13
HepG2	152.0 ± 0.3	4.6 ± 0.2	>80	0.5 ± 0.4
MCF-7R	19.6 ± 0.2	5.2 ± 0.4	15.9 ± 0.3	0.9 ± 0.2
A2780	28.8 ± 0.4	4.4 ± 0.2	14.2 ± 0.3	0.5 ± 0.2
HT-29	25.0 ± 0.3	4.8 ± 0.3	>80	$3. \pm 0.3$
A549	35.4 ± 0.4	>80	>80	2.30 ± 0.4
8505C	120.0 ± 0.2	>80	>80	0.2 ± 0.4

From the results above, **13** showed exceptionally positive potency as compared to all the positive controls towards the tested cancer cells.

Based on the IC_{50} values potency reflected in the first cancer cell chosen for further evaluation is the HepG2 cells whereby **13** showed great potential in healing HepG2 carcinoma. The ultimate aim of this study is to make **13** as the main drug in HepG2 carcinoma treatment. This is due to the observation **13** has a lower IC_{50} values as compared to all the standard drugs available in the market for HepG2 carcinoma at the present time.

The outcome for cell viability of HepG2 cells after treatment with **13** at different concentrationsis plotted in **Figure 3.2.1.1**. This shows that **13** inhibited cell proliferation in a concentration-dependent manner.
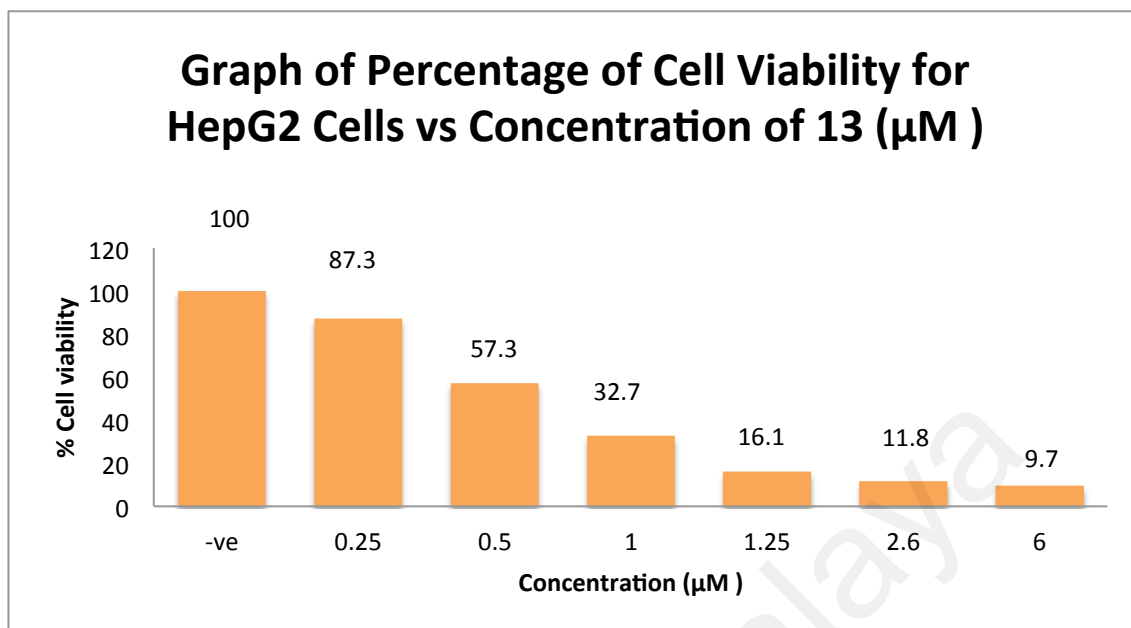
Figure 3.2.1.1: Cell viability of HepG2 cells after 24 h treatment with **13** at different concentration

3.2.1.2 BISMUTH DIETHANOL DITHIOCARBAMATE, **16**

IC_{50} values for **16** were also obtained in the same manner as for **13**. After 24 h incubation of the cancer cells with **16**, gave the results are shown in **Table 3.2.1.2**. From this deduction, **16** was found to be generally non-potent against six human cancer cell lines in testing displaying only minor activity against HepG2 cells.

Table 3.2.1.2: Cytotoxic activity of **16** and standard drugs against six human carcinoma cells after 24 h

Cell line	IC_{50} (µM)			
	Cisplatin	**Doxorubicin**	**Paclitaxel**	**16**
HepG2	152.0 ± 0.3	4.6 ± 0.2	>80	55.9 ± 0.3
MCF-7R	19.6 ± 0.2	5.2 ± 0.4	15.9 ± 0.3	>80
A2780	28.8 ± 0.4	4.4 ± 0.2	14.2 ± 0.3	>80
HT-29	25.0 ± 0.3	4.8 ± 0.3	>80	>80
A549	35.4 ± 0.4	>80	>80	>80
8505C	120.0 ± 0.2	>80	>80	>80

Complex **16** manifested the same relationship manner in cell proliferation whereby it is concentration-dependent. **Figure 3.2.1.2** displays the data obtained.
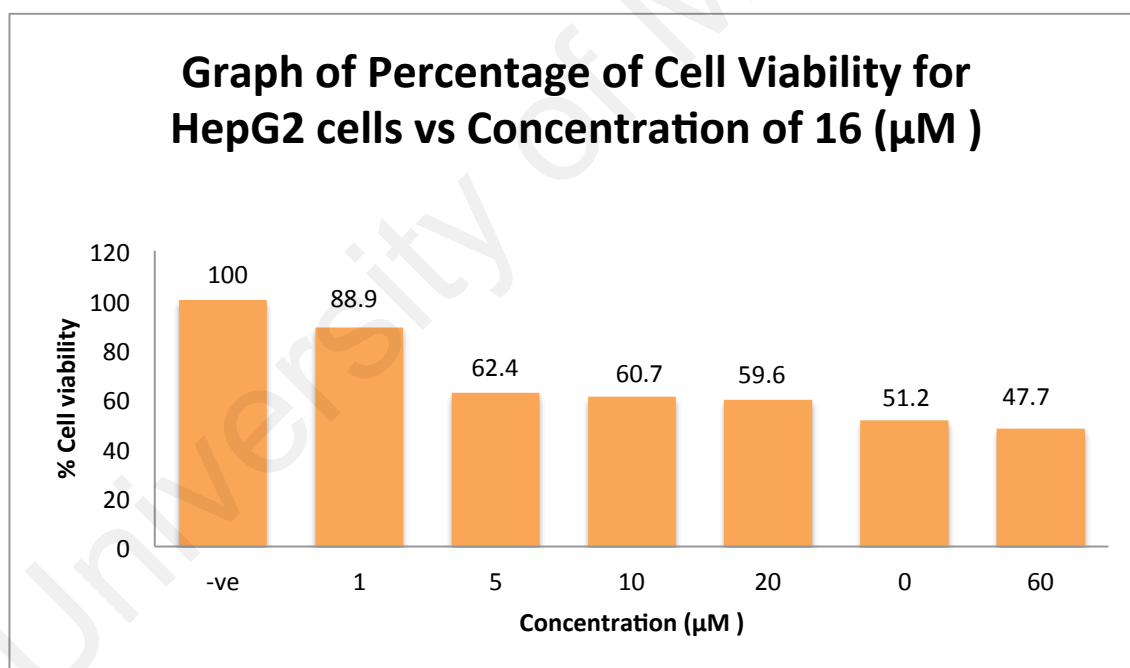
Figure 3.2.1.2: Cell viability of HepG2 cells after treatment with **16** after 24 h at different concentrations

3.2.2 MEMBRANE PERMEABILITY STUDY (AO/PI APOPTOTIC CELL STUDY)

The integrity of HepG2 cells was analysed after treatment with the IC_{50} dose of each of **13** and **16**. The AO/PI staining method was chosen due to its simplicity and availability. Through this method, an increase in plasma membrane permeability in apoptotic cells is indicated by some fluorescent dyes (Kapuscinski, 1983). Cells that had been treated with Doxorubicin (being a current drug used in the treatment of HepG2 carcinoma) and untreated cells are the control in this experiment. **Figure 3.2.2A** and **Figure 3.2.2B** shows the results of both controls.

When viewed under a fluorescence microscope, cells with an intact membrane after treatment will exhibit bright-green nuclei while cells that undergoes apoptosis will have dark-green nuclei with condensed chromatin (shown as dense green areas) after being dyed with AO (Yeh *et. al.*, 1981).

The PI dye on the other hand is resistant toward intact membrane plasma but permeable towards dying or dead cells by means of intercalating with DNA or RNA.

This occurrence will produce bright-red fluorescence hence bright-red fluorescence can be seen in necrotic cells as they have lost their membrane integrity (Foglieni*et. al.*, 2001).
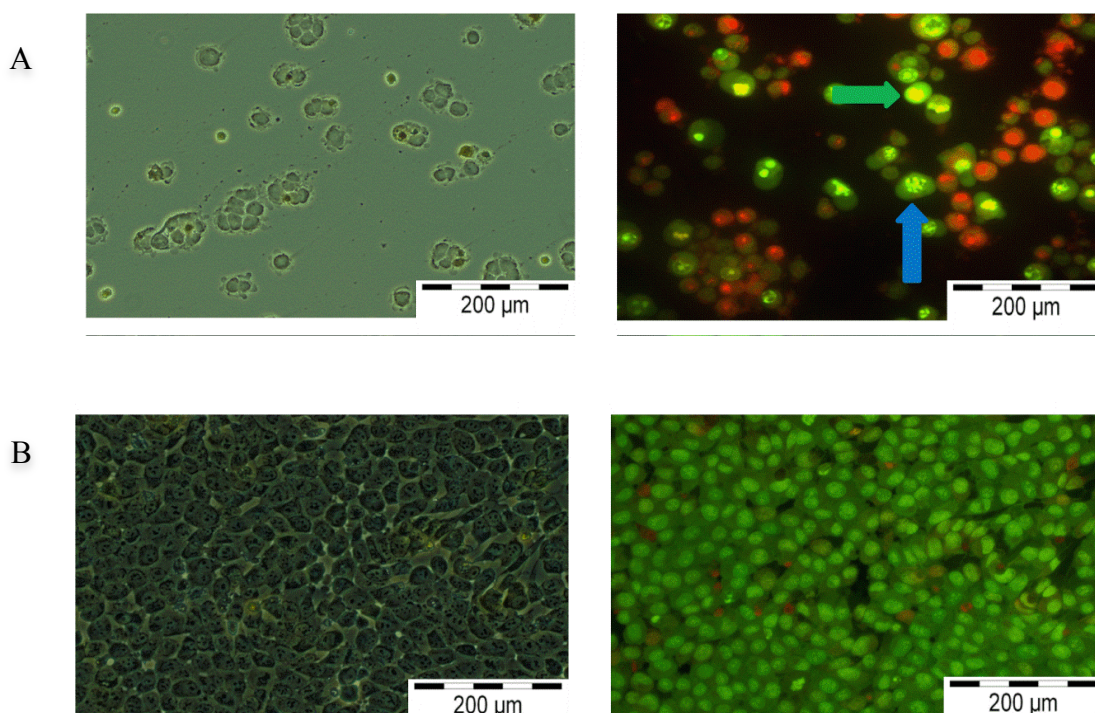
Figure 3.2.2: HepG2 cells dyed with AO/PI before and after being incubated with an IC$_{50}$ dose of A) Doxorubicin and B) nothing (untreated cells). PI produced Red-coloured stains when the integrity of the membrane plasma was disturbed, green stains shows intact membrane whereby dark-green cells with yellow/green dots of condensed nuclei indicate apoptotic cells. The green arrow in A points to a healthy cell whilst the blue arrow points to an apoptotic cell. Image B, the majority of cells showed green stains which portrays that their cell membranes are intact. Red-stained are dead cells by nature. These images have been magnified 100×.

3.2.2.1 BISMUTH DIETHYL DITHIOCARBAMATE

Most of HepG2 cells underwent apoptosis after treatment with **13** (**Figure 3.2.2.1**). The attributes of apoptotic cells were observed, condensation of nuclear chromatin and cytoplasm, membrane blebbing and the formation of apoptotic bodies. The enlargement of cell volume and formation of multinucleated cells were also noted. Vast numbers of cells were seen to have clumped up in a small amount of unorganized

colonies. None of these characteristics were seen in either the control experiment for untreated cells and doxorubicin-treated cells.
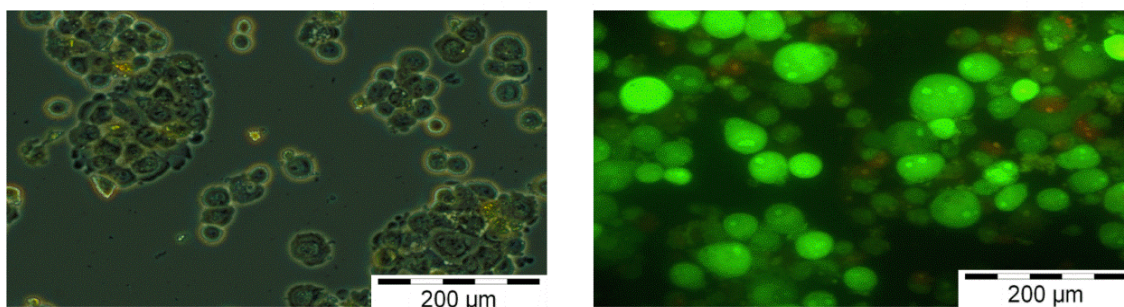
Figure 3.2.2.1: Shows HepG2 cells after incubation with the IC_{50} dose of **13** before and after being dyed with AO/PI. Dark-green cells with yellow/green dots of condensed nuclei show apoptotic cells showing its features. Also, enlargement of cell volume, formation of multinucleated cells and unorganized clusters of cells can be observed as well. This image had been magnified 100×

3.2.2.2 BISMUTH DIETHANOL DITHIOCARBAMATE

Ministration of **16** on HepG2 cells indicated that the cells undergo apoptosis as for**13**. The treated HepG2 cells show the same features of condensed nuclear chromatin and cytoplasm, blebbing of membrane plasma and apoptotic body formation. By contrast, HepG2 cells treated with **16**, showed no evidence on the expansion of cell volume and the emergence of multinucleated cells. Moreover, red-coloured fluorescence appeared on most of the **16**-treated cells with unperturbed membrane plasma, indicates that **16** also promoted necrosis concurrently. Affirmation of the above explanation are revealed in **Figure 3.2.2.2** which also displays that most of the treated cells were clumped together in an unorganized grouping after incubation with **16**.
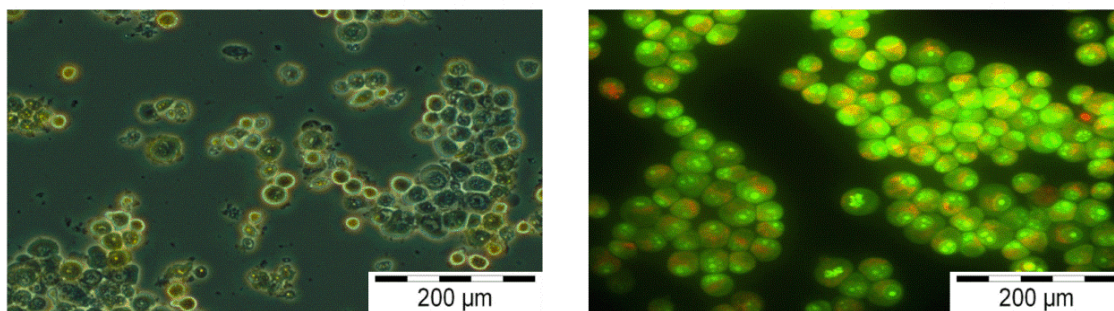
Figure 3.2.2.2: HepG2 cells before and after staining with AO/PI after being treated with the IC_{50} amount of **16**. Dark-green cells with yellow/green dots of condensed nuclei with traces of red-colour fluorescence exhibited that the cells experienced apoptosis with some traces of necrosis at the same time.Magnification of the image is at 100×

3.2.3 DNA FRAGMENTATION ANALYSIS

One of distinctive features of the lethal stages of apoptosis is chromosal DNA fragmentation. The analysis of this proceeded in a two-step method; the DNA was firstly cleaved into 50-300 kb sections and further into oligonucleosomal fragments (Rowinsky, 2005; Samejima *et. al.*, 2005). During the apoptosis process, the extrication of apoptotic signals such as p53 and DFFA genes will eventually causes DNA damage. **Figure 3.2.3** shows DNA extraction of untreated cells as the negative reference.

L1   L2
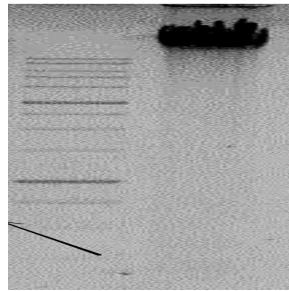
Figure 3.2.3: DNA fragmentation analysis for untreated HepG2 cells. Cultured in RPMI 1640 for 24 h, the DNA was then extracted and the fragmentation was detected by using (continued from Figure 3.2.3) electrophoresis with 2% agarose gel. L1 shows 1 kb DNA ladder for comparison. L2 is the negative control, which shows no DNA fragmentation, occurred in untreated HepG2 cells

3.2.3.1 BISMUTH DIETHYL DITHIOCARBAMATE

Figure 3.2.3.1 shows the results of DNA fragmentation analysis after treatment with **13**. Formation of ladders on L4 gel indicates DNA fragmentation took place.

L3   L4
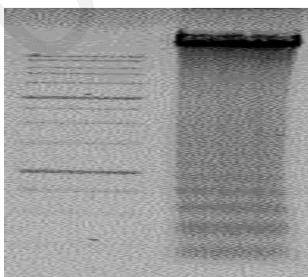
Formation of ladders on the gel

Figure 3.2.3.1: Formation of ladders indicates that after treatment with **13**, strong DNA fragmentation had occurred via apoptosis. L3 is a 1 kb DNA ladder for comparison with L4, which is DNA fragmentation analysis for HepG2 cells, treated with **13.**

3.2.3.2 BISMUTH DIETHANOL DITHIOCARBAMATE

Complex **16** was also found to induce DNA fragmentation after 24 h of incubation as shown as the formation of ladder in L6 (**Figure 3.2.3.2**).

L5   L6
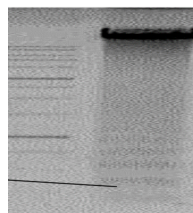
Figure 3.2.3.2: DNA ladders as shown above proves that after treatment with **16**, DNA fragmentation had occurred via apoptosis. L5 is a 1 kb DNA ladder for comparison withL6, which is DNA fragmentation analysis for HepG2 cells treated with **16**.

3.2.4   RESTRICTION ENZYME DIGESTION AND ANALYSIS

The inhibitions of twelve different restriction enzymes, which differ in their target sequences, were measured to analyse the sequence of selectivity in binding by **13** and **16**. The restriction enzymes and their target sequences are listed in **Table 3.2.4**.

To evaluate the binding selectivity of **13** and **16**, the twelve restriction enzymes were used to act on λ DNA. This is on the basis that anti-cancer action can be controlled when discrete binding transpires within DNA, either via groove binding or intercalation. Results were obtained by using the gel electrophoresis method. An accurate and duplicable protection patterns were acquired for each DNA interaction study each time for both compounds.

Table 3.2.4: List of twelve restriction enzymes and their target sequences

Tsp 509I	5'—↓ A A T T —3' 3'— T T A A ↑—5'
Hae III	5'—G C ↓G C —3' 3'—C G ↑C G —5
Sal I	5'—G ↓T C G A C—3' 3'—C A G C T ↑G—5'
Pst I	5'—C T G C A ↓G—3' 3'—G↑ A C G T C—5'
Pvu II	5'—C A G ↓C T G—3' 3'—G T C ↑ G A C—5'
Sca I	5'—A G T ↓A C T—3' 3'—T C A ↑T G A—5'
Ssp I	5'—A A ↓T A T T—3' 3'— T T A T ↑A A—5'
Ase I	5'—A T ↓T A A T—3' 3'— T A A T ↑T A—5'
Mun I	5'—C↓ A A T T G—3' 3'— G T T A A ↑C—5'
EcoR I	5'—G↓ A A T T C—3' 3'— C T T A A ↑G—5'
Nde I	5'—C A↓ T A T G—3' 3'—G T A T ↑A C—5'
Bst 11071	5'—G T A ↓ T A C—3' 3'—C A T ↑ A T G—5'

3.2.4.1 BISMUTH DIETHYL DITHIOCARBAMATE

Based on the outcome, 'AT' sequence was protected from DNase digestion by **13** in Ssp I "AATATT", Nde I "CATATG" and Bst 11071 "GTATAC". On the other hand, GC, short AT, AAT and random sequences were not shielded from DNase digestion.

These are deduced by the fact that digestion with Ssp I, Nde I and Bst 11071 did not trigger scission on λ DNA. This proposed that **13** was bound to specific DNA sequences sites and hindered it from restriction enzyme digestion (Palanichamy *et. al.*, 2012). The negative control also shows digested DNA bands, **Figure 3.2.4.1A** and **Figure 3.2.4.1B**.
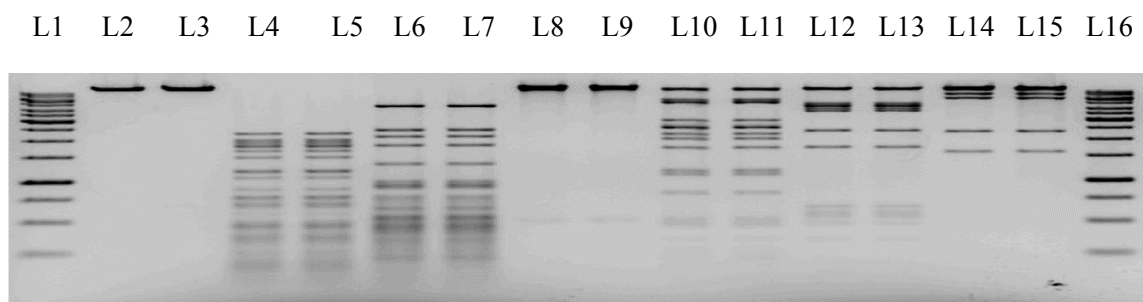
Figure 3.2.4.1A: Electrophoresis results after incubating λ DNA (0.5 μg/μL) with 5 units of restriction enzyme in the presence or absence of 10 μM of **13** for 2 h at 37 °C. Lanes 1 and 16, 1 kb DNA ladder; Lane 2, λ DNA alone (0.5 μg); Lane 3, λ DNA + 10 μM of compound as reference; Lane 4,λ DNA + 5 units of Tsp 509I (control): Lane 5, λ DNA + 5 units of Tsp 509I + 10 μM of compound; Lane 6, λ DNA + 5 units of Hae III (control): Lane 7, λ DNA + 5 units of Hae III + 10 μM of compound; Lane 8, λ DNA + 5 units of Sal I (control): Lane 9, λ DNA + 5 units of Sal I + 10 μM of compound; Lane 10, λ DNA + 5 units of Pst I (control): Lane 11, λ DNA + 5 units of Pst I + 10 μM of compound; Lane 12, λ DNA + 5 units of Pvu II (control): Lane 13, λ DNA + 5 units of (Figure 5.6.1A, continued) Pvu II + 10 μM of compound; Lane 14, λ DNA + 5 units of Sca I (control): and Lane 15, λ DNA + 5 units of Sca I + 10 μM of compound
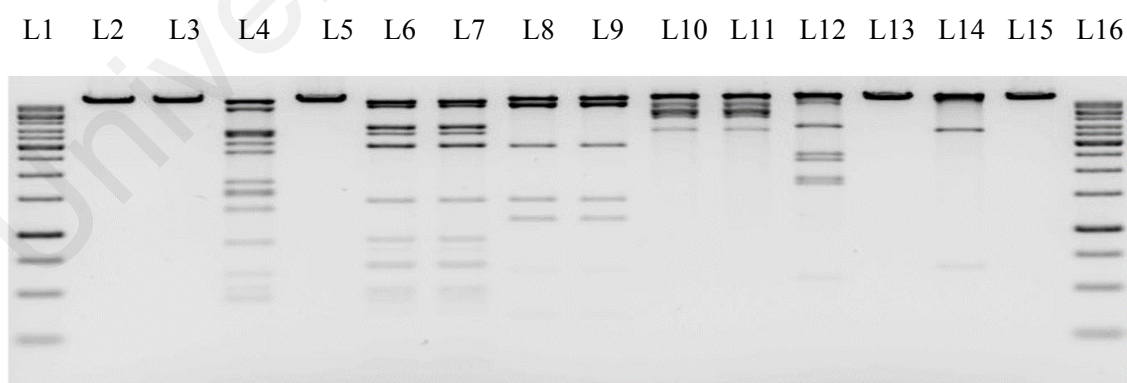
Figure 3.2.4.1B: Electrophoresis results after incubating λ DNA (0.5 μg/μL) with 5 units of restriction enzyme in the presence or absence of 10 μM of **13** for 2 h at 37 °C. Lanes 1 and 16, 1 kb DNA ladder; Lane 2, λ DNA alone (0.5 μg); Lane 3, λ DNA + 10

μM of compound as reference; Lane 4, λ DNA + 5 units of Ssp I (control): Lane 5 λ

DNA + 5 units of Ssp I + 10 μM of compound; Lane 6, λ DNA + 5 units of Ase I

(control): Lane 7, λ DNA + 5 units of Ase I + 10 μM of compound; Lane 8, λ DNA + 5

units of Mun I (control): Lane 9, λ DNA + 5 units of Mun I + 10 μM of compound;

Lane 10, λ DNA + 5 units of EcoR I (control): Lane 11, λ DNA + 5 units of EcoR I +

10 μM of compound; Lane 12, λ DNA + 5 units of Nde I (control): Lane 13, λ DNA +

5 units of Nde I + 10 μM of compound; Lane 14, λ DNA + 5 units of Bst 11071

(control): and Lane 15, λ DNA + 5 units of Bst 11071 + 10 μM of compound

3.2.4.2 BISMUTH DIETHANOL DITHIOCARBAMATE

Adversely, compound **16** failed to shield any restriction sites in all twelve tested

restriction enzymes. This was observed when the bands in the gel appeared to have no

change as compared to the control (**Figure 3.2.4.2A** and Figure **3.2.4.2B**).
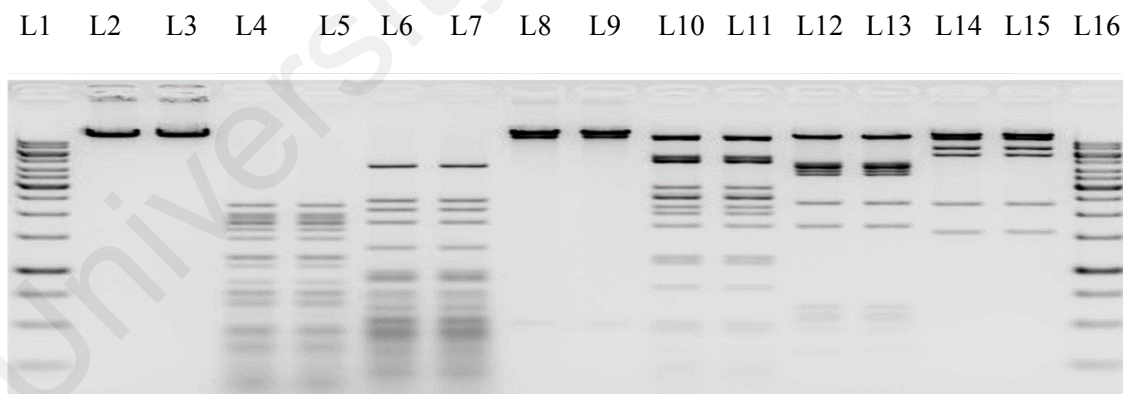
Figure 3.2.4.2A: Electrophoresis results after incubating λ DNA (0.5 μg/μL) with 5

units of restriction enzyme in the presence or absence of 10 μM of **16** for 2 h at 37 °C.

Lanes 1 and 16, 1 kb DNA ladder; Lane 2, λ DNA alone (0.5 μg); Lane 3, λ DNA + 10

μM of compound as reference; Lane 4, λ DNA + 5 units of Tsp 509I (control): Lane 5, λ

DNA + 5 units of Tsp 509I + 10 μM of compound; Lane 6, λ DNA + 5 units of Hae III

(control): Lane 7, λ DNA + 5 units of Hae III + 10 μM of compound; Lane 8, λ DNA +

5 units of Sal I (control): Lane 9, λ DNA + 5 units of Sal I + 10 μM of compound; Lane 10, λ DNA + 5 units of Pst I (control): Lane 11, λ DNA + 5 units of Pst I + 10 μM of compound; Lane 12, λ DNA + 5 units of Pvu II (control): Lane 13, λ DNA + 5 units of Pvu II + 10 μM of compound; Lane 14, λ DNA + 5 units of Sca I (control): and Lane 15, λ DNA + 5 units of Sca I + 10 μM of compound

Figure 3.2.4.2B: Electrophoresis results after incubating λ DNA (0.5 μg/μL) with 5 units of restriction enzyme in the presence or absence of 10 μM of **16** for 2 h at 37 °C. Lanes 1 and 16, 1 kb DNA ladder; Lane 2, λ DNA alone (0.5 μg); Lane 3, λ DNA + 10 μM of compound as reference; Lane 4, λ DNA + 5 units of Ssp I (control): Lane 5, λ DNA + 5 units of Ssp I + 10 μM of compound; Lane 6, λ DNA + 5 units of Ase I (control): Lane 7, λ DNA + 5 units of Ase I + 10 μM of compound; Lane 8, λ DNA + 5 units of Mun I (control): Lane 9, λ DNA + 5 units of Mun I + 10 μM of compound; Lane 10, λ DNA + 5 units of EcoR I (control): Lane 11, λ DNA + 5 units of EcoR I + 10 μM of compound; Lane 12, λ DNA + 5 units of Nde I (control): Lane 13, λ DNA + 5 units of Nde I + 10 μM of compound; Lane 14, λ DNA + 5 units of Bst 11071 (control): and Lane 15, λ DNA + 5 units of Bst 11071 + 10 μM of compound

3.2.5 INTRACELLULAR SIGNALLING CASCADES (CASPASE ACTIVITY AND ROS MEASUREMENTS)

Programmed cell death (PCD) or apoptosis is a highly controlled process to eliminate unwanted cells from the body in course of organ development, immune responses and tissue remodelling. It is found that frailty in the apoptosis pathway in cancer development is the culprit that contributes to the resistance of tumours towards chemotherapy. Consequently, many anti-cancer drugs are designed to target the particular signalling components of survival pathways and cell death (Fesik, 2005; Qiao *et. al.*, 2009; Wong, 2009). Broadly, apoptosis is defined as an individual set of biochemical stages together with morphological changes that include chromation condensation, activation of caspases and chromosomal DNA fragmentation (Kroemer *et. al.*, 2009).

To investigate the cell death pathways, an interpretation of RT^2 profiler PCR microarray analysis, caspase activity study, DNA fragmentation and ROS production measurements were evaluated. ROS production measurements are vital for the inspection the of cell death pathway induced by **13** and **16**.

3.2.5.1 BISMUTH DIETHYL DITHIOCARBAMATE

13 depicts an over-expression of pro-apoptotic genes alongside the suppression of anti-apoptotic genes after treatment of HepG2 cells. This outcome bestows the proof that the cytotoxicity of **13** is affiliated with the induction of p53/p73-dependent activation of the mitochondrial pathway of apoptosis, p53 (TP53) and p73 (TP73) were expressed concurrently. It is noteworthy that the PCR microarray analysis disclosed that

13 also induced apoptosis *via* both intrinsic and extrinsic pathways arising from diverse types of apoptosis-inducing factors.

Compound **13** were discovered to activate p53 gene expression with a 6-fold increase over p73 expression as indicated in **APPENDIX A**. This shows that the up-regulation of p53/p73 genes stipulate DNA damage in HepG2 cells, which is in accord with the DNA fragmentation results (see section 3.2.3).

Besides that, the p21 encoded gene, CDKN1A, which serves the purpose as a major inhibitor of p53-dependent apoptosis (Gartel *et. al.*, 2002), was up-regulated to 12-fold by **13**after 24 h (**Figure 3.2.5.1A** and **Figure 3.2.5.1B**).
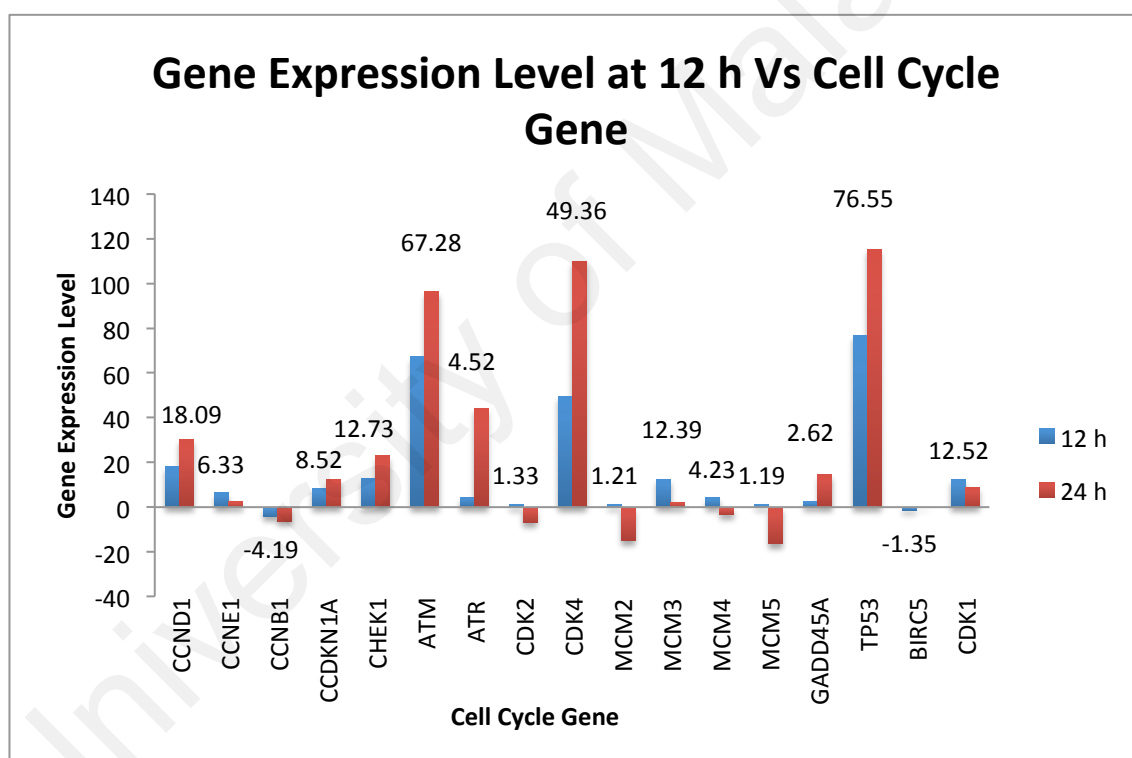
Figure 3.2.5.1A: Graph of gene expression levels after treatment with **13** against cell cycle genes. The data show the gene expression levels after 12 h treatment
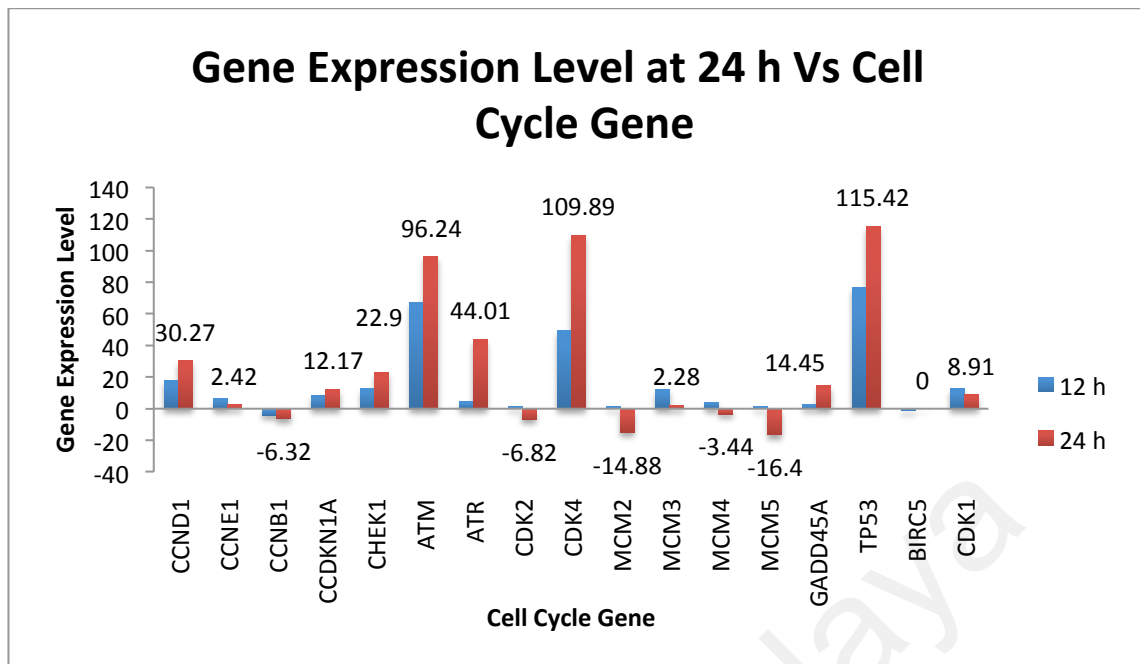
Figure 3.2.5.1B: Graph of gene expression levels after treatment with **13** against cell cycle gene. The data show gene expression levels after 24 h

In addition, another vital protein that regulates p53, the ataxia telangiectasia mutated (ATM), was also up-regulated by 98-fold after 24 h (**Figure 3.2.5.1A** and **Figure 3.2.5.1B**). The ATM gene triggers off a cell cycle controlling mechanism and apoptotic responses by selectively expressing the p53 gene (Barlow *et. al.*, 1997). Hence, both the up-regulation of the CDKN1A and ATM genes work together in the intensification of the p53 pathway.

P73, which induces apoptosis, was seen to be amplified after treatment of **13**. This is because of the presence of c-Abl protein that also leads to the in augaration of apoptosis (Dobbelstein *et. al.*, 2005) (see **APPENDIX A**). Further, a cell death inducer, the BNIP3L protein, was highly expressed over 55-fold, in cells treated with **13**. This unveils the proof for the operation of the p53 gene as in turn; it can increase the expression of BNIP3L gene that is well known to be highly produced in wild-type p53-expressing cells (Fei *et. al.*, 2004).

A second mechanism of p53/p73-induced apoptosis was ushered-in by the BCL-2-associated X-protein (BAX). BAX also stimulates mitochondrial translocation and cytochrome c liberation. To sum things up, mitochondrial permeability is administered by a family of proto-oncogenes, examples being anti-apoptotic (BCL-2) and pro-apoptotic (BAD, BAX) (Tsujimoto *et. al.*, 2000). The presence of BAX into the mitochondrial membrane causes an increase in membrane permeability that in turn promoting apoptosis once being triggered (Eskes *et. al.*, 1998; Gross *et. al.*, 1999). From the results obtained, **13** (also see **APPENDIX A**) cause the deactivation of BCL-2, thus the rise of BAX, which increases the potential in the mitochondrial membrane, in the disappearance of anti-apoptotic protein, BCL-2.

The ultimate occurrence that leads to apoptosis is the loss of mitochondrial trans-membrane potential (Petit *et. al.*, 1996). In consequence of treatment, ΔΨm (intrinsic mitochondrial membrane potential) was affected, ensued by the destruction of the mitochondrial membrane and the liberation of proteins such as cytochrome C from the intermembrane region (Kroemer *et. al.*, 2007). Cytochrome c which cohered to apoptotic activating factor-1 (APAF-1), was notably extracted in HepG2 treated cells by **13** which selects the activation of caspase 9, a key inactivating caspase-3, the most formidable effector caspase (see **APPENDIX A**) The increase in ΔΨm also causes the release of AIF. AIF triggered DNase that in turn promotes apoptosis (Li *et. al.*, 2001; Saelens *et. al.*, 2004; van Loo *et. al.*, 2001). **Figure 3.2.5.1D** depicts the downwards shift (from M2 to M1) in the fluorescence response due to presence of cytochrome c in treated HepG2 cell by **13** after 12 h and 24 h. **Figure 3.2.5.1C** shows that the negative control samples has low levels of cytochrome C loss.

12 h   24 h
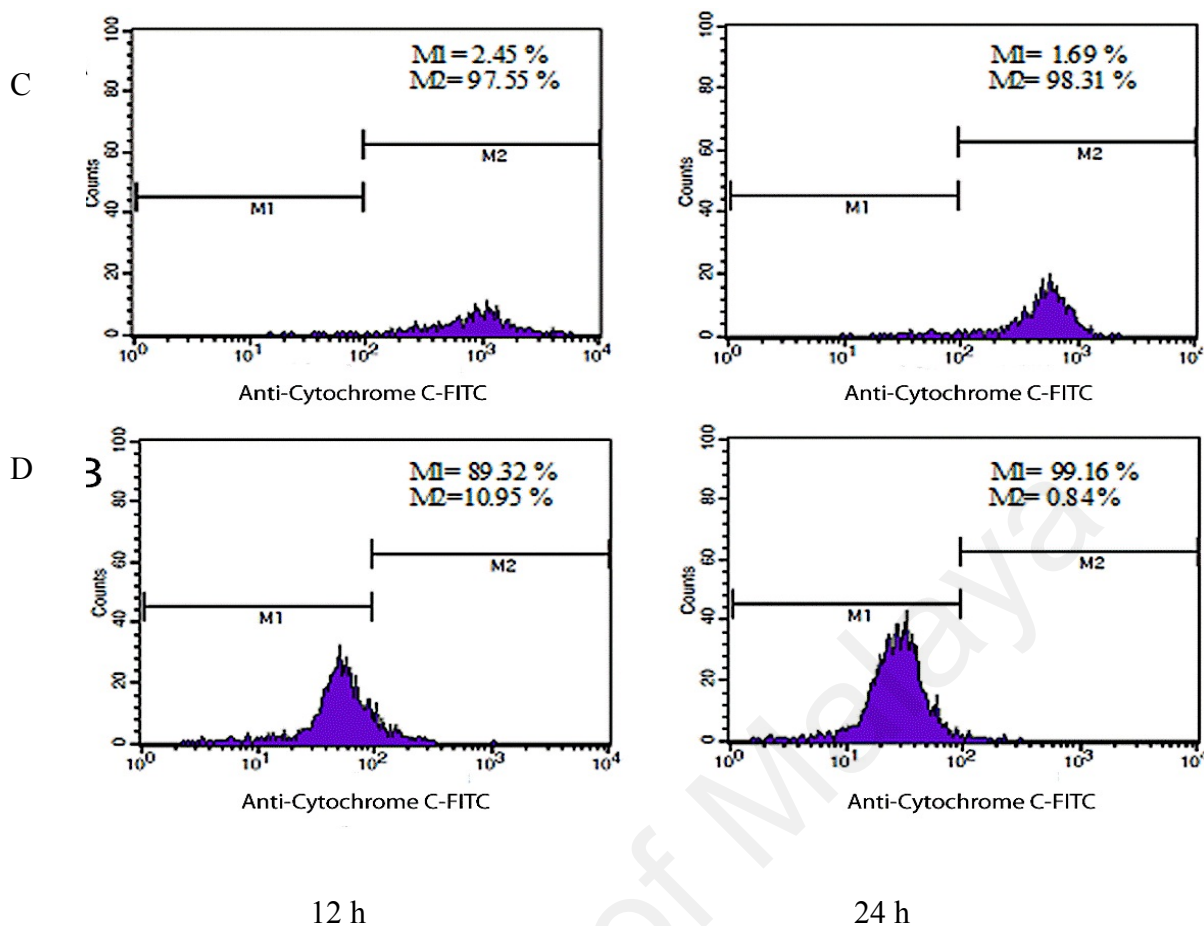
Figure 3.2.5.1C and **Figure 3.2.5.1D**: Histograms showing cells stained using the FlowCellect Cytochrome C Kit^TM. **Figure 3.2.5.1C** results from the untreated HepG2 cells after 12 h and 24 h (negative control); **Figure 3.2.5.1D** HepG2 cells treated with 0.53 μM of **13** for 12 h and 24 h

Another after-effect from the increase of mitochondrial membrane potential is the liberation of ROS which plays a vital role in apoptosis prompted by chemotherapeutic agents via the activation of the mitochondria-mediated apoptosis pathways (Le Bras *et. al.*, 2005; Skulachev, 1996). One proposal is that ROS could also affect TNFR (tumour necrosis factor receptor) and FAS (tumour necrosis factor superfamily) receptor-mediated apoptosis (Krammer, 1999). Cellular ROS generation exceeded about 32% as compared to the negative control after treatment with **13**. This indicates that **13** instigated notable H_2O_2 generation (**Figure 3.2.5.1E**).

Graph of ROS Production vs HepG2 Cells
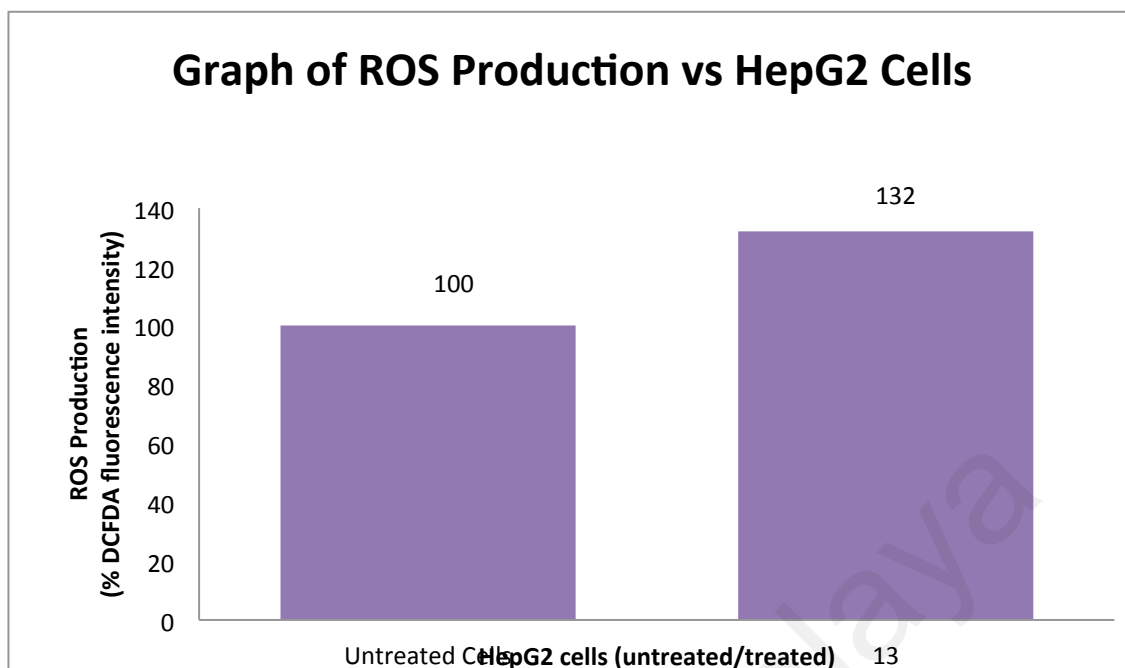
Figure 3.2.5.1E: Interaction of **13** with HepG2 cells giving rise to ROS production. Measurements were made after treatment at the IC_{50} dose of 0.53 μM for 16 h and labelled with carboxy-H2DCFDA for 1 h, prior to evaluating the fluorescence response

From this outcome, it is suggested that **13** activates the intrinsic pathway by boosting the ROS production and supressing the mitochondrial function, which imparts apoptotic cell death in HepG2 cells. Drugs which can injure the functional integrity of mitochondria could be of importance in anti-cancer therapy (Caruso *et al.*, 2007).

Not only that, we also found that the treatment of HepG2 cells with **13** brings about an extrinsic pathway by activating death receptors of the tumour necrosis factor receptor superfamily, member 6 (FAS) and the tumour necrosis factor receptor (TNFR1A) gene expression. Consequently, after the release of FAS and raising the enzymatic activities, caspase-8, -10, -9 and -3 were triggered (see **APPENDIX A**), **Table 3.2.5.1A** and **3.2.5.1B).**

Table 3.2.5.1A: Quantification of caspases -3/7, -8 and -9 in HepG2 in the presence of **13** by measuring the green fluorescent signal at excitation wavelength = 490 nm and emission wavelength = 520 nm. The green fluorescent signal shows the amount of active caspases existing in the cells at the time the reagent was added. The data were collected by taking the means and standard deviation from four independent experiments that were conducted in triplicate**.**

Caspase	Absorbance	
	Control	13
Caspase 3/7	126 ± 0.3	26946.0 ± 0.3
Caspase 8	135 ± 0.3	25782.0 ± 0.4
Caspase 9	130 ± 0.2	21805.0 ± 0.3

Table 3.2.5.1B: Quantification of AFC in HepG2 cell cultured in the presence of **13** upon cleavage of the AEVD-AFC substrate by caspase-10. AEVD-AFC emits blue light (λmax = 400 nm); upon cleavage of the substrate by caspase-10, free AFC emits yellow-green fluorescence (λmax = 505 nm). Means and standard deviations from four independent experiments conducted in triplicate

Caspase	Absorbance	
	Control	13
Caspase 10	124.0 ± 0.3	1483.0 ± 0.2

Generally, FAS and TNFR1 takes in the FAS-associated protein with death domain (FADD) together with procaspase-8 and -10 and incorporate them to the receptor. Procaspase-8 and procaspase-10 are controlled by FADD leading to auto-cleavage and activation that in turn triggers the effector caspase to start the cell death process(Abd El-Ghany *et. al.*, 2009; Thorburn, 2004).On the other hand, caspase-8 and -10 are able to cut the BCL-2 family member bid, a bridging death receptor that acts as a molecular linker, and also truncate BH3 interacting-domain death antagonist (tBID) which is linked to BAX, a pro-apoptotic protein via intercepting the mitochondria pathway causing a disturbance in the mitochondrial membrane potential and

deployment of cytochrome c(Gomes *et. al.*, 2005; LeBel *et. al.*, 1992; Yin, 2006). To support the claim in the proposed apoptotic pathway mechanisms, compound **13** was found to also express BID in HepG2 cells (see **APPENDIX A**).

Besides activating the mitochondrial and FAS death receptor apoptotic routes, **13** also instigates another death receptor-dependent pathway, a chain of pro-apoptotic genes, i.e. CD40 (CD40 gene), CD40L (CD40LG), TNF-α (TNF) and TNF-R1 (p55/TNFRSF1A) (see **APPENDIX A**). One of the genes, CD40 is a member of TNF family and is well known for its vital role in regulating immune and homeostasis (Loskog *et. al.*, 2009). Based on experimental evidence, it has been suggested that the CD40 pathway can be used in cancer therapy as it can restore an anti-tumour response in the host ensued by normalisation of the tumour microenvironment and arresting the growth of CD40-positive tumours (Loskog *et. al.*, 2009). Moreover, CD-40 also contains a death domain look-alike, cytoplasmic motif, which is involved in the commencement of TNF-R1 and CD95-dependent apoptosis, which in turn stimulates cell death in mesenchyme origin cells, tumour cells and a particular types of transformed cell lines (Airoldi *et al.*, 2003; Eliopoulos *et al.*, 1996; Hess *et al.*, 1998). Furthermore, CD-40 has the potential to activate membrane-anchored TNF-α and TNF-R1 (p55) and then caspase-8 and -3 to stimulate the death receptor-dependent pathway (Grell *et al.*, 1999).

In another route, in HepG2 cells, **13** also highly expressed death-associated protein kinase 1 (DAPK1), a tumour suppressor, by about 43-fold (see **APPENDIX A**). Significantly, over-expression of siDAPK1, aided the expression of the protein for transcription factor Rel/nuclear factor-kappaB (NF-κB)-targeted genes (Hess *et. al.*, 1996). Nf-κB plays an important role in balancing the gene transcription and in the process of cell proliferation (Kodama *et. al.*, 2005; Yoo *et. al.*, 2012). Protein expression for anti-proliferation genes (e.g. COX-2 and ICAM-1), and anti apoptosis

genes such as XIAP, which obstructs apoptosis triggered by a multiple variety of stimuli and initiates both the principle death pathways, was suppressed by DAPK1 *(LaCasse et. al.,* 1998). Due to its critical function in that it acts at the point of convergence of both extrinsic and intrinsic death pathways on effector caspase initiation, XIAP is rightfully classified as one of the most efficient apoptotic inhibitors (Eckelman *et. al.*, 2006). Put simply, XIAP suppresses the activities of a number of caspases, in particular caspases-3, -7 and -9, through the modulation of direct-enzyme inhibition or ubiquitin-mediated proteasome degradation (Eckelman *et al.*, 2006). Highly expressed in most cancer cells and tumour specimens, the deactivation of XIAP will cause cancer cells to undergo apoptosis(LaCasse, 2013; Yang *et. al.*, 2003). Notably, **13** significantly down-regulates XIAP after 24 h of treatment in HepG2 cells.

3.2.5.2 BISMUTH DIETHANOL DITHIOCARBAMATE

16 also causes an over-expression of pro-apoptotic genes alongside the suppression of anti-apoptotic genes after application to HepG2 cells. Both p53 (TP53) and p73 (TP73) were expressed concurrently. This outcome proves that the cytotoxicity of **16** is affiliated with the induction of p53/p73-dependent activation of the mitochondrial pathway of apoptosis, showing the anti-cancer properties.

Compound **16**discovered to stimulate p53 gene expression at a 10-fold increase over p73 expression as displayed in **APPENDIX A**. This shows that the up-regulation of p53/p73 genes causes DNA damage in HepG2 cells, which is compatible with the DNA fragmentation results (see section 3.2.3).

Besides that, the p21 encoded gene, CDKN1A, which is a major inhibitor of p53-dependent apoptosis (Gartel *et. al.*, 2002), was up-regulated 22-fold by **16** after 24 h (**Figure3.2.5.2A** and **Figure3.2.5.2B**).
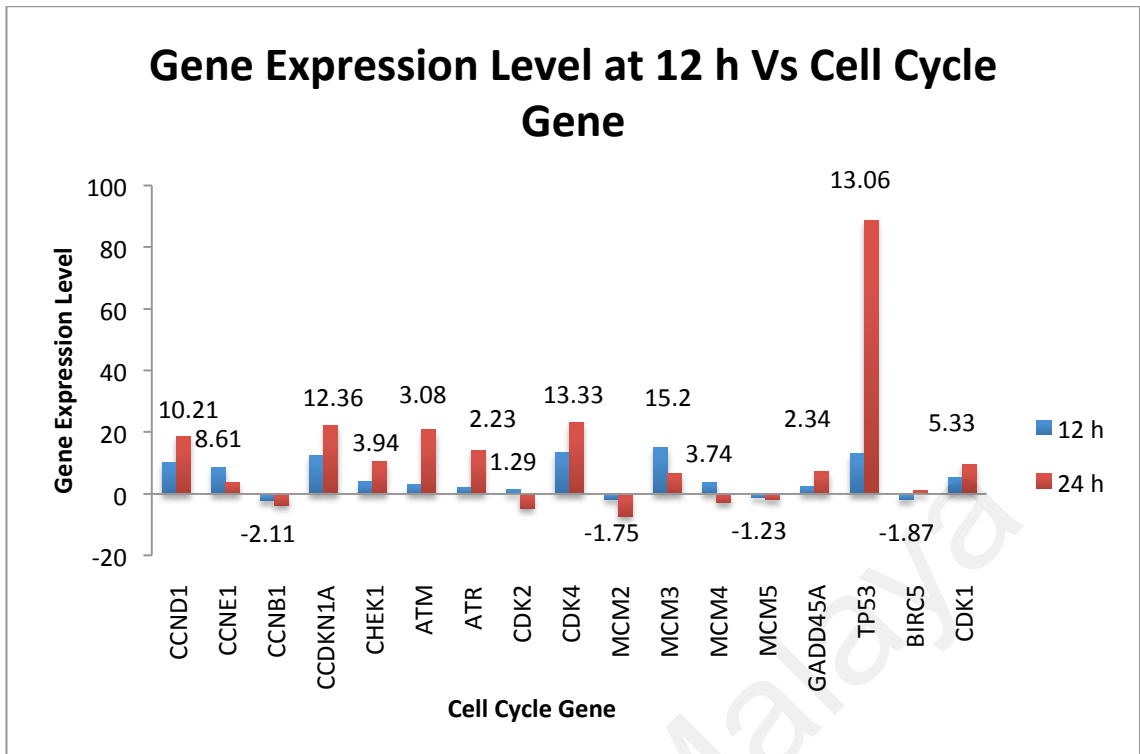
Figure 3.2.5.2A: Graph of gene expression levels after treatment with **16** against cell cycle gene. The data shows the gene expression levels after 12 h treatment
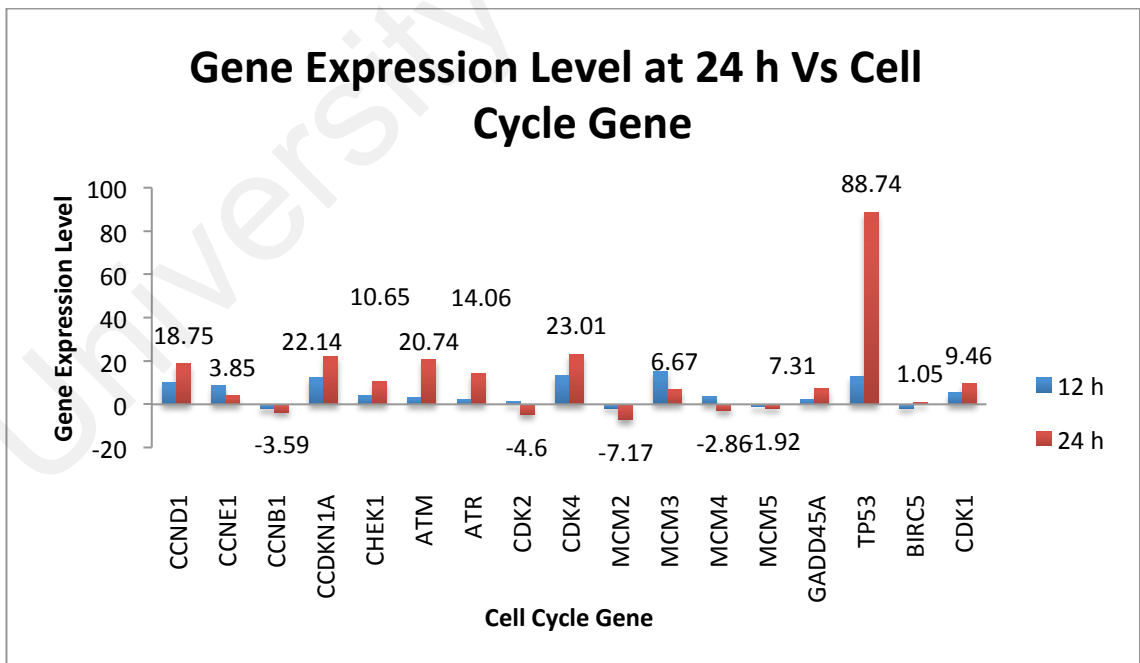
Figure 3.2.5.2B: Graph of gene expression levels after treatment with **16** against cell cycle gene. The data shows the gene expression levels after 24 h treatment

Further, the ATM protein was also up-regulate 21-fold after 24 h (**Figure 3.2.5.2A** and **Figure 3.2.5.2B**) by **13**, hence displaying the same outcome as for p53 gene expression.

16 also increased p73-induced apoptosis in the presence of c-Abl protein (Dobbelstein *et al.*, 2005) (see **APPENDIX A**). A cell death inducer, BNIP3L protein was highly expressed by 23-fold, in cells treated with **16** *via* p53 gene expression. This unveils the proof for the operation of the p53 gene as this in turn can increase the expression of the BNIP3L gene which is well known to be highly produced in wild-type p53-expressing cells (Fei *et al.*, 2004).

From the foregoing, **16** (see **APPENDIX A**) causes the deactivation of BCL-2, which in turn gives rise to BAX which increases the potential in the mitochondrial membrane without causing the disappearance of anti-apoptotic protein, BCL-2.

The presence of cytochrome c was notably extracted in HepG2 cells treated with**16** which assists in the activation of caspase-9, and thereby caspase-3 (see **APPENDIX A**). **Figure 3.2.5.2C** displays the downwards shift (from M2 to M1) in the fluorescence response due to presence of cytochrome c in treated HepG2 cells by **16** after 12 h and 24 h. Figure 3.2.5.1C (see section 3.2.5.1) shows that the negative control samples has low levels of cytochrome C loss.

Cellular ROS generation exceeded about 21% as compared to the negative control after treatment with **16**, which proves a pronounced generation of hydrogen peroxide, H_2O_2 (**Figure 3.2.5.2D**).

From this outcome, it is indicated that **16** activates the intrinsic pathway by boosting the ROS production and restrained the mitochondrial function which causes apoptotic cell death in HepG2 cells. Drugs which can injure the functional integrity of mitochondria could be of importance in anti-cancer therapy (Caruso *et al.*, 2007).
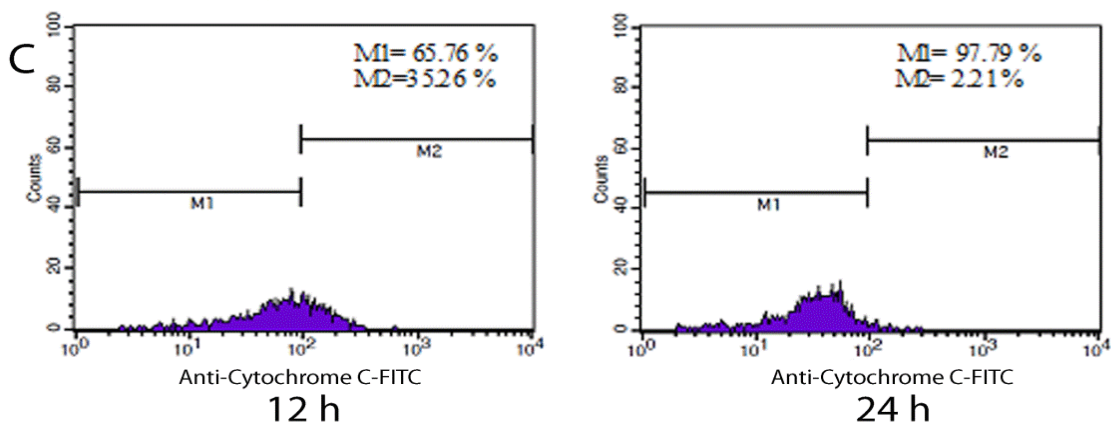
Figure 3.2.5.2C: Histograms showing cells stained using the FlowCellect Cytochrome C Kit^{TM} resulting from HepG2 cells treated with 55.9 μM of **16** for 12 h and 24 h
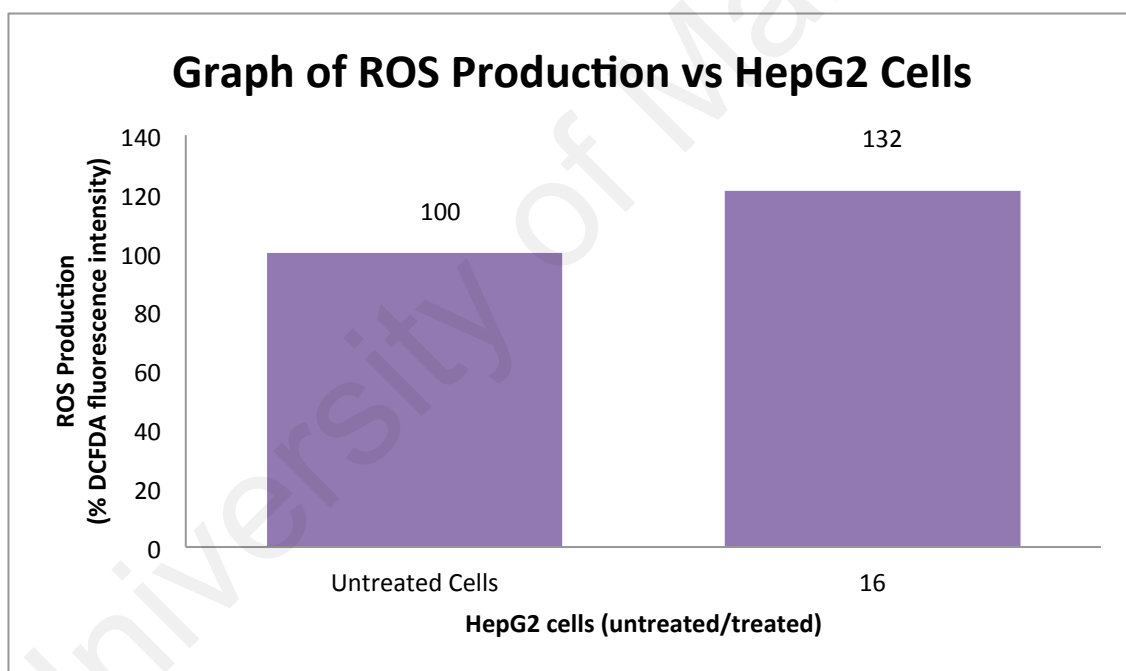
Figure 3.7.2D: Interaction of **16** with HepG2 cells giving rise to ROS production. Measurements were made after treatment at the IC$_{50}$ dose of 55.9 μM for 16 h and labelled with carboxy-H2DCFDA for 1 h, prior to evaluating the fluorescence response

Treatment of HepG2 cells by **16** also causes an extrinsic pathway in the same way as **13** whereby the release of FAS and the raising of enzymatic activities, caspase-8, -10, -9 and -3 were triggered (see **APPENDIX A**, **Table 3.2.5.2A** and **3.2.5.2B**).

Table 3.7.2A: Quantification of caspases -3/7, -8 and -9 in HepG2 in the presence of **16** by measuring the green fluorescent signal at excitation wavelength = 490 nm and emission wavelength = 520 nm. The green fluorescent signal shows the amount of active caspases exist in the cells at the time the reagent was added. Data were collected by taking the means and standard deviation from four independent experiments that were conducted in triplicate

Caspase	Absorbance	
	Control	16
Caspase 3/7	126.0 ± 0.3	6365.0 ± 0.3
Caspase 8	135.0 ± 0.3	22018.0 ± 0.4
Caspase 9	130.0 ± 0.2	13085.0 ± 0.3

Table 3.2.5.2B: Quantification of AFC in HepG2 cell cultured in the presence of **16** upon cleavage of the AEVD-AFC substrate by caspase-10. AEVD-AFC emits blue light (λmax = 400 nm); upon cleavage of the substrate by caspase-10, free AFC emits yellow-green fluorescence (λmax = 505 nm) (Means and standard deviations from four independent experiments conducted in triplicate)

Caspase	Absorbance	
	Control	16
Caspase 10	124.0 ± 0.3	12760.0 ± 0.2

Compound **16** was found to also express BID in HepG2 cells (see APPENDIX A) indicating the same apoptotic pathway mechanism as exerted by **13**.

Unlike **13**, **16** did not express a significant amount of death-associated protein kinase 1 (DAPK1), a tumour suppressor. This has the result of lowering the expression

of protein for transcription factor Rel/nuclear factor-kappaB (NF-κB)-targeted genes (Hess *et. al.*, 1996). The 5-fold increase of XIAP expression by **16** defers the cell death process in HepG2 cells. High amounts of XIAP will cause metastasis in cancer cells and increase the durability of cancer cell lines towards chemotherapy(LaCasse, 2013; Yang *et al.*, 2003).

3.2.6 CELL CYCLE ANALYSIS

To have an in-depth study in tumour growth operation, the comprehension of cell cycle analysis is the basic knowledge that needs to be revealed. The area of metal-based drugs has seen several gold compounds that displayed anti-cancer activities via the modulation of cell cycle and the obstruction of cancer cells growth (Gandin *et al.*, 2010; Gouvea *et al.*, 2012). In this particular study, HepG2 cells were treated with **13** and **16** at different time periods (6, 12 and 24 h) to inspect whether the growth-inhibitory effect was associated with the inauguration of cell cycle arrest and/or apoptosis. The cell cycle analysis was analysed using flow cytometry.

The principal mechanism in anti-cancer drug treatment is via cell cycle arrest and apoptosis (Bremer *et. al.*, 2006; Sakaue-Sawano *et. al.*, 2011). Prior to the present findings, some anti-cancer agents are found to arrest G_1 phase of the cell cycle together with the decrease in the expression of cyclin D1 and/or cyclin E in cancer cells (Cheng *et al.*, 2005; Oh *et. al.*, 2010).

Due to its important role in G_2/M phase regulation, cyclin B1 (CCNB1) combine with cdc2 (CDK1) to form a cdc2-cyclinB$_1$ complex. The shut down of the complex operation hindered the transition from the G_2 to M phase (Grana *et. al.*, 1995).Phosphate 3, cdc25c, which acts as a M-phase inducer, plays an essential role in the dephosphorylation of cdc2, hence precluding the activation of the cdc2-cyclinB$_1$

complex (Jin *et. al.*, 1996).Moreover, cyclin-dependent kinase inhibitor p21 (CDKN1A) controls the cell cycle process. Significantly, the level of p21 rises at the G_2/M transition in a number of cancer cells (Cho *et al.*, 2011; Dash *et al.*, 2005; Niculescu *et al.*, 1998; Zhao *et al.*, 2009).

Two protein kinases of the PI-3 PIKK family, ATM and Rad3-related protein, activate the signalling network to paralysed cell cycle progression thus terminating the DNA replication resulting in DNA damage. Crucial for regulating G2/M arrest after double-strands break is the serine/threonine-protein kinase (Chek1), an enzyme that is encoded in humans by the CHEK1 gene that causes the downgrading effects of ATR and ATM (Ting *et. al.*, 2004; Yarden *et. al.*, 2002). As a reaction to replication stress, both mitotic entry and S-phase replication were delayed by chek1, which thus stabilizes the stalled replication fork (Sorensen *et. al.*, 2012).

Research has shown that mini-chromosome maintenance (MCM) proteins of which six (MCM2-7), could be useful as proliferation markers in an array of cancers(Padmanabhan *et. al.*, 2004). Mainly, MCM proteins consist of a group of six highly conserved and highly homologous proteins that are essential in forming pre-replication complexes, which are accountable for permitting DNA replication (Takisawa *et. al.*, 2000). Hence, the increased expression in MCM proteins is pronounced in most premalignant proliferative states and solid tumours.

The p53 also play a significant role at the G_2/M checkpoint (Passalaris *et. al.*, 1999). Inauguration of GADD45 in a variety of cancer cells that leads to the initiation of p53, a retaliation to DNA damage (Zhan *et. al.*, 1994; Zhan et al., 1996). Furthermore, during the in vitro process, GADD45 was also found to effectively destabilize cdc2-cyclin B_1 complexes, indicating that the cause may be to accommodate cdc2/cyclin inactivation in vivo (Zhan et al., 1999).

3.2.6.1 Bismuth Diethyl Dithiocarbamate

The growth of HepG2 cells were inhibited by **13** through cell cycle arrest at S and G_2/M phases. This correlates with the decrease in the percentage of cells in G_0/G_1 phase at a time-dependent relationship up to 24 h (**Figure 3.2.6.1A** and **Figure 3.2.6.1B**). It was observed that the obvious changes in the cell population in the G_1 phase and in the case of proteins that are related to G_1 phase such as Ckd4 (**Figure 3.2.5.1A** and **Figure 3.2.5.1B**). Moreover, exposure to **13** was closely related to cellular phenotypic changes, examples being cell shrinkage and density (refer to **Figure 3.2.1**).
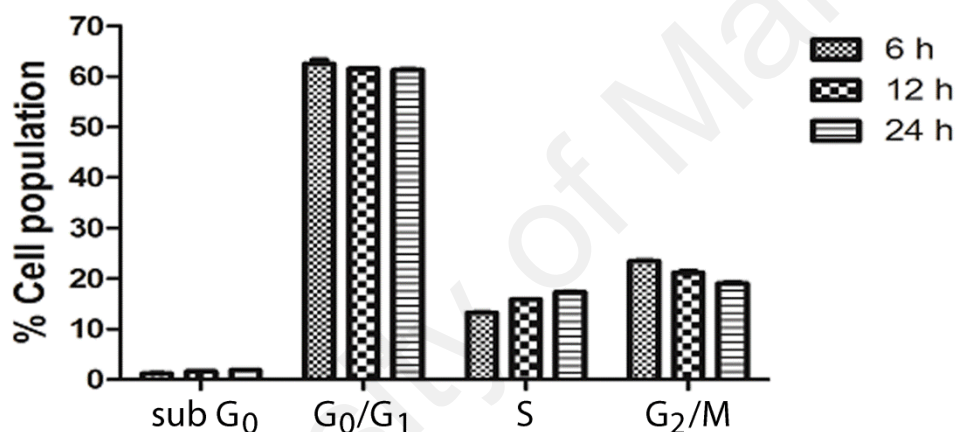
Figure 3.2.6.1A: Effect of **13** on cell cycle distribution in HepG2 cells. Cells were incubated at doses corresponding to the IC_{50} value (0.53 μM) for 6, 12 and 24 h and the cell cycle was ascertained by FACS analysis. The data are representative examples of triplicate independent tests. *pα0.05 versus control group
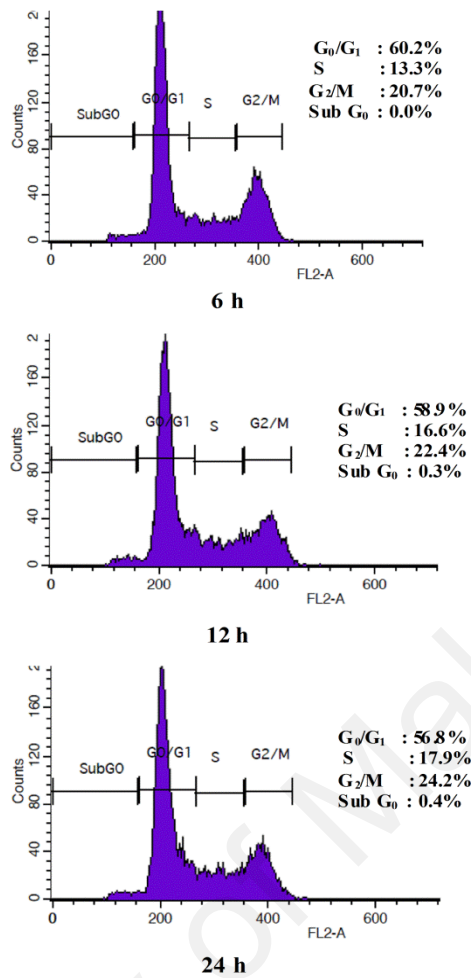
Figure 3.2.6.1B: Effect of **13** on cell cycle distribution in cultured HepG2 cells. Cells were incubated at doses of $IC_{50} = 0.53$ μm for 6, 12 and 24 h, the distribution was confirmed via FACS analysis

On the other hand, cell cycle analysis shows that upon application of **13** causes significant numbers ofHepG2 cells to be arrested at S and G_2/M phases. This is shown in the increase in cyclin D1 ($CCND_1$) and cyclin E ($CCNE_1$) expression after 24 h of treatment (**Figure 3.2.5.1B**). This suggests that the decrease in cyclin D1 and cyclin E1 production aids in the cell cycle arrest at the S phase via the modulation of the essential S phase passage.

The anti-cancer activities in HepG2 cells by 13 were partly caused by its potential to activate the growth inhibition at the G_2/M phase by down-regulating cdc2, cyclin B_1 and p21 gene expression. (See **Figure 3.2.5.1A**, **Figure3.2.5.1B** and **APPENDIX A**).

On the other hand, **13**also up-regulated CHEK1 after incubation for 24 h, by about 23-fold, together with ATR and ATM (see **Figure 3.2.5.1A** and **Figure 3.2.5.1B**). These results were verified by the flow cytometry analysis where **13** caused 24% of cell cycle arrest at the G_2/M checkpoint (see **Figure 3.2.6.1A**).

After treatment with **13**, a down-regulation of the MCM2-5 gene was observed thus reducing the expression of the MCM protein that acts as chemo-preventive agent (see **Figure 3.2.5.1A** and **Figure 3.2.5.1B**).

GADD45 on the other hand was up-regulated by around 15-fold after treatment with **13** as compared to the control (see **Figure 3.2.5.1A** and **Figure 3.2.5.1B**).

3.2.6.2 BISMUTH DIETHANOL DITHIOCARBAMATE

Complex **16** also inhibited the growth of HepG2 through cell cycle arrest at the S and G_2/M phases. Likewise, the increase in the number of cells at S and G_2/M phases was proportionate to the decrease in the percentage of cells at G_0/G_1 phase in a time-dependent relationship up to 24 h (**Figure 3.2.6.2A** and **Figure 3.2.6.2B**). Notable changes were observed in the cell population in the G_1 phase and on the contrary proteins that are related to G_1 phase such as Ckd4 (**Figure 3.2.5.2A** and **Figure 3.2.5.2B**). Furthermore, the introduction of **16** was linked to cellular phenotypic changes, for instance being cell shrinkage and density (refer to **Figure 3.2.2**).
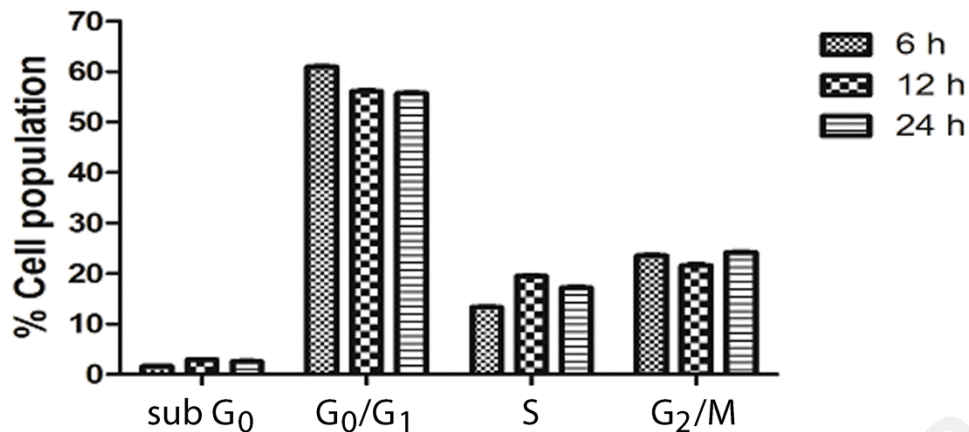
Figure 3.2.6.2A: Cell cycle distribution in HepG2 cells after treatment with **16**. Cells were incubated at doses corresponding to the IC_{50} value (55.9 μM) for 6, 12 and 24 h, and the cell cycle was ascertained by FACS analysis. The data are representative examples of triplicate independent tests. *pα0.05 versus control group.

Further, as a consequence to the exposure of **16**, the cell cycle analysis showed a significant numbers of HepG2 cells were arrested at the S and G_2/M phases, and decreases in the expression of cyclin D1 ($CCND_1$) and cyclin E ($CCNE_1$) after 24 h of incubation (**Figure 3.2.5.2B**). This shows the reduction in cyclin D1 and cyclin E1 production promotes cell cycle arrest at S phase to control the pivotal S phase passage.

The cytotoxicity activity caused by **16** in HepG2 cells was due to its potential to initiate the growth inhibition at the G_2/M phase by the down-regulation of cdc2, cyclin B_1 and p21 gene expression (see **Figure 3.2.5.2A**, **Figure 3.2.5.2A** and **APPENDIX A**).

Besides that, this observation **16** also up-regulated CHEK1 by about 11-fold after being applied for 24 h, together with ATR and ATM (see **Figure 3.2.5.2A** and **Figure 3.2.5.2B**). These findings were confirmed by the flow cytometry analysis where **16** affected the cell cycle arrest at G_2/M checkpoint by 18% (see **Figure 3.2.6.2A**).
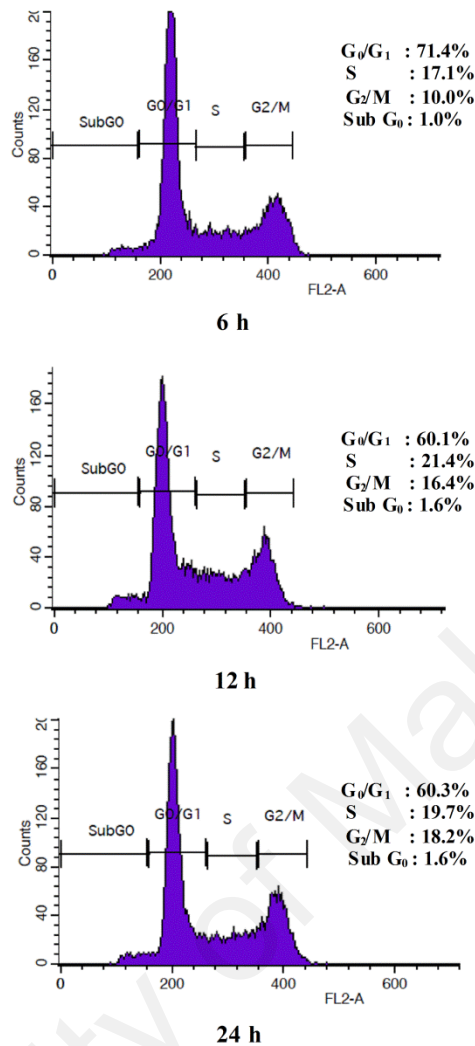
Figure 3.2.6.2B: Effect of **16** on cell cycle distribution in cultured HepG2 cells. Cells were incubated at doses of IC_{50} = 59 μm for 6, 12 and 24 h, and the distribution was confirmed via FACS analysis

After administration of **16**, theMCM2-5 gene was down-regulated therefore reducing the expression of the MCM protein (see **Figure 3.2.5.2A** and **Figure 3.2.5.2B**).

The outcome of treatment with **16** also shows that GADD45 was up-regulated by more or less 7-fold as compared to the control (see **Figure 3.2.5.2A** and **Figure 3.2.5.2B**).

What remains as a challenge in cancer treatment is metastasis, a process where tumour cells from the main tumour are being spread to other organs, which in turn happens to be one of the main cause of death in cancer patients (Eckhardt *et. al.*, 2012).

There are a few factors that are taken into account in cell invasion studies. For example the fact that Nuclear factor-kappa B (NF-кB) are activated by a survivin (BIRC5)-XIAP that leads to cell motility kinases focal adhesion kinase (FAK) and c-Src tyrosine kinase (c-Src) activation that eventually will usher in cancer progression and metastasis (Mehrotra *et. al.*, 2010). Being a heterodimeric DNA-binding protein, NF-кb inhere two crucial components, p50 and p65, has been established to have a great impact on the evolvement and distant metastasis of human carcinoma (Meylan *et. al.*, 2009; Pikarsky *et. al.*, 2004; Tan *et. al.*, 2011; Wu *et. al.*, 2009). Selectively bound to DNA, the activated NF-кB will pilot the expression of a wide variety of genes that will regulate apoptosis, assist cell proliferation, angiogenesis and stimulate invasion and metastasis (Park *et. al.*, 2007; Wu *et. al.*, 2009). Further, cell migration and invasion can be increased or decreased by an XIAP-deficiency in cell, under certain conditions (Mehrotra *et. al.*, 2010).

To date, a prevention of metastasis has not been found therefore study on tumour metastasis is of vital interest in cancer therapy.

3.2.7.1 BISMUTH DIETHYL DITHIOCARBAMATE

An invasion assay was carried out and it was found that **13** inhibited cell invasion. **Figure 3.2.7.2A** shows that after treatment with **13** at IC_{50} value of 0.53 μm,

the invasion rate of HepG2 Cells through matrigel (*pα0.05) decreased to 3.96 ± 0.52 % (normalized to 100 %).

Also found that down regulation of survivin and XIAP by **13**causes inhibition of metastasis in HepG2 cells (**Figure 3.2.7.2B**).

3.2.7.2 Bismuth Diethanol Dithiocarbamate

Compound **16** also expressed the decrement of invasion rate to 40.22 ± 2.36 % (normalized to 100 %) in HepG2 cells upon treatment with its IC_{50} value of 55. 9 μm (**Figure 3.2.7.2A** and **Figure 3.2.7.2B**).

| 1% DMSO only | **13** | **16** |
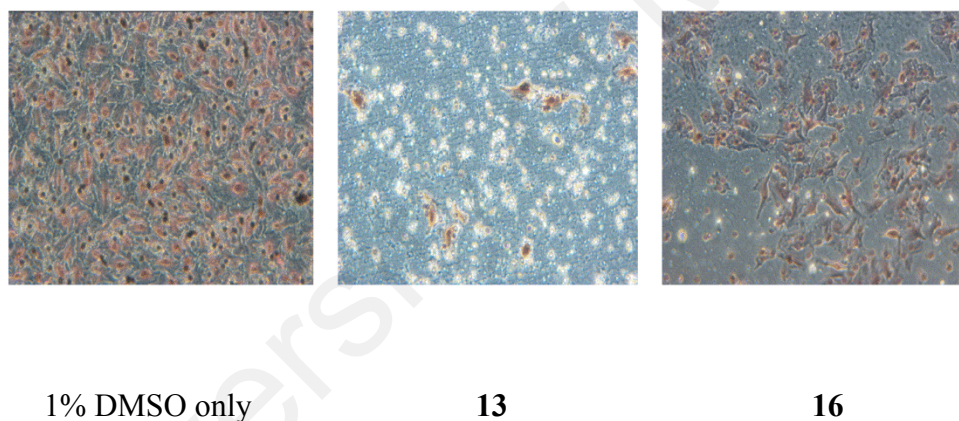
Figure 3.2.7.2A: Matrigel invasion assay showing **13** and **16** inhibited cell invasion. Photos were taken at 200× magnification and are representative of three independent experiments.
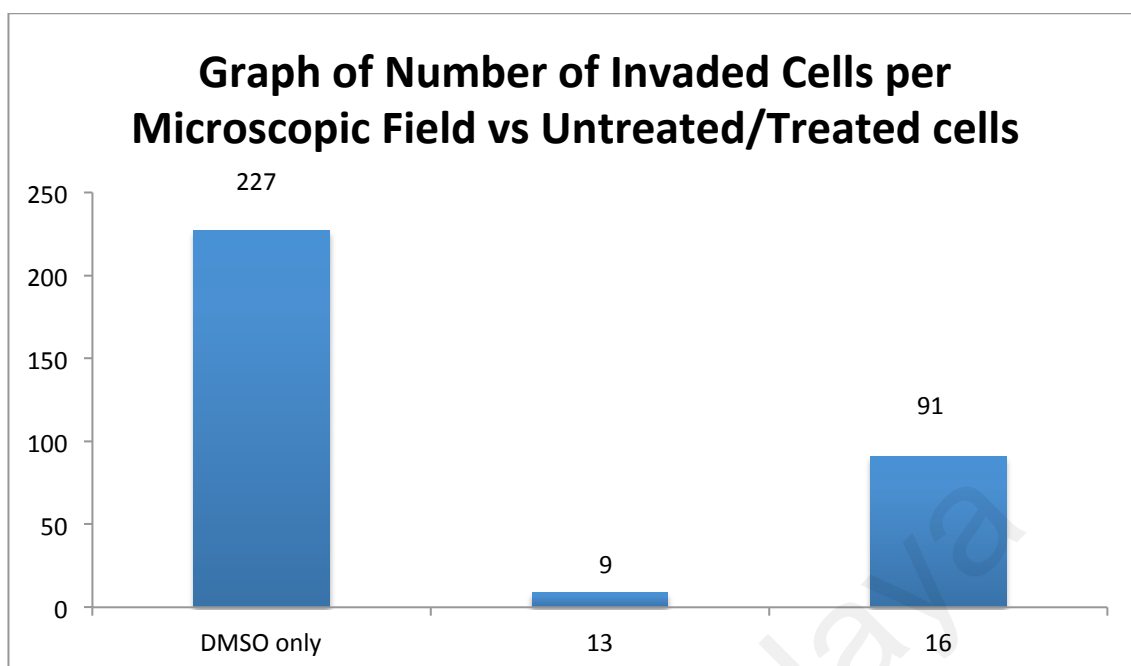
Figure 3.2.7.2B: Graphical representation of the numbers of invaded cells per microscopic field when treated with **13** and **16**. Data were shown as mean ± SEM from three independent experiments. *pα0.05, compared to DMSO only. The invasions rate of **13** and **16** are 3.96 ± 0.52 % and 40.22 ± 2.36 %, respectively (normalized to 100%).

CHAPTER 4 : CONCLUSION

A total of twelve bismuth and antimony complexes with six different dithiocarbamate ligands were successfully synthesized and fully characterised.

All twelve complexes were submitted to our collaborators at the Faculty of Medicine and Health Sciences, Universiti Putra Malaysia for further biological evaluation against an array of human carcinoma cell lines. At the present time, **13** was found to be exceptionally potent on HepG2 cells as compared to current drugs in use for HepG2 treatment. It's activity was compared to that exhibited by **16**, investigated due to it's greater solubility in water, hence, the initial thought that **16** could exert a higher potency towards HepG2 cells based on its water soluble ligand. The study proved otherwise.

To compliment research on partial biological properties, the twelve complexes could also be useful as synthetic precursors for Sb_2S_3 and Bi_2S_3 nanoparticle generation. The research on metal-based drugs and their nanoparticles can enhance the efficiency of the complexes as a drug or other medicinal purposes. To this end, twelve complexes have been sent out to University of Bath, United Kingdom, for an aerosol-assisted chemical vapour deposition (AAVD) study to determine their ability in this context. Three recommendations can be made out of this study are:

• To investigate more prospective bismuth compounds since they are generally non-toxic to humans despite being a non-essential metal in the body. One in particular is bismuth subgallate. It has been widely used as a remedy for various gastrointestinal diseases. However, due to its hydrophobic nature, future studies could improve its solubility properties and hence could diversify its medicinal use perhaps in cancer drug development

• Exploring othe rpotential metals. Examples such as arsenic, come to mind. Being in the same group as both bismuth and antimony, arsenic has similar chemical properties and thus possesses potential in drug development. Eventhough, arsenic is well known as a toxin and implicated as a carcinogenic agent, the rise of development in Trisenox (Arsenic Oxide) in the treatment of Acute Promyelocytic Leukaemia (Zhu *et. al.*, 2002) offers another dimension to exploit arsenic compounds. Various organoarsenic compounds also have been investigated for its medicinal properties. For example, 4-(N-(S-glutathionylacetyl)amino)AS, which was found to exhibit growth suppressing activity towards a variety of cancer cells (Dilda *et. al.*, 2005). It is highly possible for arsenic metal to form a complex with dithiocarbamate ligands which may exhibit good activity towards a range of carcinoma. Currently, two arsenic compounds, arsenic diethyl dithiocarbamate and arsenic pyrrolidine dithiocarbamate, have been synthesized and sent for initial biological evaluation to inspect its toxicity before any further tests to be made; result are not represented herein

• Enquire more on other equally active dithiocarbamate ligands, ethylene bis(dithiocarbamate) (EBDC), for example as such. This specific ligand has shown wide uses not only as a drug to cure fungi infections but has its own agricultural uses as well. EBDC could be complexed with bismuth and antimony to investigate its other possibilities and towards discovering enhanced drugs that are of vital importance in sustaining ones life

REFERENCES

Abd El-Ghany, R. M., Sharaf, N. M., Kassem, L. A., Mahran, L. G., & Heikal, O. A. (2009). Thymoquinone triggers anti-apoptotic signaling targeting death ligand and apoptotic regulators in a model of hepatic ischemia reperfusion injury. *Drug Discovery & Therapeutics, 3*(6), 296-306.

Airoldi, I., Lualdi, S., Bruno, S., Raffaghello, L., Occhino, M., Gambini, C., & Corrias, M. V. (2003). Expression of costimulatory molecules in human neuroblastoma. Evidence that CD40+ neuroblastoma cells undergo apoptosis following interaction with CD40L. *British Journal of Cancer, 88*(10), 1527-1536.

Aly, A. A., Brown, A. B., Bedair, T. M. I. & Ishak, E. A. (2012). Dithiocarbamate Salts: Biological Activity, Preparation, and Utility in Organic Synthesis. *Journal of Sulfur Chemistry, 33*(5), 605-607.

Amir, M. K., Khan, S. Z., Hayat, F., Hassan, A., Butler, I. S. & Rehman, Z. E. (2016). Anticancer activity, DNA-binding and DNA-denaturing aptitude of palladium(II) dithiocarbamates. *Journal of Sulfur Chemistry, 452*, 31-40.

Banti, C. N., Kourkoumelis, N., Tsiafoulis, C. G., Skoulika, S., & Hadjikakou, S. K. (2017). Silver(I) complexes of methyl xanthate against human adenocarcinoma breast cancer cells. *Polyhedron, 121*, 115-122.

Barlow, C., Brown, K. D., Deng, C. X., Tagle, D. A., & Wynshaw-Boris, A. (1997). Atm selectively regulates distinct p53-dependent cell-cycle checkpoint and apoptotic pathways. *Nature Genetics, 17*(4), 453-456.

Bhalla, R., Burt, J., Hector, A. L., Levason, W., Luthra, S. K., McRobbie, G., Monzittu, F. M. & Reid, G. (2016). Complexes of aluminium, gallium and indium trifluorides with neutral oxygen donor ligands: Synthesis, properties and reactions. *Polyhedron, 106*, 65-74.

Bodenner, D. L., Dedon, P. C., Keng, P. C. & Borch, R. (1986). Effect of Diethyldithiocarbamate on *cis*-Diamminedichloroplatinum(II)-induced Cytotoxicity, DNA Cross-Linking, and γ-Glutamyl Transpeptidase Inhibition. *Cancer Research, 46*, 2745-2750.

Bremer, E., van Dam, G., Kroesen, B. J., de Leij, L., & Helfrich, W. (2006). Targeted induction of apoptosis for cancer therapy: current progress and prospects. *Trends in Molecular Medicine, 12*(8), 382-393.

Caruso, F., Villa, R., Rossi, M., Pettinari, C., Paduano, F., Pennati, M. & Zaffaroni, N. (2007). Mitochondria are primary targets in apoptosis induced by the mixed phosphine gold species chlorotriphenylphosphine-1,3-bis(diphenylphosphino)propanegold(I) in melanoma cell lines. *Biochemical Pharmacology, 73*(6), 773-781.

Chauhan, H. P. S., Carpenter, J. & Joshi, S. (2014). M Synthetic aspects, spectral, thermal studies and antimicrobial screening on *bis*(*N,N*-

dimethyldithiocarbamato-*S,S′*)antimony(III) complexes with oxo or thio donor ligands. *Spectrochimica Acta Part A: Molecular and Biomolecular Spectroscopy, 130*, 230-237.

Chauhan, H. P. S., Joshi, S. & Carpenter, J. (2016). Mixed bismuth(III) complexes with sulfur donor ligands. *Journal of Analysis and Calorimetry, 124*(1), 117-130.

Cheng, C. C., Yang, S. M., Huang, C. Y., Chen, J. C., Chang, W. M., & Hsu, S. L. (2005). Molecular mechanisms of ginsenoside Rh2-mediated G1 growth arrest and apoptosis in human lung adenocarcinoma A549 cells. *Cancer Chemotherapy & Pharmacology, 55*(6), 531-540.

Chian S. L. & Tiekink, E. R. T. (2007). Prevalence of intermolecular Bi … S interactions in bismuth dithiocarbamate compounds: $Bi(S_2CNR_2)_3$. *Zeitschrift Fur Kristallographie, 222*, 532.

Cho, J. H., Lee, J. G., Yang, Y. I., Kim, J. H., Ahn, J. H., Baek, N. I. & Choi, J. H. (2011). Eupatilin, a dietary flavonoid, induces G2/M cell cycle arrest in human endometrial cancer cells. *Food & Chemical Toxicology, 49*(8), 1737-1744.

Collinson, S. R. & Schröder, M. (2011). *Encyclopedia of Inorganic and Bioinorganic Chemistry*. Wiley: John Wiley & Sons.

Dash, B. C., & El-Deiry, W. S. (2005). Phosphorylation of p21 in G2/M promotes cyclin B-Cdc2 kinase activity. *Molecular and Cellular Biology, 25*(8), 3364-3387.

Dilda, P. J., Don, A. S., Tanabe, K. M., Higgins, V. J., Allen, J. D., Dawes, I. W. & Hogg, P. J. (2005). *Journal of the National Cancer Institute, 97*, 1539-1547.

Dobbelstein, M., Strano, S., Roth, J., & Blandino, G. (2005). p73-induced apoptosis: a question of compartments and cooperation. *Biochemical and Biophysical Research Communication, 331*(3), 688-693.

Eckelman, B. P., Salvesen, G. S., & Scott, F. L. (2006). Human inhibitor of apoptosis proteins: why XIAP is the black sheep of the family. *EMBO Reports, 7*(10), 988-994.

Eckhardt, B. L., Francis, P. A., Parker, B. S., & Anderson, R. L. (2012). Strategies for the discovery and development of therapies for metastatic breast cancer. *Nature Reviews Drug Discovery, 11*(6), 479-497.

Eliopoulos, A. G., Dawson, C. W., Mosialos, G., Floettmann, J. E., Rowe, M., Armitage, R. J. & Young, L. S. (1996). CD40-induced growth inhibition in epithelial cells is mimicked by Epstein-Barr Virus-encoded LMP1: involvement of TRAF3 as a common mediator. *Oncogene, 13*(10), 2243-2254.

Eskes, R., Antonsson, B., Osen-Sand, A., Montessuit, S., Richter, C., Sadoul, R., & Martinou, J. C. (1998). Bax-induced cytochrome C release from mitochondria is independent of the permeability transition pore but highly dependent on Mg^{2+} ions. *Journal of Cell Biology, 143*(1), 217-224.

Fei, P., Wang, W., Kim, S. H., Wang, S., Burns, T. F., Sax, J. K. & El-Deiry, W. S. (2004). Bnip3L is induced by p53 under hypoxia, and its knockdown promotes tumor growth. *Cancer Cell, 6*(6), 597-609.

Ferreira, I. P., Piló, E. D. L., Recio-Despaigne, A. A., Da Silva, J. G., Ramos, J. P., Marques, L. B., Prazeres, P. H. D. M., Takahashi, J. A. & Souza-Fagundes, E. M. (2016). Bismuth(III) complexes with 2-acetylpyridine- and 2-benzoylpyridine-derived hydrazones: Antimicrobial and cytotoxic activities and effects on the clonogenic survival of human solid tumor cells. *Bioorganic & Medicinal Chemistry, 24*, 2988–2998.

Fesik, S. W. (2005). Promoting apoptosis as a strategy for cancer drug discovery. *Nature Reviews Cancer, 5*(11), 876-885.

Fiorillo, A. A. & Galbraith, G. M. (2004). A Valence Bond Description of Coordinate Covalent Bonding. *The Journal of Physical Chemistry, 108* (23), 5126-5130.

Foglieni, C., Meoni, C. & Davalli, A. M. (2001). Fluorescent dyes for cell viability: an application on prefixed conditions. *Histochemistry and Cell Biology, 115*(3), 223-229.

Frézard, F., Martins, P. S., Barbosa, M. C. M., Pimenta, A. M., Ferreira, W. A., de Melo, J. E., Mangrum, J. B. & Demicheli, C. (2008). *Journal of Inorganic Biochemistry, 102*, 656-665.

G, Hogarth. (2012). Metal-dithiocarbamate complexes: chemistry and biological activity. *Mini Reviews in Medicinal Chemistry, 12*, 1202 - 12015.

Gandin, V., Fernandes, A. P., Rigobello, M. P., Dani, B., Sorrentino, F., Tisato, F. & Marzano, C. (2010). Cancer cell death induced by phosphine gold(I) compounds targeting thioredoxin reductase. *Biochemical Pharmacology, 79*(2), 90-101.

Gartel, A. L. & Tyner, A. L. (2002). The role of the cyclin-dependent kinase inhibitor p21 in apoptosis. *Molecular Cancer Therapeutics, 1*(8), 639-649.

Garnovskii, A. D., Burlov, A. S., Lysenko, K. A., Garnovskii, D. A., Borodkina, G. I., Ponomarenko, A. G., Chigarenko, G. G., Nikolaevskii, S. A. & Minkin, V. I. (2009). Tribochemically active chelate complexes of salicylideneimines. *Russian Journal of Coordination Chemistry, 35*, 120.

Ge, G. R. & Sun, H. (2007). Bioinorganic Chemistry of Bismuth and Antimony: target Sites for Metallodrugs. *Accounts of Chemical Research, 40*, 267-274.

Gomes, A., Fernandes, E., & Lima, J. L. (2005). Fluorescence probes used for detection of reactive oxygen species. *Journal of Biochemical and Biophysical Methods, 65*(2-3), 45-80.

Gouvea, L. R., Garcia, L.S., Lachter, D. R., Nunes, P. R., de Castro Pereira, F., Silveira-Lacerda, E. P. & Teixeira, L. R. (2012). Atypical fluoroquinolone gold(III) chelates as potential anticancer agents: relevance of DNA and protein interactions for their mechanism of action. *European Journal of Medicinal Chemistry, 55*, 67-73.

Grana, X., & Reddy, E. P. (1995). Cell cycle control in mammalian cells: role of cyclins, cyclin dependent kinases (CDKs), growth suppressor genes and cyclin-dependent kinase inhibitors (CKIs). *Oncogene, 11*(2), 211-219.

Grell, M., Zimmermann, G., Gottfried, E., Chen, C. M., Grunwald, U., Huang, D. C. & Strasser, A. (1999). Induction of cell death by tumour necrosis factor (TNF) receptor 2, CD40 and CD30: a role for TNF-R1 activation by endogenous membrane-anchored TNF. *EMBO Journal, 18*(11), 3034-3043.

Gross, A., McDonnell, J. M., & Korsmeyer, S. J. (1999). BCL-2 family members and the mitochondria in apoptosis. *Genes & Development, 13*(15), 1899-1911.

Haldar, A. K., Sen, P. & Roy, S. (2011). Use of Antimony in the Treatment of Leishmaniasis: Current Status and Future Directions. *Molecular Biology International, 2011*.

Han, A., Ozturk, I. I., Banti, C. N., Kourkoumelis, N., Manoli, M., Tasiopoulus, A. J., Owczarzak, A. M., Kubicki, M. & Hadijikakou, S. K. (2014). Antimony (III) halide compounds of thioureas: Structures and Biological Activity. *Polyhedron, 79*, 151-160.

Handong Y., Chuanhua, W. & Yong W. (2004). *Indian Journal of Chemistry, Section A:Inorganic,Bio-inorganic,Physical,Theoretical and Analytical Chemistry, 43*, 1439.

Handong Y., Zhai, J., Yu-Ying, S. & Da-Qi W. (2008). Synthesis, characterizations and crystal structures of new antimony (III) complexes with dithiocarbamate ligands. *Polyhedron, 27*(2), 663-670.

Hannon, M. J. (2007). Metal-based anticancer drugs: From a past anchored in platinum chemistry to a post-genomic future of diverse chemistry and biology. *Pure and Applied Chemistry, 79*(12), 2243-2261.

Hess, S., & Engelmann, H. (1996). A novel function of CD40: induction of cell death in transformed cells. *The Journal of Experimental Medicine, 183*(1), 159-167.

Hess, S., Gottfried, E., Smola, H., Grunwald, U., Schuchmann, M., & Engelmann, H. (1998). CD40 induces resistance to TNF-mediated apoptosis in a fibroblast cell line. *European Journal of Immunology, 28*(11), 3594-3604.

Hongyu, L., Chian, S. L., Jinzhu, W., Ho, P. C., de Vos, D. & Tiekink, E. R. T. (2007). Cytotoxicity, qualitative structure–activity relationship (QSAR), and anti-tumor activity of bismuth dithiocarbamate complexes. *Journal of Inorgnic Biochemistry, 101*, 809-816.

Jabali, B. & Ali, H. A. (2016). New zinc(II) complexes of the Non-steroidal Anti-Inflammatory Drug (indomethacin) and various nitrogen donor ligands. Synthesis, characterization and biological activity. *Polyhedron, 117*, 249-258.

Jamaludin, N. Z., Zheng-Jie, G., Yoke, K. C., Kok-Pian, A., Jiun, H. S., Chai, H. K., Abidin, F. Z., Halim, S. N. A. & Ng, S. W. (2013). Phosphanegold(I) dithiocarbamates, $R_3PAu[SC(=S)N(^iPr)CH_2CH_2OH]$ for R = Ph, Cy and Et:

Role of phosphane-bound R substituents upon in vitro cytotoxicity against MCF-7R breast cancer cells and cell death pathways. *European Journal of Medicinal Chemistry, 67*, 127-141.

Joshi, S., Chauhan, H. P. S. & Carpenter, N. (2017). Preparation, spectroscopic characterization and antimicrobial activities of mixed metal (Sb and Bi) bridged derivatives with mixed sulfur donor ligands. *Journal of Molecular Structure, 1128*, 221-229.

Jin, P., Gu, Y., & Morgan, D. O. (1996). Role of inhibitory CDC2 phosphorylation in radiation-induced G2 arrest in human cells. *Journal of Cell Biology, 134*(4), 963-970.

Low, K. Y., Baba, I., Farina, Y., Othman, A. H., Ibrahim, A. R. Fun, H-K. & Ng, S. W. (2001). *Main Group Metal Chemistry, 24*, 451.

Kant, R., Chandrashekar, A. K. & Kumar, A. (2008). Synthesis and Biological Activity on Some Organoantimony (III) Compounds. *Phosphorus, Sulfur and Silicon, 183*, 1410-1419.

Kapuscinski J., Darzynkiewicz Z., Melamed M. R. & Traganos F. (1983). Interactions of acridine orange with nucleic acid: properties of acridine orange with single stranded ribonucleic acid. *Biochemical Pharmacology, 32*(24), 3679-3664.

Kavounis, C. A., Kokkou, S. C., Rentzeperis, P. J. & Karagiannidis, P. (1980). *Acta Crystallographica Section B: Structural Science, Crystal Engineering and Materials, 36*, 2954.

Kemahli, E., Yildiz, M., Firat, T., Özyalvaçli, M. E., Üyetürk, U., Yilmaz, B. & Gücük, A. (2016). An experimental study on effects of pyrrolidine dithiocarbamate on ischemia-reperfusion injury in testis. *Canadian Urological Association Journal, 10*(3-4), E104–E109.

Kodama, N., Asakawa, A., Inui, A., Masuda, Y., & Nanba, H. (2005). Enhancement of cytotoxicity of NK cells by D-Fraction, a polysaccharide from Grifola frondosa. *Oncology Reports, 13*(3), 497-502.

Kotnik, M., Oblak, M., Canderluh, P.S., Pre-zelj, A., Humljan, J., Plantan, I., Urleb, U. & Solmajer, T. (2008). *WO2008043733A*.

Krammer, P. H. (1999). CD95(APO-1/Fas)-mediated apoptosis: live and let die. *Advances in Immunology, 71*, 163-210.

Kroemer, G., Galluzzi, L. & Brenner, C. (2007). Mitochondrial membrane permeabilization in cell death. *Physiological Reviews, 87*(1), 99-163.

Kroemer, G., Galluzzi, L., Vandenabeele, P., Abrams, J., Alnemri, E. S. & Baehrecke, E. H. (2009). Classification of cell death: recommendations of the Nomenclature Committee on Cell Death. *Cell Death & Differentiation, 16*(1), 3-11.

LaCasse, E. C. (2013). Pulling the plug on a cancer cell by eliminating XIAP with AEG35156. *Cancer Letters, 332*(2), 215-224.

LaCasse, E. C., Baird, S., Korneluk, R. G., & MacKenzie, A. E. (1998). The inhibitors of apoptosis (IAPs) and their emerging role in cancer. *Oncogene, 17*(25), 3247-3259.

Lal, Nand. (2014). Dithiocarbamates: A Versatile Class of Compounds in Medicinal Chemistry. *Chemistry & Biology Interface, 4*(6), 321-340.

Lalagani, A., Sardashti, M. K., Khalaj, M., Gajda, R. & Woźniak, K. (2017). Syntheses and structural characterization of Cu(II) and Mn(II) coordination polymers with the neutral flexible bidentate N-donor ligands. *Inorganica Chimica Acta, 457*, 136-144.

Le Bras, M., Clement, M. V., Pervaiz, S., & Brenner, C. (2005). Reactive oxygen species and the mitochondrial signaling pathway of cell death. *Histology & Histopathology, 20*(1), 205-219.

LeBel, C. P., Ischiropoulos, H., & Bondy, S. C. (1992). Evaluation of the probe 2',7'-dichlorofluorescin as an indicator of reactive oxygen species formation and oxidative stress. *Chemical Research in Toxicology, 5*(2), 227-231.

Li, H., Lai, C. S., Wu, J., Ho, P. C., de Vos, D., & Tiekink, E. R. (2007). Cytotoxicity, qualitative structure-activity relationship (QSAR), and anti-tumor activity of bismuth dithiocarbamate complexes. *Journal of Inorganic Biochemistry, 101*(5), 809-816.

Li, L. Y., Luo, X., & Wang, X. (2001). Endonuclease G is an apoptotic DNase when released from mitochondria. *Nature, 412*(6842), 95-99.

Liebmann, J. E., Cook, J.A., Lipschlutz, C., Teangue, D., Gisher, J. & Mitchell, J.B. (1993). *British Journal of Cancer, 68*, 1104-1109.

Lippert, B. & Miguel, P. J. S. (2016). *Coordination Chemistry Reviews, 327-328*, 333-348.

Loskog, A. S., & Eliopoulos, A. G. (2009). The Janus faces of CD40 in cancer. *Seminars in Immunology, 21*(5), 301-307.

Martirosyan, G. G., Kurtikyan, T. S., Azizyan, A. S., Iretskii, A. V. & Ford, P. C. (2013). Crystal structure, antibacterial and cytotoxic activities of a new complex of bismuth(III) with sulfapyridine. *Journal of Inorganic Biochemistry, 121*, 129-133.

Marzano I. M. (1), Franco M. S., Silva, P. P., Augusti, R., Santos, G. C., Fernandes, N. G., Bucciarelli-Rodriguez, M., Chartone-Souza, E. & Pereira-Maia, E. C. (2013). Crystal structure, antibacterial and cytotoxic activities of a new complex of bismuth(III) with sulfapyridine. *Molecules, 18*(2), 1464-1476.

Mensforth, E. J., Languino, L. R. & Batten, S. R. (2013). Coordination polymers of sulphur-donor ligands. *Inorganica Chimica Acta, 403*, 9-24.

Mehrotra, S., Hill, M. R., Raskett, C. M., Mercurio, A. M., Dohi, T., & Altieri, D. C. (2010). IAP regulation of metastasis. *Cancer Cell, 17*(1), 53-64.

Meylan, E., Dooley, A. L., Feldser, D. M., Shen, L., Turk, E., Ouyang, C., & Jacks, T. (2009). Requirement for NF-kappa B signalling in a mouse model of lung adenocarcinoma. *Nature, 462*(7269), 104-107.

Milacic, V., Chen, D., Giovagnini, L., Diez, A., Fregona, D., & Doua, Q. P. (2008). Pyrrolidine dithiocarbamate-zinc(II) and -copper(II) complexes induce apoptosis in tumor cells by inhibiting the proteasomal activity. *Toxicology and Applied Pharmacology, 231*(1), 24-33.

Nabipour, H., Ghammamy, S., Ashuri, S. & Aghbolagh, Z. S. (2010). Synthesis of a New Dithiocarbamate Compound and Study of Its Biological Properties. *The Journal of Organic Chemistry, 2*, 57-80.

Niculescu, A. B. (3), Chen, X., Smeets, M., Hengst, L., Prives, C., & Reed, S. I. (1998). Effects of p21(Cip1/Waf1) at both the G1/S and the G2/M cell cycle transitions: pRb is a critical determinant in blocking DNA replication and in preventing endoreduplication. *Molecular and Cellular Biology, 18*(1), 629-643.

Oh, H. L., Lee, D. K., Lim, H., & Lee, C. H. (2010). HY253, a novel decahydrofluorene analog, from Aralia continentalis, induces cell cycle arrest at the G1 phase and cytochrome c-mediated apoptosis in human lung cancer A549 cells. *Journal of Ethnopharmacology, 129*(1), 135-139.

Ozturk, I. I., Banti, C. N., Kourkoumelis, N., Manos, M. J., Tasiopoulos, A. J., Owczarzak, A. M., Kubicki, M. & Hadjikakou, S. K. (2014). Synthesis, characterization and biological activity of antimony(III) or bismuth(III) chloride complexes with dithiocarbamate ligands derived from thiuram degradation. *Polyhedron, 67*, 89-103.

Padmanabhan, V., Callas, P., Philips, G., Trainer, T. D., & Beatty, B. G. (2004). DNA replication regulation protein Mcm7 as a marker of proliferation in prostate cancer. *Journal of Clinical Pathology, 57*(10), 1057-1062.

Palanichamy, K., Sreejayan, N., & Ontko, A. C. (2012). Overcoming cisplatin resistance using gold(III) mimics: anticancer activity of novel gold(III) polypyridyl complexes. *Journal of Inorganic Biochemistry, 106*(1), 32-42.

Park, B. K., Zhang, H., Zeng, Q., Dai, J., Keller, E. T., Giordano, T., & Wang, C. Y. (2007). NF-kappaB in breast cancer cells promotes osteolytic bone metastasis by inducing osteoclastogenesis via GM-CSF. *Nature Medicine, 13*(1), 62-69.

Passalaris, T. M., Benanti, J. A., Gewin, L., Kiyono, T., & Galloway, D. A. (1999). The G(2) checkpoint is maintained by redundant pathways. *Molecular and Cellular Biology, 19*(9), 5872-5881.

Petit, P. X., Susin, S. A., Zamzami, N., Mignotte, B., & Kroemer, G. (1996). Mitochondria and programmed cell death: back to the future. *Febs Letters, 396*(1), 7-13.

Pikarsky, E., Porat, R. M., Stein, I., Abramovitch, R., Amit, S., Kasem, S. & Ben-Neriah, Y. (2004). NF-kappaB functions as a tumour promoter in inflammation-associated cancer. *Nature, 431*(7007), 461-466.

Qu, L., Zhang, M., Li, L. & Shu, W. Y. (1996). Synthesis and application of antimony

and N,N-diethyldithiocarbamate. *Transactions of Nonferrous Metals Society of China, 6*(3), 54-57.

Que, M., Zhang, Y. C., Liu, Z. D. & Zhou, H. P. (2009). *Acta Crystallographica Section E: Structure Reports Online, 65*, m311.

Qiao, L., & Wong, B. C. (2009). Targeting apoptosis as an approach for gastrointestinal cancer therapy. *Drug Resistance Updates, 12*(3), 55-64.

Rowinsky, E. K. (2005). Targeted induction of apoptosis in cancer management: The emerging role of tumor necrosis factor-related apoptosis-inducing ligand receptor activating agents. *Journal of Clinical Oncology, 23*(36), 9394-9407.

Ruizhuo, O., Yang, Y., Xiao, T., Kai, F., Yaoqin, Y, Huihong, T., Xiaoshen, Z., Tianyu, Z., Penghui, C., Fei, X., Ning, G., Yuhao, L. & Yuqing, M. (2017). Potent anticancer activity of a new bismuth (III) complex against human lung cancer cells. *Journal of Inorganic Biochemistry, 168*, 18-26.

Sadler, P. J., Li, H. & Sun, H. (1999). Coordination Chemistry of Metals in Medicine: Target Sites for Bismuth. *Coordination Chemistry Reviews, 185-186*, 689-709.

Saelens, X., Festjens, N., Vande Walle, L., van Gurp, M., van Loo, G., & Vandenabeele, P. (2004). Toxic proteins released from mitochondria in cell death. *Oncogene, 23*(16), 2861-2874.

Sakaue-Sawano, A., Kobayashi, T., Ohtawa, K., & Miyawaki, A. (2011). Drug-induced cell cycle modulation leading to cell-cycle arrest, nuclear mis-segregation, or endoreplication. *BMC Cell Biology, 12*, 2.

Samejima, K., & Earnshaw, W. C. (2005). Trashing the genome: the role of nucleases during apoptosis. *Nature Reviews Molecular Cell Biology, 6*(9), 677-688.

Schreck, R., Meier, B., Mannel, D. M., Droge, W. & Baeuerle, P. A. (1992). Dithiocarbamates as Potent Inhibitors of Nuclear Factor kB Activation in Intact Cells. *Journal Experimental Medicine, 175*, 1181-1194.

Skulachev, V. P. (1996). Why are mitochondria involved in apoptosis? Permeability transition pores and apoptosis as selective mechanisms to eliminate superoxide-producing mitochondria and cell. *Febs Letters, 397*(1), 7-10.

Sorensen, C. S., & Syljuasen, R. G. (2012). Safeguarding genome integrity: the checkpoint kinases ATR, CHK1 and WEE1 restrain CDK activity during normal DNA replication. *Nucleic Acids Research, 40*(2), 477-486. 7

Sun, H. (2011). Biological chemistry of arsenic, antimony and bismuth.

Sun, H., Zhang, L., & Szeto, K. Y. (2004). Bismuth in medicine. *Metal Ions in Biological System, 41*, 333-378.

Sun, R. Z., Guo, Y. C., Liu, W. M., Chen, S. Y. & Feng, Y. Q. (2012). Syntheses, Crystal Structures and Antibacterial Activities of Complexes [(C9H18NS2)3M(III)] (M = Sb and Bi). *Jiegou Huaxue, 31*, 655.

Takisawa, H., Mimura, S., & Kubota, Y. (2000). Eukaryotic DNA replication: from pre-replication complex to initiation complex. *Current Opinion in Cell Biology, 12*(6), 690-696.

Tamilvanan, S., Gurumoorthy, G., Thirumaran, S. & Ciattini, S. (2017). E Synthesis, characterization, cytotoxicity and antimicrobial studies on Bi(III) dithiocarbamate complexes containing furfuryl group and their use for the preparation of Bi_2O_3 nanoparticles. *Polyhedron 121*, 70-79.

Tan, W., Zhang, W., Strasner, A., Grivennikov, S., Cheng, J. Q., Hoffman, R. M., & Karin, M. (2011). Tumour-infiltrating regulatory T cells stimulate mammary cancer metastasis through RANKL-RANK signalling. *Nature, 470*(7335), 548-553.

Tan, Y. S., Ooi, K. K., Ang, K. P., Akim, A. M., Cheah, Y. K., Halim, S. N. A., Seng, H. L. & Tiekink, E. R. T. (2015). Tumour-infiltrating regulatory T cells stimulate mammary cancer metastasis through RANKL-RANK signalling. *Journal of Inorganic Biochemistry, 150*, 48-62.

Thorburn, A. (2004). Death receptor-induced cell killing. *Cell Signal, 16*(2), 139-144.

Tiekink, E.R.T. & Young, D.J. (2006). *Acta Crystallographica Section E: Structure Reports Online, 62*, m1887.

Ting, N. S., & Lee, W. H. (2004). The DNA double-strand break response pathway: becoming more BRCAish than ever. *DNA Repair, 3*(8-9), 935-944.

Tsujimoto, Y., & Shimizu, S. (2000). Bcl-2 family: life-or-death switch. *Febs Letters, 466*(1), 6-10.

Tunç, T., Karacan, M. S., Ertabaklar, H., Sarı, M., Karacan N. & Büyükgüngör, O. (2015). Antimony(III) complexes with 2-amino-4,6-dimethoxypyrimidines: Synthesis, characterization and biological evaluation. *Journal of Photochemistry and Photobiology B: Biology, 153*, 206-214.

van Loo, G., Schotte, P., van Gurp, M., Demol, H., Hoorelbeke, B., Gevaert, K., . . . Vandenabeele, P. (2001). Endonuclease G: a mitochondrial protein released in apoptosis and involved in caspase-independent DNA degradation. *Cell Death & Differentiation, 8*(12), 1136-1142.

Venkatachalam, V., Ramalingam, K., Bocelli, G. & Cantoni, A. (1997). *Inorganica Chimica Acta, 23*, 261.

Williams, D. R. (1971). *The Metals of Life: The solution Chemistry of Metal Ions in Biological Systems*. Great Britain: The Camelot Press LTD.

Williams, R. J. & Fraústo da Silva, J. J. R. (2001). *Biological Chemistry of the Elements*. Oxford: Oxford University Press.

Wong, K. K. (2009). Recent developments in anti-cancer agents targeting the Ras/Raf/ MEK/ERK pathway. *Recent Patents on Anti-cancer Drug Discovery, 4*(1), 28-35.

Wu, Y., Deng, J., Rychahou, P. G., Qiu, S., Evers, B. M., & Zhou, B. P. (2009). Stabilization of snail by NF-kappaB is required for inflammation-induced cell migration and invasion. *Cancer Cell, 15*(5), 416-428.

Yadav & Prasad, R. N. (2012). Metals in oncology: an overview. *Academic Voices, A Multidisciplinary Journal, 2*(1), 54-58.

Yan, S., Jin, L. & Sun, H. (2005). *51Sb Antimony in medicine, in Metallotherapeutic Drugs and Metal-Based Diagnostic Agents: The use of Metals in Medicine* (M. G. a. E. R. T. Tiekink Ed.): John wiley & Sons, Ltd, Chichester.

Yang, L., Cao, Z., Yan, H., & Wood, W. C. (2003). Coexistence of high levels of apoptotic signaling and inhibitor of apoptosis proteins in human tumor cells: implication for cancer specific therapy. *Cancer Research, 63*(20), 6815-6824.

Yarden, R. I., Pardo-Reoyo, S., Sgagias, M., Cowan, K. H., & Brody, L. C. (2002). BRCA1 regulates the G2/M checkpoint by activating Chk1 kinase upon DNA damage. *Nature Genetics, 30*(3), 285-289.

Yeh, C. J., Hsi, B. L. & Faulk, W. P. (1981). Propidium iodide as a nuclear marker in immunofluorescence. II. Use with cellular identification and viability studies. *Journal of Immunology Methods, 43*(3), 269-275.

Yin, X. M. (2006). Bid, a BH3-only multi-functional molecule, is at the cross road of life and death. *Gene, 369*, 7-19.

Yi-Yun, G., Guo-Xiu, G., Qi, Y. & En-Qing, G. (2017). A series of 1D-to-3D coordination polymers from an unsymmetrical tetracarboxylic acid and various N-donor ligands: Syntheses, structures and photoluminescence properties. *Polyhedron, 124*, 68-76.

Yoo, H. J., Byun, H. J., Kim, B. R., Lee, K. H., Park, S. Y., & Rho, S. B. (2012). DAPk1 inhibits NF-kappaB activation through TNF-alpha and INF-gamma-induced apoptosis. *Cell Signalling, 24*(7), 1471-1477.

Zhan, Q., Antinore, M. J., Wang, X. W., Carrier, F., Smith, M. L., Harris, C. C., & Fornace, A. J., Jr. (1999). Association with Cdc2 and inhibition of Cdc2/Cyclin B1 kinase activity by the p53-regulated protein Gadd45. *Oncogene, 18*(18), 2892-2900.

Zhan, Q., Bae, I., Kastan, M. B., & Fornace, A. J., Jr. (1994). The p53-dependent gamma-ray response of GADD45. *Cancer Research, 54*(10), 2755-2760.

Zhan, Q., Fan, S., Smith, M. L., Bae, I., Yu, K., Alamo, I., Jr., & Fornace, A. J., Jr. (1996). Abrogation of p53 function affects gadd gene responses to DNA base-damaging agents and starvation. *DNA and Cell Biology, 15*(10), 805-815.

Zhao, R., Xiang, N., Domann, F. E., & Zhong, W. (2009). Effects of selenite and genistein on G2/M cell cycle arrest and apoptosis in human prostate cancer cells. *Nutrition and Cancer, 61*(3), 397-407.

Zhu, J., Chen, Z., Lallemand-Breitanbach, V. & de Thé, H. (2002). How acute promyelocytic leukaemia revived arsenic. *Nature Reviews Cancer,* (2), 705-714.

LIST OF PUBLICATIONS AND PAPERS PRESENTED

Ishak, D. H. A., Ooi, K. K., Ang, K. P., Akim, A. M., Cheah, Y. K., Nordin, N., Halim, S. N. A., Seng, H. L. & Tiekink, E. R. T. (2014). A bismuth diethyl dithiocarbamate compound promotes apoptosis in HepG2 carcinoma cell cycle arrest and inhibits cell invasion through the modulation of NF-κB activation pathway. *Journal of Inorganic Biochemistry, 130*, 38-51.

Paper was presented at the following conference and symposiums:

1. *Joint Malaysia-UK Symposium on Inorganic Chemistry*. Kuala Lumpur, MYS, December 2013. **Awarded Best Poster Prize (RCN:207890) by The Royal Society of Chemistry (RSC), United Kingdom.**

2. *5th UM-CU-NUS Trilateral Mini Symposium and Scientific Meeting.* Kuala Lumpur, MYS, February 2014.

3. *12th Chemistry Conference for Young Scientists (ChemCYS).* Blankenberge, BE, February 2014. **Awarded ChemCYS Best Poster Presentation in the field of Biochemistry & Biotechnology by The Royal Flemish Chemistry Society (Youth Division), Chemistry Conference for Young Scientists and European Young Chemists Network (EYCN).**

4. *University of Malaya Chemical Crystallography Symposium.* Kuala Lumpur, MYS, May 2014.

5. *University of Malaya Pharmaceutical Co-Crystal Symposium.* Kuala Lumpur, MYS, July 2014.

Gene expression level in HepG2 cell lines after treatment with **13** and **16** as compared to untreated cell. The data represents the mean of **13** and **16**-induced fold-change in gene expression relative to control-treated cells (n = 3), $p < 0.05$. .Note that:

a) ▌Corresponds to up-regulated genes
b) ▌Indicates that the genes are being down-regulated

	Up-down regulation in fold (as compared to control group)			Up-down regulation in fold (as compared to control group)	
	1	2		1	2
ABL1	58.13	253.96	**CASP7**	27.69	159.62
AKT1	72.06	241.94	**CASP8**	37.57	14.32
APAF1	33.17	12.62	**CASP9**	103.34	160.95
BAD	34.56	49.81	**CD40**	12.33	1.01
BAG1	-11.62	21.51	**CD40LG**	8.64	1.01
BAG3	-54.99	172.26	**CFLAR**	28.47	46.48
BAG4	-14.13	236.96	**CIDEA**	-1.19	-1.19
BAK1	64.50	164.11	**CIDEB**	23.77	134.22
BAX	34.99	14.04	**CRADD**	37.04	112.87
BCL10	11.64	26.51	**DAPK1**	42.54	1.01
BCL2	-16.63	-6.33	**DFFA**	103.34	59.16
BCL2A1	9.59	18.75	**FADD**	7.42	18.23
BCL2L1	-5.70	61.33	**FAS**	42.85	131.46
BCL2L10	-8.41	1.01	**FASLG**	6.03	8.39
BCL2L11	3.08	8.16	**GADD45A**	4.26	2.62
BCL2L2	35.54	123.51	**HRK**	10.06	18.11
BCLAF1	93.78	393.03	**IGF1R**	-212.13	-86.91
BFAR	1.55	2.88	**LTA**	9.52	11.22
BID	13.37	2.16	**LTBR**	215.45	395.76
BIK	7.52	8.22	**MCL1**	36.53	69.00
NAIP	24.44	67.11	**NOL3**	82.21	160.73
BIRC2	-1.35	1.85	**PYCARD**	1.04	1.01
BIRC3	-185.95	-30.94	**RIPK2**	37.82	180.83
XIAP	-68.65	4.90	**TNF**	-7.94	-7.95
BIRC6	-56.06	-24.28	**TNFRSF10A**	22.49	65.73
BIRC8	-18417.65	-4842.45	**TNFRSF10B**	250.94	928.32
BNIP1	75.12	179.58	**TNFRSF11B**	6.28	20.80
BNIP2	227.73	595.72	**TNFRSF1A**	138.26	225.73
BNIP3	-87.96	-49.92	**TNFRSF21**	12.65	51.57
BNIP3L	55.28	22.65	**TNFRSF25**	1.01	93.60
BRAF	-22.92	-8.18	**CD27**	-1.88	-1.32
NOD1	22.03	99.63	**TNFRSF9**	1.01	1.01
CARD6	1.01	1.09	**TNFSF10**	2.95	2.03
CARD8	3.10	3.50	**CD70**	2.93	3.29
CASP1	44.67	54.51	**TNFSF8**	7.47	5.42
CASP10	1.01	4.43	**TP53**	113.08	90.63
CASP14	1.01	33.32	**TP53BP2**	4.41	22.76
CASP2	58.94	304.12	**TP73**	18.79	8.62
CASP3	97.69	4.91	**TRADD**	35.29	92.31
CASP4	8.64	9.31	**TRAF2**	-1.05	77.11
CASP5	3.41	3.36	**TRAF3**	-3.14	73.46
CASP6	38.35	109.78	**TRAF4**	-11.74	51.98
ABL1	58.13	253.96	**CASP7**	27.69	159.62
AKT1	72.06	241.94	**CASP8**	37.57	14.32
APAF1	33.17	12.62	**CASP9**	103.34	160.95
BAD	34.56	49.81	**CD40**	12.33	1.01
BAG1	-11.62	21.51	**CD40LG**	8.64	1.01
BAG3	-54.99	172.26	**CFLAR**	28.47	46.48
BAG4	-14.13	236.96	**CIDEA**	-1.19	-1.19
BAK1	64.50	164.11	**CIDEB**	23.77	134.22
BAX	34.99	14.04	**CRADD**	37.04	112.87